論文 / 著書情報
Article / Book Information

題目(和文)	スルホン酸が結合したアモルファスカーボンの酸触媒能に関する研究
Title(English)	Studies on catalysis of amorphous carbon with sulfonic acid groups
著者(和文)	菅沼学史
Author(English)	satoshi suganuma
出典(和文)	学位:博士(理学), 学位授与機関:東京工業大学, 報告番号:甲第8640号, 授与年月日:2012年3月26日, 学位の種別:課程博士, 審査員:原 亨和
Citation(English)	Degree:Doctor (Science), Conferring organization: Tokyo Institute of Technology, Report number:甲第8640号, Conferred date:2012/3/26, Degree Type:Course doctor, Examiner:
学位種別(和文)	博士論文
Type(English)	Doctoral Thesis

Studies on Catalysis of Amorphous Carbon with Sulfonic Acid Groups

（和訳：スルホン酸が結合したアモルファスカーボンの酸触媒能に関する研究）

Department of Electronic Chemistry
Interdisciplinary Graduate School of Science and Engineering
Tokyo Institute of Technology

Satoshi Suganuma

2012　Doctor Thesis

Studies on Catalysis of Amorphous Carbon with Sulfonic Acid Groups

（和訳：スルホン酸が結合したアモルファスカーボンの酸触媒能に関する研究）

Department of Electronic Chemistry
Interdisciplinary Graduate School of Science and Engineering
Tokyo Institute of Technology

Satoshi Suganuma

This thesis was submitted to Tokyo Institute of Technology
for the degree of Doctor of Science.

2012　Doctor Thesis

Contents

Chapter 1 ***General Introduction***

1-1 Background 1

1-2 Solid acid catalyst

1-2-1 Clays 3

1-2-2 Zeolites 4

1-2-3 Heteropolyacids 6

1-2-4 Metal oxides and mixed metal oxides 7

1-2-5 Metal sulfates and phosphates 8

1-2-6 Ion-exchange resins 9

1-2-7 Sulfonated mesoporous silicas 11

1-2-8 Carbon-based solid acids 12

1-2-9 Water-tolerant Lewis acids 13

1-3 Transformation of carbohydrate by solid acid catalysts 15

1-3-1 Hydrolysis of polysaccharides into monosaccharides 16

1-3-2 Conversion of monosaccharides 16

1-3-2-1 Production of HMF 17

1-3-2-2 Production of furfural 19

1-3-2-3 Production of lactic acid and lactate-derivatives 19

1-4 Outline of this thesis 21

References 22

Chapter 2 ***Synthesis and Acid Catalysis of Cellulose-Derived Carbon-Based Solid Acid***

2-1 Abstract 28

2-2 Introduction 28

2-3 Experimental 29

2-4 Results and discussion 31

2-5 Conclusion 34

References and notes 35

Chapter 3 ***Hydrolysis of Cellulose by Amorphous Carbon Bearing SO_3H, COOH, and OH Groups***

3-1 Abstract 42

3-2 Introduction 42

3-3 Experimental 43

3-4 Results and discussion 45

3-5 Conclusion 50

References and notes 51

Chapter 4 ***SO_3H-Bearing Amorphous Carbon derived from Polyvinyl Chloride as a Heterogeneous Acid Catalyst***

4-1 Abstract 59
4-2 Introduction 59
4-3 Experimental 60
4-4 Results and discussion 61
4-5 Conclusion 64
References and notes 65

Chapter 5 ***SO_3H-bearing Mesoporous Carbon as a Highly Selective Catalyst***

5-1 Abstract 72
5-2 Introduction 72
5-3 Experimental 73
5-4 Results and discussion 75
5-5 Conclusion 79
References and notes 80

Chapter 6 ***Summary*** 91

List of publications 93

Acknowledgements 94

Appendix 1 Lactic Acid Synthesis over Hydrous Ta_2O_5 as a Heterogeneous Lewis Acid Catalyst

1-1 Abstract 95
1-2 Introduction 95
1-3 Experimental 96
1-4 Results and discussion 97
1-5 Conclusion 99
References and notes 100

Chapter 1

General Introduction

1-1 Background

Catalysts made great contribution to the development of chemical industry in the 20th century. Early in the century, synthesis of NH_3 catalyzed by iron-based catalysts led to increased production volume of food, resulting in an enormous increase in population. Coal chemistry was developed by catalysts, such as the synthetic process of CH_3OH using copper-based catalysts and gasoline using cobalt-based catalysts from syngas (CO and H_2) obtained by gasification of coal. In second half of 20th century, the industrial chemical production based on petroleum refinery was developed by Co-Mo sulfide, zeolites, and platinum group metals (especially Rh, Pd, and Pt), and has also continuously expanded into the manufacture of a variety of fine chemicals. But the E factor, defined as the mass ratio of waste to desired product, in fine chemical processes is 5-50 kg(waste)/kg(product). This value is much higher than that of <1-5 kg(waste)/kg(product) for bulk chemical processes, because production of fine chemicals involves multi-step syntheses and the use of stoichiometric amounts of unrecyclable catalysts that are converted into worthless waste after completion of reactions [1]. One of the solutions to this problem is the widespread replacement of harmful catalysts with reusable and easily separable alternatives.

Acid catalysts are the most conventionally used catalysts in chemical industry, including the production of petrochemicals (petroleum refinery), pharmaceuticals, agrochemicals, and fragrances. Acid catalyzed processes include catalytic cracking, alkylation, isomerization, hydration/dehydration, esterification, hydrolysis, and a variety of condensation reactions [2]. They produce more than 1×10^{11} kg/year of important products [3]. Many chemical reactions in industrial processes are known to be catalyzed by traditional Brønsted acids (H_2SO_4, HF, HCl, *p*-toluenesulfonic acid) or Lewis acids ($AlCl_3$, $ZnCl_2$, BF_3) in liquid-phase systems. These acid catalysts are responsible for corrosion of the reactor or reaction apparatus, and shows low activity and selectivity in some reactions. Recovery of the catalyst from the reaction mixture accompanies energy-inefficient special processes represented by distillation, which results in a significant increase in environmental load as well as production cost [4]. Homogeneous acids are removed from the reaction mixture by neutralization treatment which converts useful catalysts into worthless inorganic salts. Even though only catalytic amounts are generally, but not always, used in the oil refining and petrochemical industries, the absolute quantities of waste generated are considerable owing to the enormous production volumes involved. In the fine chemical industries the production volumes are much smaller but these acids are also used in stoichiometric quantities [5]. In order to

overcome the difficulties in separation and reusability, homogeneous Brønsted and Lewis acid catalysts have been replaced with recyclable solid counterparts, applied to diversified reactions [1,5-8]. The use of solid acids provides additional benefits [8]: contamination of the product by trace amounts of neutralized catalyst is generally avoided. Therefore, a wide variety of solid catalysts, for example, zeolites [4,9,10], pure and mixed metal oxides [4,11,12], supported heteropolyacids [4,13,14], ion-exchange resins [15,16], and supported Lewis acids [6], have been developed on this purpose. These solid acids have been used predominantly in large-scale industrial processes such as alkylation, isomerization, dehydration, condensation, etherification, and the formation of alcohols from olefins [1].

A prominent example in solid acid-catalyzed reaction in chemical industry is the manufacture of caprolactam, the raw material for Nylon-6. The conventional process involves the reaction of cyclohexanone with hydroxylamine sulfate, producing cyclohexanone oxime which is subjected to the Beckmann rearrangement in the presence of stoichiometric amounts of sulfuric acid. The overall process generates ca. 4.5 kg of ammonium sulfate per 1.0 kg of caprolactam over the 2 steps [1]. Ichitani and coworkers at Sumitomo chemical company [17,18] developed a vapor phase Beckmann rearrangement over a high-silica MFI zeolite. This process is combined with the technology developed by Enichem [19], for the ammoximation of cyclohexanone with NH_3/H_2O_2 over the titanium-containing zeolite catalyst (TS-1) described earlier, thus affording caprolactam in >98% yield without the production of hazardous salt. This process is currently being commercialized in Japan.

The efforts have been devoted to the development of a stable solid catalyst which has the acid sites with the required acidity (type and strength) and reactivity to promote a given type of chemical reaction. A difficulty in the use of solid acids is the severe poisoning of the acid sites by water, and in fact most solid acids lose their catalytic activities in aqueous solution. For reactions in which water participates as a reactants or product, such as hydrolysis, hydration, and esterification, only a few solid acids are acceptable in terms of the activity, stability and insolubility in water [14]. Development of new water-tolerant solid acids would have a major impact in industrial applications. It would especially be attractive in water-tolerant Lewis acids, because most Lewis acids are hygroscopic and thus are immediately deactivated or decomposed in the presence of even a small amount of water, which often limits their use in organic synthesis [14]. In addition, Brønsted and Lewis acid catalysts have been required for the conversion of biomass-derived carbohydrate, which attracts attention as a sustainable source of carbon to supply compounds needed in the transportation and chemical sectors. Application of solid acid catalysts to carbohydrate conversion in water can realize sustainable development of a society in the future [20,21].

In this chapter, structure and acid catalysis for some important solid acids with Brønsted and/or Lewis acid sites have been summarized in the following section.

1-2 Solid acid catalyst

1-2-1 Clays

Clays are produced in enormous quantities in nature and have found a wide variety of applications including catalysts [1,4,11,12]. They were widely used as solid acid catalysts in oil refining from the 1930s until the mid-1960s when they were replaced by the zeolites. Clay minerals consist of layered (alumino)silicates in which the basic building blocks – SiO_4 tetrahedral and MO_6 octahedral (M= Al^{3+}, Mg^{2+}, Fe^{3+}, Fe^{2+}, etc.) – polymerize to form two-dimensional sheets [1,4,11,12]. One of the most commonly used clays is montmorillonite in which each layer is composed of an octahedral sheet sandwiched between two tetrahedral silicate sheets (thickness: c.a. 1.0 nm) (Figure 1-1). The octahedral sheet typically comprises oxygens attached to Al^{3+} or some lower valence cations such as Mg^{2+}. The overall layer has a net negative charge which is compensated by hydrated cations occupying the interlayer spaces. Immersion in water results in a swelling of the clay by incorporation of excess amounts of water into interlayers and exposure of the intercalated cations, making them accessible for exchangeable cations. The interlayer cations are largely responsible for the Brønsted and/or Lewis acidity. Acid strength of the clays depends largely on the electronegativity of the cations; both the amount and strength of Brønsted and Lewis acid sites can be enhanced by cation exchange or treatment with mineral acid, e.g. H_2SO_4.

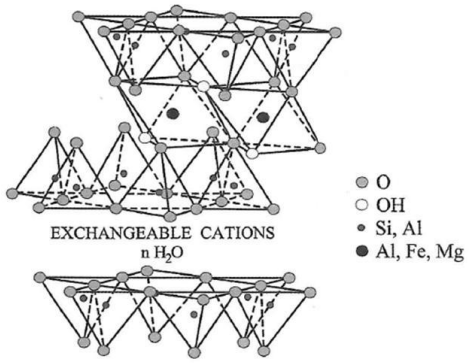

Figure 1-1. Structure of montmorillonite clay

An Al^{3+}-exchanged montmorillonite effectively promotes various acid-catalyzed reactions. H_2SO_4 treatment of natural montmorillonite affords the much more active and widely used acid catalyst known as K-10 or KSF (Sud-Chemie or Fluka, respectively). For instance, K-10 has been successfully used as a catalyst in the Friedel-Crafts alkylation [22]. Clays are also effective supports for Lewis acids such as $ZnCl_2$ or $FeCl_3$ [23]. Montmorillonite-supported $ZnCl_2$, known as Clayzic, has been extensively studied as a catalyst in e.g. the Friedel-Crafts alkylation [24, 25].

A serious shortcoming of clays is their limited thermal stability. Heating of exchanged clays results in a loss of water, accompanied by collapse of the layered structure, thereby dramatically decreasing the effective surface area. This problem was resolved by developing pillared clays [26-28], in which the interlayers are expanded with pillaring agents. Inorganic polyoxocations such as $[Al_{13}O_4(OH)_{24}(H_2O)_{12}]^{7+}$ are popular pillaring agents but a variety of organic and organometallic

pillaring agents have also been used. Pillaring with Al_{13} provides an interlayer space of ca. 0.8 nm after drying.

1-2-2 Zeolites

Zeolites are crystalline aluminosilicates with the following formula in the as-synthesized form: $xM_{2/n}O{\cdot}xAl_2O_3{\cdot}ySiO_2{\cdot}wH_2O$ where M is a inorganic cation (group 1 or 2) or an organic cation, and *n* and *w* represent the cation valence and the number of water molecules contained in the voids, respectively. Zeolites consist of tetrahedral building blocks that are linked through oxygen atoms producing a three-dimensional network, and have channels and cavities of molecular dimensions in the structure. The channel size is conventionally defined as ultralarge (>12-), large (12-), medium (10-), or small (8-membered ring) pores. A summary of zeolites with different pore size is given in Table 1-1. These molecular sieves have highly developed microporous structure, high surface area, and large pore volume, which are capable of adsorbing great amounts of small molecules such as hydrocarbons. This fact combined with the possibility to generate active site inside the channels and cavities of zeolites produces a very unique type of catalysts, which can be considered as a catalytic microreactor [10].

Table 1-1. Representative zeolites and its ring size for the main channel

Molecular sieve Type	Framework structure type (IUPAC CODE)	Type species	Window size
Small pore	LTA	A	8
	CHA	chabazite	
Medium pore	MFI	ZSM-5, silicalite	10
	FER	ferrierite	
	TON	theta-1	
Large pore	FAU	Faujasite, X, Y	12
	*BEA	Beta	
	MOR	mordenite	
Ultralarge	AET	MCM-37	14

A large number of zeolites are reported, some of which are naturally obtained, but most of which have been synthesized under hydrothermal condition [29]. The basic ingredients – SiO_2, Na_2SiO_3 or $Si(OR)_4$, and Al_2O_3, $NaAlO_2$, or $Al(OR)_3$ – together with a structure directing agent (template), usually an alkylamine or tetraalkylammonium salt, are added to aqueous alkaline solution (pH 8-12). This process results in the formation of a monomeric and oligomeric silicate species through a sol-gel reaction. Gradual heating of this mixture up to 200 °C results in dissolution of the gel to form clusters of SiO_4/AlO_4^- units which constitute the basic building blocks for the zeolite structure. In the presence of the template, these building blocks are polymerized each

other to form the zeolites. At this point, the zeolite still contains the organic molecules in the structure. This is subsequently removed by calcination, i.e. heating the material at 400-600 °C in air [1].

Zeolite structure containing only SiO_2 tetrahedra would be electrically neutral and no acidity would be developed on its surface. Brønsted acid sites are developed when Si^{4+} is isomorphically substituted by a trivalent metal cation, for instance $A1^{3+}$, and a negative charge is created in the lattice, which is compensated by a proton. The proton is attached to the oxygen atom connected to neighbor silicon and aluminum atoms, resulting in the bridged hydroxyl group which is responsible for the Brønsted acid site (Figure 1-2). The Brønsted acid strength is related to the Si/Al ratio [30]. The number of proton donor (hydroxyl groups) corresponds to the number of aluminum atoms present in the structure. The acid strength increases with decreasing aluminum content [31] (but note that complete replacement of aluminum affords a material with lower acidity [32]).

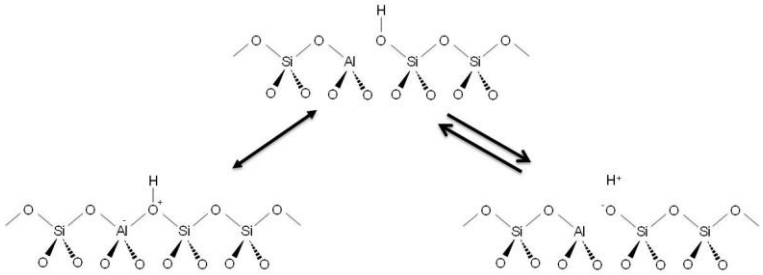

Figure 1-2. The acid form of zeolites

Pertinent examples of zeolite-catalyzed reactions in organic synthesis include the Friedel-Crafts alkylations, isomerizations, cracking, amination, hydration, and esterification [2]. The Friedel-Crafts alkylation of aromatics has been widely used in both bulk and fine chemical industries. For example, ethylbenzene (the raw material for styrene manufacture) is obtained by alkylation of benzene with ethylene over acidic zeolite. In 1980, a breakthrough in the alkylation technology was achieved with the application of the medium pore zeolite, H-ZSM-5, as a stable and recyclable catalyst (Mobil-Badger process) [2]. A benefit of this process is suppression of polyalkylation owing to the shape selective properties of micropores in H-ZSM-5. In another case, Sumitomo chemical [4,33-37] commercialized a vapor phase Beckmann rearrangement of cyclohexanone oxime to caprolactam with a high-silica MFI (ZSM-5 type) zeolite. The activity of the catalyst was proportional to its external surface area. This, together with the fact that caprolactam is not incorporated easily into the pores of the zeolite, suggests that the reaction takes place on the external surface, possibly at the pore openings. Ichihashi et al. [34,35] proposed that the reaction takes place in silanol nest resulting from dealumination, as was also suggested by Hölderich et.al. [38]

Acid-catalyzed processes in water using zeolites as solid acids were also reported. Asahi Kasei commercialized the hydration process of cyclohexene using a high-silica H-ZSM5 zeolite [39], combining a partial hydrogenation of benzene. This process involves a biphasic system, the organic (cyclohexene) and the aqueous phase containing the zeolite. The product, cyclohexanol, is exclusively distributed in the organic phase (cyclohexene phase), and can be recovered readily by

distillation. It was found that various zeolites having Si/Al ratios > 10 were active for the hydration reaction [40]. Zeolites with high Si/Al ratios are more hydrophobic than those with low Si/Al ratios, which is essential for the activity of the zeolites in water. In addition, the difference of the selectivity depending on the zeolites can be attributable to size and shape of micropores [40,41], therefore suggesting that this reaction took place inside the pores of the zeolites.

1-2-3 Heteropolyacids

Heteropolyacids (HPAs) are protonic acids that incorporate polyoxometalate anions (heteropolyanions) having metal-oxygen octahedral as the basic structural units into the complex cluster [13,42-49]. The first characterized and the well-known HPA is the Keggin heteropolyanion typically represented by the formula $XM_{12}O_{40}^{x-8}$ where X is the central atom (Si^{4+}, P^{5+}, etc.), *x* is its oxidation state, and M is the metal ion (Mo^{6+} or W^{6+}). The M^{6+} ions can be substituted by various metal ions, e.g., V^{5+}, Co^{2+}, Zn^{2+}, etc. The Keggin anion is composed of a central tetrahedron XO_4 surrounded by 12 edge- and corner-sharing metal-oxygen octahedra MO_6 (Figure 1-3) [49]. The octahedra are arranged in four M_3O_{13} groups. Each group is formed by three octahedra sharing edges and having a common oxygen atom which is also shared with the central tetrahedron XO_4. Among a wide variety of HPAs, the Keggin type HPA is the most stable and more easily available material; these are the most important factors for practical applications.

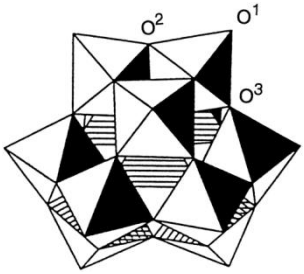

Figure 1-3. The Keggin structure of the $XM_{12}O_{40}^{x-8}$ anion (α-isomer) [49]: terminal (O^1), edge-bridging (O^2), and corner-bridging (O^3) oxygen atoms.

Many HPAs exhibit superacidity. For example, $H_3PW_{12}O_{40}$ has a higher acid strength (H_0=-13.16) than CF_3SO_3H or H_2SO_4. They were prepared simply by mixing phosphate and tungstate in the required amounts at the appropriate pH [44]. But, an inherent drawback of HPAs is their solubility in polar solvents, such as water and alcohol, which severely limits their application as recyclable solid acid catalysts in the liquid phase reactions. In order to overcome this problem, HPAs have been immobilized on supportant materials such as silica [50], carbon [51,52], or acidic ion-exchange resin [53]. For example, silica-occluded $H_3PW_{12}O_{40}$ was used as an insoluble solid acid catalyst in several liquid phase reactions such as ester hydrolysis, esterification, hydration, and the Friedel-Crafts alkylations [4].

The salts of HPA with large cations such as Cs^+ possess high surface area and have also been used as water-insoluble catalyst [14,54]. Partial substitution for proton by Cs^+ ions resulted in

unique changes in the surface area and hence in the amount of acidic site on the surface. The amount of acidic site on the surface showed a maximum for $Cs_xH_{3-x}PW_{12}O_{40}$ compounds with x = 2.5 [14]. $Cs_{2.5}H_{0.5}PW_{12}O_{40}$ (abbreviated $Cs_{2.5}$) has mesopores as well as microporous that are formed by interparticle voids among nanocrystallites [55]. $Cs_{2.5}$ showed significantly higher activities than original $H_3PW_{12}O_{40}$ and other solid acid catalysts for various acid-catalyzed reactions in water [56-60]. For instance, the catalytic activity of $Cs_{2.5}$ for the hydrolysis of ethyl acetate in excess water was compared with those of typical solid acids [56]. The activity of $Cs_{2.5}$ (per weight) was 3 and 35 times higher than those of H-ZSM-5 (Si/Al = 40) and H-ZSM-5 (Si/Al = 628), respectively. It would seem that the hydrophobicity and strong acidity of $Cs_{2.5}$ are responsible for its high activity. Three types of test reactions were used in water [56-60]: (1) the hydration of 2,3-dimethyl-2-butene, (2) the hydrolysis of 2-methylphenyl acetate, and (3) the hydrolysis of maltose. $Cs_{2.5}$ exhibited significantly superior activity for the reactions against other solid acids, because the acid sites of $Cs_{2.5}$ were shielded from water, due to the hydrophobic character of the $Cs_{2.5}$ surface. Another feature of $Cs_{2.5}$ is mesopores, in which bulk reactants such as maltose can diffuse smoothly and access to acid sites. However, $Cs_{2.5}$ has disadvanteges in the leaching out of heteropolyanions, and less-presipitation in an aqueous phase after the reaction. When $Cs_{2.5}$ was bonded to an amine functionalized SiO_2, the composite was entirely insoluble and water-tolerant solid acid, and exhibited stable and high catalytic performance in the hydrolysis of ethyl acetate and the hydration of α-pinene [61].

1-2-4 Metal oxides and mixed metal oxides

Hydrated niobium pentoxide (Nb_2O_5•nH_2O), usually called as niobic acid, was found to have Brønsted acid sites with high acid strength (H_0= -5.6) when calcined at relatively low temperatures (373 – 573 K), though the surface of niobic acid calcined above 773 K was almost neutral [2,62]. The acid sites on niobic acid are thought to be isolated OH groups as Brønsted acid sites, which are derived from distorted octahedral NbO_6, NbO_7, or NbO_8 species [63]. Niobic acid shows stable catalytic activity for acid-catalyzed reactions in which water molecules participate or are liberated. In fact, it showed excellent stability as an acid catalyst for hydrolysis [64,65], esterification [66], and hydration reactions [67]. Sugi et al. have reported the Nb_2O_5-catalyzed hydrolysis of phenyloxirane into 1,2-dihydroxybenzene in water under mild conditions [64,65]. When the reaction was performed in water at reflux temperature, niobic acid exhibited the highest activity among the solid acids. Aluminosilicate catalysts showed lower selectivity than niobic acid, due to effectively enhancing isomerization (side reaction). The diol selectivity for niobic acid was higher than that for other solid acids, e.g. aluminosilicates or Nafion. The activity of hydrolysis and the ratio of hydrolysis to isomerization (H/I) depended on the calcination temperature of niobic acid in a mixture of dioxane and water (90:10 v/v). Because the activity significantly decreased after calcination above 723 K and the H/I ratio steadily decreased with the calcination temperature, it can be suggested that the structural changes of the surface occurred after the calcination above 723 K.

Hydrated tantalum oxide as well as hydrated niobium oxide displayed strong acid properties, and catalyzed the aldol-condensation of acetone and the hydration of isobutene [68].

MoO_3-ZrO_2 is one of the available mixed metal oxides as a solid acid catalyst. The catalysts were prepared from the mixtures of H_2MoO_4 and zirconia gel with various ratios.[69]. NH_3 temperature programmed desorption (NH_3-TPD) measurement revealed that the acid strength of MoO_3-ZrO_2 is lower than those of SiO_2-Al_2O_3, H-ZSM-5, mordenite, and $Cs_{2.5}H_{0.5}PW_{12}O_{40}$ [69]. MoO_3/ZrO_2 calcined at 1073 K was highly active in the hydrolysis of ethyl acetate in excess water and esterification of acetic acid with ethanol [70]. The dependence of the calcination temperature on the conversion of ethyl acetate or acetic acid is unique. When MoO_3-ZrO_2 was calcined at temperatures below 773 K, the conversions of ethyl acetate and acetic acid were less than 7 and 15%, respectively. For calcination temperatures below 573 K, MoO_3-ZrO_2 showed less activity for hydrolysis than ZrO_2 itself. However, the activity of MoO_3-ZrO_2 significantly improved as the calcination temperatures was increased to 873-1073 K. The acid strength was independent of the calcination temperature and the acid amount continuously decreased with the increase of calcination temperature. On the other hand, the hydrophobicity of the surface was enhanced by the thermal treatment at high temperatures. The high reactivity of MoO_3-ZrO_2 is therefore predominantly attributable to the enhanced hydrophobic nature of the surface brought about the thermal treatment.

Amorphous zirconium tungstate $ZrW_{2\text{-}8}O_{0.5\text{-}3.5}$ has shown higher catalytic activity for ethylene hydration than partially reduced tungsten oxide, such as W_2O_5 [71]. Zirconium tungstate with a composition of W/Zr = 2 provided the highest activity for the reaction. Because of the high activity and insolubility in water, zirconium tungstate holds promise as an alternative for the problematic phosphoric acid catalyst. Tin tungstate, 13 % W-added stannia, generates remarkable acidity on the surface when calcined at 1273 K [72,73]. This material showed high catalytic activity in the dehydration of methanol into dimethyl ether and the esterification of *n*-octanoic acid with methanol to methyl *n*-octanoate. The 5 %- and 10 %- WO_3/SnO_2 compounds calcined at 1273 K showed activities much higher than mordenite and SiO_2-AlO_3 in the presence of water.

1-2-5 Metal sulfates and phosphates

Many studies have been reported concerning solid superacidity of sulfated metal oxides, where sulfated zirconia (SO_4^{2-}/ZrO_2) is a typical example of those superacids [74]. Commonly, the sulfated metal oxides have been prepared by the following procedures: (i) preparation of amorphous metal oxide gels as precursors; (ii) treatment of the gels with sulfate ion by exposure to a H_2SO_4 solution or by impregnation with $(NH_4)_2SO_4$; (iii) calcination of the sulfated materials at a high temperature in air. Among the sulfated metal oxides, SO_4^{2-}/ZrO_2 is well known as one of the strongest solid superacids; its acid strength is lower than -16 on the Hammett function scale [75]. Sulfated zirconia catalyst exhibited excellent catalytic activity for acylation, condensation and esterification reactions [76]. A number of studies have investigated the nature of acid sites for sulfated zirconia in order to

know how the surface acidity of zirconium oxide is greatly enhanced by sulfated ions [77,78]. An representative model of acid sites on sulfated zirconia is shown in Figure 1-5, where two oxygens are bonded to Zr in addition to coordination of a S=O group with Zr. The active site is not on the metals, but on the S atoms. The addition of water causes the breaking of this coordination and brings about strong Brønsted acid sites [79].

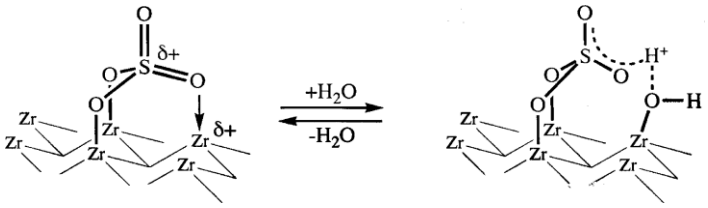

Figure 1-5. Sulfated zirconia structure models.

Zirconium phosphonates, $Zr(O_3PR)_2$, are layered compounds synthesized in amorphous forms under aqueous conditions through the reaction of a soluble zirconium salt and phosphoric or organophosphoric acid. Segawa et al.[14] synthesized several types of zirconium phosphonates, $Zr(O_3PR)_2$, either as a single component with one type of R, or as composite zirconium phosphonates with two different R groups, where R could be -OH, $-CH_3$, $-C_6H_5$, $-C_{12}H_{25}$, $-C_{22}H_{45}$, $-CH_2COOH$, $-C_2H_4COOH$, or $-CH_2SO_3H$. In the hydrolysis of ethyl acetate in water and esterification of acetic acid with ethanol, $Zr(O_3PCH_2SO_3H)_2$ exhibited high catalytic activity in comparison to the other zirconium phoshonates, due to the strong acidity for SO_3H groups. However, $Zr(O_3PCH_2SO_3H)_2$ is problematic in terms of dissolution in polar solvents. When a second functional group ($-O_3PC_{12}H_{25}$) was introduced at phosphor moiety, the resulting zirconium phosphonate, $Zr[(O_3PCH_2SO_3H)_x\text{-}(O_3PC_{12}H_{25})_{1-x}]_2$ at $x < 0.7$, was insoluble in water [80].

Niobium phosphates shows high catalytic performance for dehydration of fructose to 5-(hydroxymethyl)-2-furaldehyde (abbreviated HMF) in water. Two kinds of niobium phosphate (P/N1 and P/N2) were reported; P/N1 was obtained by the stirring of niobic acid (CBMM) and H_3PO_4, followed by calcination, and P/N2 was prepared from P/N1 and NaCl [81]. When P/N1 and P/N2 were used as catalysts, a high selectivity toward HMF was observed with no detectable amounts of by-product, such as levulinic and formic acid. These catalysts have both Brønsted and Lewis acid sites. Although structure of Brønsted and Lewis acid sites for niobium phosphate is similar to that of niobic acid, the Brønsted acid strength of niobium phosphates is weaker than that of original niobic acid. Lewis acid sites for niobium phosphate can be assigned to coordinatively unsaturated Nb^{+5} sites.

1-2-6 Ion-exchange resins

Two main classes of ion-exchange resins are sulfonated polystyrene (Amberlyst- and Dow- type resin) and perfluorosulfonic acid-based catalyst (Nafion). Structure of these resins is shown in Figure 1-6 [82,83]. Amberlyst-15 is a macroreticular sulfonated polystyrene-based

ion-exchangeable resin with 20 % divinylbenzene, and consists of agglomeration of very small microspheres interspersed with macropores. Nafion resin, a copolymer consisting of tetrafluoroethylene and perfluoro-2-(fluorosulfonylethoxy)propyl vinyl ether, is SO_3H-bonded perfluorinated resin. The terminal $-CF_2CF_2SO_3H$ groups show strong acid strength. The physical properties of these cation-exchange resins are shown in Table 1-2 [82,83]. One of the main differences between sulfonated polystyrene and perfluorinated resin with sulfonic acids is the acid strength. It is generally accepted that sulfonic acids bonded to perfluorinated polymer are strong acids with values of the Hammet acidity function (H_0) from -11 to -13, whereas that of Amberlyst-15 is -2.2. Another important difference is the number of acid sites, which is ~5-fold greater for the Amberlyst-15 than that of Nafion.

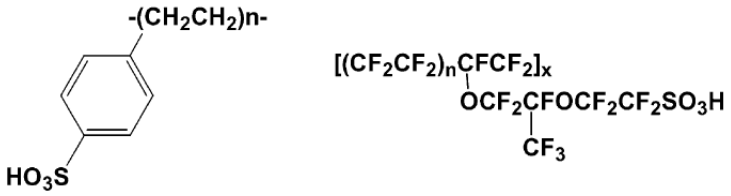

Figure 1-6. Structure of polymer resins.

Table 1-2. Physical properties of cation-exchange resins.

Catalyst	Surface area ($m^2 \cdot g^{-1}$)	Pore volume ($mL \cdot g^{-1}$)	Capacity (mequiv of $H^+ \cdot g^{-1}$)	Max operating temperature (°C)	H_0
Amberlyst-15	50	0.35	4.8	120	-2.2
Nafion-NR50	0.02	*A*	0.9	280	-12
Nafion-silica nanocomposite	200	0.7	0.15	280	>-12

[a] Nonporous structure

Examples of Nafion-catalyzed reactions are dehydration of *tert*-butyl alcohol to isobutylene, alkylation of phenol, bisphenol A synthesis, hydration of propene, decomposition of cumene hydroperoxide, and hydrolysis of ester [84,85]. Due to the small surface area (0.02 $m^2\ g^{-1}$), most of the SO_3H groups are generally buried within the polymer beads. However, Nafion can incorporate large amounts of hydrophilic reactants or solvents into the bulk, which provides smooth access of reactants in solution to SO_3H groups and results in high catalytic performance. On the other hand, the active sites of Nafion were largely inaccessible to hydrophobic reactant and solvent. As a result, Nafion resin exhibited low catalytic activities for hydrophobic reactions.

Cation-exchange resins have been used as solid acids in the etherification of olefins with alcohols, e.g. the coupling of isobutene with methanol to form methyl *t*-butyl ether (MTBE), one of the octane boosters in the fuel for motor vehicles. Commercially, MTBE is produced in the liquid phase over macroporous sulfonic acid resin such as Amberlyst-15 [86], which can function also as an acid catalyst in non-swelling solvents. Other examples of acid-catalyzed reactions using Amberlyst-15 are esterification, etherification and acetalizations [87,88]. However, a serious

shortcoming of Amberlyst-15 is limited thermal stability up to 120 °C.

To increase the accessibility for acid sites in non-swelling reactant or solvent, a new class of solid acid catalyst based upon a high surface area Nafion-silica nanocomposite has been developed [89,90]. Nafion resin-silica nanocomposites with high surface areas can function as effective acid catalysts in non-swelling solvents and reactants. Nafion-silica nanocomposites showed higher catalytic activity than that of Amberlyst-15 for the esterification of cyclic olefins with saturated and unsaturated carboxylic acids [83]. Esterification of dicyclopentadiene with acrylic acid was catalyzed effectively using Nafion-silica (13% w/w) composite. For nitration of benzene, Nafion-silica composite was found to be a better catalyst than Nafion resin [83]. Okuyama et al. [91] reported the hydrolysis of ethyl acetate and esterification of acrylic acid with 1-butanol using a new silica composite of the perfluorocarbonsulfonic acid resin, Aciplex (Asahi Chemical Co.). The Aciplex-silica composite showed higher activity than typical solid acids, such as $Cs_{2.5}H_{0.5}PW_{12}O_{40}$, H-ZSM-5, and SO_4^{2-}/ZrO_2 for the reactions. Aciplex-silica composite was superior in activity to Nafion-silica composite for the reactions. While the acid strength of the Aciplex-silica composite was similar to that of Nafion-SiO_2, the acid amount of the Aciplex-SiO_2 is about 2 times higher than that of Nafion-SiO_2. This difference would bring about the difference in activity [91,92].

1-2-7 Sulfonated mesoporous silicas

Sulfonated hybrid materials were prepared by modification of inorganic solid surface with organic sulfonic acid group. Combining properties of organic and inorganic components in a single composite material is well-considered approach to optimize the number, dispersion, accessibility, and strength of the acid sites [93-95]. To prevent leaching weakly bound active sites, covalent attachment of sulfonic acids to the inorganic matrix is the preferred technique (Figure 1-7) [4,96]. The MCMs group of mesoporous materials comprises lamellar MCM-50, cubic MCM-48 and the hexagonal MCM-41 structures [97-103]. Preparation of sulfonated ordered mesoporous silicas leads to materials with a high surface area, a narrow pore size distribution, excellent site accessibility, high loading, and high acid strength [104-106].

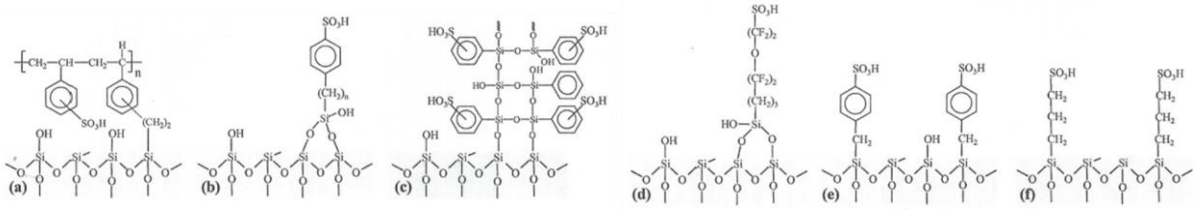

Figure 1-7. Sulfonated mesoporous silicas: (a) sulfonated polystyrene-silica hybrid prepared via the sol-gel technique; alkylphenylsulfonic acid; (c) sulfonated polyphenylsilsesquioxane; (d) perfluorosulfonic acid; (e) benzylsulfonic acids attached to a chlorinated silica; (f) sulfonated polysiloxane.

There are generally two preparation procedures: one is post-synthetic immobilization of sulfonic

acid groups via grafting and coating and another is one-pot sol-gel synthesis with structure-directing agents. In the former, preformed MCM-41 can be functionalized by a sol-gel reaction of surface silanols or siloxanes with silylating agents such as 3-mercaptopropyltrimethoxysilane. After oxidation of the immobilized thiol groups with H_2O_2, a solid sulfonic acid is obtained [104,105,107,108]. In the latter, hybrid ordered mesoporous silicas can be obtained, processing a sol containing $RSi(OR')_3$ and TEOS or TMOS in the presence of a self-assembling surfactant. For example, hybrid MCM type materials with covalently linked phenyl or alkyl groups were prepared in a micellar cetyltrimethylammonium bromide solution [109]. In a similar approach, dodecylamine was used as the structure-directing agent to obtain HMS type materials with immobilized organic groups (HMS = hexagonal mesoporous silica) [110]. The synthesis of MCM- and HMS- type materials with mercaptopropyl groups was achieved by use of 3-mercaptopropyltriethoxysilane (MPTS) or its methoxy analogue [104-106,111]. Even typical non-ionic surfactants such as the poly(ethylene oxide)-poly(propylene oxide) block copolymer, commercially available as Pluronic 123, have been used to prepare such hybrid materials [112]. In the sulfonic acid form, the prepared materials typically have a high surface area (> 500 m^2 g^{-1}), a considerably large pore volume (> 0.40 mL g^{-1}) and a narrow pore size distribution.

Mesoporous sulfonic acids are of particular interest for reactions involving bulk reactants that are too large to be incorporated into the smaller pores of conventional porous solid acids. Sulfonic acid bearing MCM-41 prepared via post-synthetic silylation was used for esterification of lauric acid with glycerol [113,114]. The resulting MCM-41 silicas containing both methyl and sulfonic acid groups were active for the reaction [115]. Higher monoglycerol yields were obtained with lauric acid rather than oleic acid. The activity of the materials was clearly superior to that of zeolite Beta or Y in bisphenol-A synthesis, the D-sorbitol dehydration–esterification forming isosorbide dilaurate and the hydroxylation of methylfuran with acetone [104,105,116].

1-2-8 Carbon-based solid acids

Our groups have reported that a partially carbonized organic compound with a high density of sulfonic acid (SO_3H) groups can function as an efficient solid acid catalyst [117-120]. The material consists of flexible polycyclic carbon nanosheets with SO_3H, COOH, and phenolic hydroxyl (OH) in a three-dimensional network that can be readily prepared by partial carbonization of natural organic compounds, such as sugar, starch, and cellulose, followed by sulfonation of the resulting amorphous carbon (Figure 1-8) [118-120]. The carbon material can incorporate large amounts of hydrophilic molecules, including water, into the carbon bulk, because of the high density of hydrophilic functional groups bound to the flexible carbon sheets. This incorporation provides good access for reactants in solution to the SO_3H groups in the carbon material, which gives rise to high catalytic performance, despite the small surface area (< 5 m^2 g^{-1}). The carbon-based solid acid showed higher catalytic performance than that of conventional solid acids in esterification, hydration, and hydrolysis [117,120]. The sugar-derived carbon material also exhibited remarkable

activity in the esterification of higher fatty acids such as oleic and stearic acids with ethanol [118,119]. However, because hydrophilic functional groups prevent incorporation of hydrophobic molecules into the carbon bulk where most of the SO_3H groups are presented, hydrophobic reactions proceed only on outer surface with small surface areas, resulting in poor or no catalytic activity. In order to develop active SO_3H-bearing carbon catalysts with large surface area available for hydrophobic acid-catalyzed reactions, SO_3H-bearing amorphous carbon/mesoporous silica composites have been developed by carbonization of loading D-glucose into the pores of mesoporous silica, followed by sulfonation with fuming H_2SO_4 [121]. The composites exhibited high catalytic performance for the dimerization of α-methylstyrene, hydrophobic reactant, although bulk carbon-based solid acid showed no catalysis for the reaction. The selectivity of the composite catalysts for unsaturated dimers exceeded for 98 %.

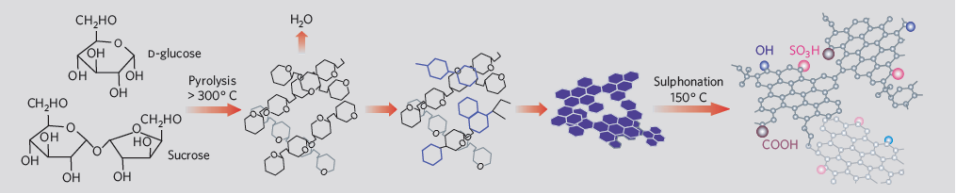

Figure 1-8. Preparation from sucrose and D-glucose of a solid catalyst.

Sulfonated mesoporous carbons, named as Starbon acids, were reported by Clark et al. [122]. Mesoporous expanded-starch was used as the precursor without the need for a templating agent, utilizing the natural ability of the amylose and amylopectin polymer chains within starch to assemble themselves into organized, largely mesoporous structures [123,124]. Starbon acids exhibited high catalytic performance in the esterification of organic diacids, such as succinic acid, fumaric acid, and itaconic acid, with ethanol in water.

Feng et al. reported the functionalization of ordered mesoporous carbon with sulfonic acid-containing aryl groups under mild conditions [125]. Hexagonal tube-like CMK-5 was chosen as the substrate because this material has uniform mesoporosity and large surface area, which is suitable as a host material for the modification with sulfonic acid groups. CMK-5 was synthesized using Al-SBA-15 as the hard template and furfuryl alcohol as the carbon precursor. Treatment of CMK-5 with aryl radical species, produced by homogeneous reduction of 4-benzene-diazoniumsulfonate with hypophosphorous acid, resulted in the formation of SO_3H-bearing CMK-5. The resulting material showed high catalytic activity in the esterification of acetic acid and formation of bisphenol-A [125].

1-2-9 Water-tolerant Lewis acids

Lewis acids have been used for a wide variety of catalytic reactions, such as C-C and C-X (X = N, O, P) bond formation, oxidation and reduction, and rearrangement [126,127]. Traditionally, Lewis acids such as $AlCl_3$, BF_3, $TiCl_4$, $SnCl_4$, etc., have been employed in these reactions. More

than stoichometric amounts of the Lewis acid are needed in many cases because the acid-base adduct as intermediate formed between the catalyst and the product (the product is often more basic than the substrates) needs to decompose, in way to add water to the reaction mixture. But, this way also leads to hydrolysis of the conventional Lewis acids, prohibiting its reuse and generating aqueous effluent containing copious amounts of inorganic salts [1]. Thus, the development of stable in water and highly reusable Lewis acids has been desired.

Recently, Kobayashi et al. reported that some inorganic triflates represented by $Sc(OTf)_3$, $Yb(OTf)_3$, and $La(OTf)_3$ can function as stable and highly active Lewis acid catalysts in the presence of water [128-130]. In 1994, they found that $Sc(OTf)_3$ could successfully work as Lewis acid catalyst in both water and organic solvents. Lewis acid on $Sc(OTf)_3$ realized to activate carbonyl or nitrogen-containing compounds even in the presence of water. $Yb(OTf)_3$ accelerated the hydroxymethylation of silyl enol ether with aqueous formalin solution to give the corresponding ketone [131-134]. They revealed that catalytic activity of Lewis acids is dependent on the hydrolysis constant (K_h) and water exchange rate constant (WERC) for substitution of inner-sphere ligands of the metal cation [129]. Active catalysts were found to have pK_h values in the range 4-10: cations having a pK_h of less than 4 are easily hydrolyzed while those with a pK_h greater than 10 display only weak Lewis acidity. From a viewpoint of green chemistry, it would be more attractive to perform the Lewis acid-catalyzed reactions in pure water using inorganic triflates. This was achieved by adding the surfactant (sodium dodecyl sulfate: SDS) to the aqueous solution [129]. A further extension of this concept resulted in the development of lanthanide salts with dodecyl sulfate, so-called Lewis acid-surfactant catalysts (LASC) which combine the Lewis acidity of the metal cation with the surfactant properties of the anion [135]. These LASCs, e.g. $Sc(DS)_3$, exhibited high catalytic performance in water. LASCs were shown to catalyze a variety of reactions, such as Michael additions and a three component α-aminophosphonate synthesis in pure water [129,135].

Use of polymer-supported catalysts offers several advantages, such as separation and isolation, as well as reuse of the catalyst. Nafion-Sc, which was prepared by treatment of Nafion resin with $ScCl_3 \bullet 6H_2O$ in acetonitrile under reflux conditions, was active for the allylation reactions of carbonyl compounds with tetraallyltin under aqueous conditions [136]. The Diels-Alder reaction was accelerated by Nafion-Sc in H_2O-CH_3OH-toluene at room temperature [137]. Nafion-Sc also worked efficiently for the imino Diels-Alder reaction to afford the corresponding adducts in high yields. Nafion-Sc was recovered simply by filtration and washing with a suitable solvent, with minimal loss of activity. In the reaction of benzaldehyde with tetraallytin in H_2O-MeOH-toluene (1:7:4) at room temperature, the yields were 91% (15 h), 81% (48 h), and 93% (40 h) for the first, second, and third runs, respectively[14] .

Another alternative to conventional Lewis acids is to incorporate heteroatoms into, for example, zeolites or mesoporous silicas [6]. At the beginning with the discovery of titanium silicate-1(TS-1) in the early 1980s, isolated Lewis acid sites in crystalline microporous materials could be formed with the absence of Brønsted acid sites [138]. TS-1 is active in many organic transformations, and is able to maintain activity even in the presence of water [139]. TS-1, in combination with aqueous solutions of hydrogen peroxide (H_2O_2), has provided the industrial implementation of various

reactions, including phenol hydroxylation, cyclohexanone ammoxidation, and propene oxide synthesis, with great simplification of the processes and reduction of waste and hazards [140-142]. The tetrahedrally coordinated Ti^{4+} species can act as a Lewis acid site by using empty d^0 orbitals to accept electron pairs from reactants. The successful catalytic performance obtained with Ti-containing zeolites was applied to the way for the development of new zeolites and mesoporous materials containing different metals in framework. Sn, Zr, Ta, and Nb have been successfully incorporated into the framework of zeolite Beta and MCM-41, exhibiting peculiar catalytic properties different from Ti-based zeolites in the presence of water [143-151]. Recently, Sn-Beta and Ti-Beta was found to show highly catalytic activity for the isomerization of glucose into fructose in aqueous media [152]. A detailed NMR study revealed that when Sn-Beta was used as catalyst, glucose isomerization proceeded through an intramolecular hydride shift. This is similar pathway to Meerwein-Ponndorf-Verley (MPV) reactions mediated by Lewis acids involving a six-membered transition state between the metal center, the carbonyl group, and the hydroxyl group in the sugar (Figure 1-9) [153].

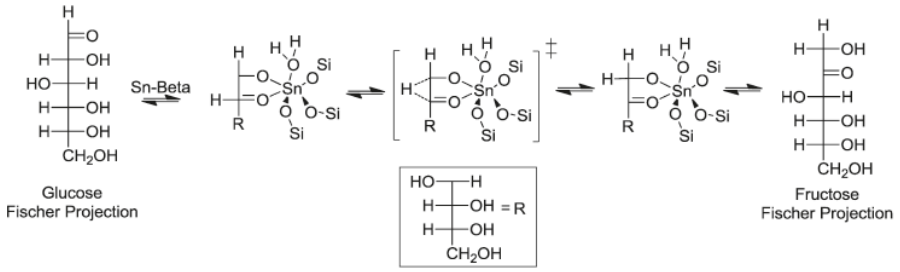

Figure 1-9. Proposed glucose isomerization reaction mechanism catalyzed by Sn–Beta.

1-3 Transformation of carbohydrate by solid acid catalysts

Carbohydrates are among the most abundant organic compounds on earth and represent the major portion of the world's renewable biomass, of which less than 5 % is used by mankind annually [154]. The bulk of the renewable carbohydrate-biomass comprises polysaccharides. Cellulose and hemicellulose in lignocellulose consists of two types of monosaccharides: hexoses (six-carbon sugars) and pentoses (five-carbon sugars). Various strategies for efficient use of carbohydrates as a chemical feedstock are being established in the interest of supplementing, and ultimately replacing petroleum resources [2,155-157]. There are two ways to transform carbohydrates into bioproducts: one is fermentation process, and the other is the chemical transformation by using a catalyst. In conversion of carbohydrates, the thermal instability is a major obstacle. Fermentation processes have proven to be more applicable than catalytic ones, in part because of their ability to operate at low temperatures. On the other hand, catalysts often offer improved process design options, resulting in higher productivity and reduced costs related to product work-up. Indeed, catalytic processes have indicated to be scalable and able to supply numerous low-cost products from petroleum.

1-3-1 Hydrolysis of polysaccharides into monosaccharides

In order to use carbohydrates, polysaccharides are converted into monosaccharides by chemical or enzymatic processes. Hydrolysis of polysaccharides can generally allow the energy-efficient conversion [2], and is typically carried out using acid catalysts at temperature ranging from 370 to 570 K, depending on the structure and nature of the polysaccharides [158]. Acid hydrolysis proceeds by C-O-C bond cleavage at the intermediate oxygen atom between two sugar molecules [159]. Hydrolysis reaction often accompanies further degradation of sugars to small organic products such as furfural and 5-hydroxymethylfurfural (HMF). Cellulose, the most abundant polysaccharide with β-glycosidic linkage, is the most difficult material to be hydrolyzed because of its high crystallinity. Hemicellulose is more open to attack at oxygen linkages to break down the oligomers into single sugar molecules. Besides polysaccharides in lignocellulose, soluble starch (a polyglucan with α-glycosidic linkage obtained from corn and rice) and inulin (a polyfructan obtained from chicory) can be hydrolyzed to form glucose and fructose, respectively. Hydrolysis of polysaccharide, especially cellulose, is catalyzed by concentrated or diluted sulfuric acid. Recently, solid acid catalysts have been applied to the cellulose hydrolysis as a replacement of liquid sulfuric acid. Layered transition-metal oxide [160], heteropolyacid [161], SO_3H-appended silica/carbon composites [162], and magnetic silica [163] are found to be active for the reaction. Although these solid acids are potential candidates, further development of the catalysts is required to improve the catalytic performance because the hydrolysis is carried out at the interface between the solid surface and macromolecular cellulose, resulting in poor accessibility of the substrate with active sites.

1-3-2 Conversion of monosaccharides

Monosaccharides obtained by hydrolysis of polysaccharides can be transformed into important basic nonpetroleum chemicals: furfural (2-furancarboxaldehyde) and 5-hydroxymethylfurfural (HMF) arising from dehydration of pentoses and hexoses, respectively (Scheme 1-1) [156]. Monosaccharides including glucose, fructose, and xylose can also serve as feedstock for the production of lactic acid through trioses. The proposed reaction networks for the production from hexoses suggested that trioses, such as dihydroxyacetone, glyceraldehyde, and pyruvaldehyde, are prevalent intermediate species (Scheme1-2) [164].

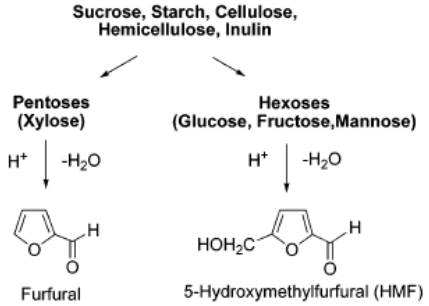

Scheme 1-1. Products synthesized from monosaccharides

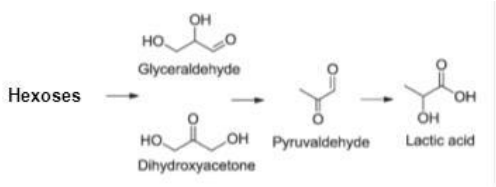

Scheme 1-2. Proposed intermediates in the conversion of hexoses into lactic acid

1-3-2-1 Production of HMF

HMF is a versatile and multi-functional compound and a good starting point for the synthesis of precursors of pharmaceuticals, thermoresistant polymers, and macrocyclic compounds, and particularly for the synthesis of dialdehydes, ethers, amino alcohols, and other organic intermediates [156,158,165]. These may lead to the possibility of numerous chemical products such as solvents, surface-active agents, phytosanitary products, and resins [156,158,165]. HMF is formed from hexoses through removing three water molecules in the acid-catalyzed dehydration reaction (Scheme 1-3) [165]. In the aqueous system, HMF enters into a consecutive reaction sequence taking up two molecules of water, and forms levulinic and formic acid as semifinal products. The cross-polymerization reactions lead to the production of colored soluble polymers and insoluble brown humins [166]. In order to prevent the side reactions and obtain a high yield of HMF, one can design and employ a suitable catalyst tuned to the formation of HMF, while not promoting the consecutive reactions or alternatively the continuous removal of HMF from the reaction mixture. The catalysts used are generally classified as mineral acid, organic acid and solid acid catalysts. Among these catalysts, solid acid catalysts have several advantages over liquid acid catalysts: (a) they facilitate the separation of product from reaction mixture and can be easily recycled; (b) they can work at relatively high temperatures, thus shortening the reaction time and favoring the formation of HMF instead of its decomposition during a prolonged reaction period; (c) they are capable of adjusting the surface acidity to improve the selectivity of HMF [167].

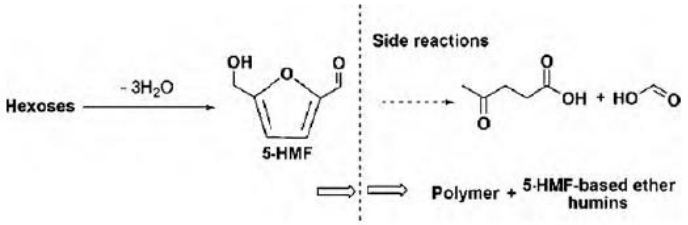

Scheme 1-3. The production of HMF and the corresponding side reactions

The most convenient method for the preparation of HMF is the acid-catalyzed dehydration of fructose. Fructose can be obtained by acid-catalyzed hydrolysis of sucrose and inulin or by selective isomerization of glucose to fructose. The representative results of fructose dehydration reported are summarized in Table 1-3. Biphasic systems (a mixture of aqueous and organic solvent) are typically used to boost HMF yields by effectively lowering reactant, product, and water concentration, or by separating the product from the reactant into different phases [168-170]. Anatase TiO_2 catalyzed the

production of 5-HMF from fructose under microwave irradiation [171]. The catalytic activity of niobium phosphate was superior to that of niobic acid in the aqueous phase, which was related to the more effective surface acidity of niobium phosphate in polar media [172,173]. Vanadyl phosphate exhibited higher catalytic performance than niobium phosphate [174]. When cubic zirconium pyrophosphate (C-ZrP_2O_4) was employed in the dehydration, a 44.3% yield of HMF in a 99.8% selectivity was obtained at 100 ºC within 0.5 h [175]. Meanwhile, γ-titanium phosphate also exhibited promising performance (a 35.3% yield of HMF in 96.1% selectivity) under similar conditions.

Table 1-3. The catalytic reaction results for the fructose dehydration with typical solid acid catalysts

Catalyst	Solvent	Temp. (K)	Time (min.)	Conv. (%)	HMF selectivity (%)	Ref.
Dowex 50wx8-100	Acetone/DMSO	423	10	96.4	85.2	[168]
Dowex 50wx8-100	Acetone/H_2O	423	15	95.1	77.2	[169]
H-form mordenite	H_2O-MIBK	438	60	76.0	91.1	[170]
Anatase TiO_2	H_2O	473	5	83.6	45.6	[171]
Niobium phosphate	H_2O	373	120	61.4	35.2	[172,173]
Vanadyl phosphate	H_2O	323	60	50.2	83.5	[174]
Cubic zirconium Phosphate	H_2O	373	30	44.4	99.8	[175]

Glucose, the most abundant sugar in biomass, is used in industry as a source of HMF because its cost is much lower than of fructose [176]. However, in pure water, glucose dehydration to HMF is extremely nonselective, because the direct dehydration of glucose requires harsher conditions (i.e., higher temperatures, longer residence times, and higher acidity) in comparison with those required to the dehydration of fructose, thus leading to higher byproduct formation [164]. An alternative strategy to generate high HMF yields from glucose involves a two-step process whereby glucose is first isomerized into fructose, followed by the dehydration of fructose into HMF (Scheme 1-4). Combination of basic Mg/Al hydrotalcites and acidic resins has been used to dehydrate glucose into HMF in dimethylformamide at 353 K [177,178]. Lewis acids can also be potentially used in combination with Brønsted acids to catalyze glucose to HMF cascade reactions. However, water-compatible Lewis acids in water are expected to have low catalytic activity not only because they progressively deactivate but also because water provides a coordinating polar environment that masks possible complex formation with low-coordinate metal species. Recently, Sn–Beta zeolites have been used in conjunction with homogeneous Brønsted acids in biphasic systems to effectively dehydrate saccharides into HMF [179]. In this system, Sn–Beta catalyzed a Lewis-acid-mediated isomerization of glucose into fructose, whereas the mineral acid catalyzed the dehydration of fructose into HMF.

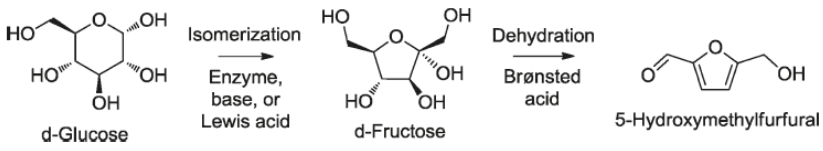

Scheme 1-4. Two-step process for the conversion of glucose into HMF.

1-3-2-2 Production of furfural

Furfural is one of the versatile and renewable chemicals with a wide industrial application profile both as a solvent and as a building block for the synthesis of various chemicals, including tetrahydrofuran, agrochemicals, pharmaceuticals, fragrances, and furan-based resins [180-182]. Furfural is formed from xylose through removing three water molecules in the acid-catalyzed dehydration reaction (Scheme 1-5). The by-products formed in this reaction result mainly from consecutive condensation reactions between furfural and intermediates of the xylose-to-furfural conversion [180]. For dehydration of xylose as well as glucose and fructose, heterogeneous catalytic processes offer several advantages over liquid acid catalysts. Attempts have been made to develop such processes, and the use of zeolites (faujasites and mordenites) was reported for the reaction at 443 K in a mixture of water and metylisobutyl ketone or toluene [183]. Mordenite was more selective to furfural than faujasite, achieving selectivities between 90 and 95%; however, conversion was low (about 30%). Valente et al. have studied the hydrolysis of xylose to furfural by heteropolyacids [184], MCM-functionalized sulfonic acid [185], and microporous and mesoporous niobium silicates [186] as catalysts at 413 K, using DMSO and water/toluene solvents. The dehydration over microporous niobium silicates gives xylose conversions up to 90% and furfural yields up to 50%. These yields are significantly higher than those achieved under the same reaction conditions with HY or mordenite zeolites.

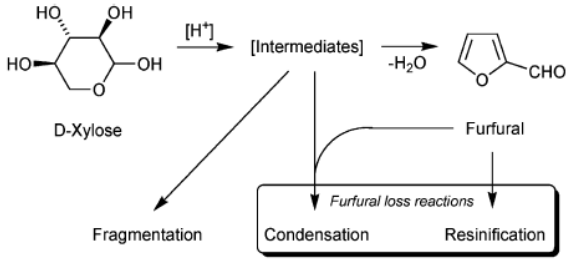

Scheme 1-5. Simplified reaction scheme of the dehydration of xylose to furfural and some side reactions.

1-3-2-3 Production of lactic acid and lactate-derivatives

Lactic acid is an important chemical used widely in the pharmaceutical, food, cosmetic and chemical industries [187]. Recent growth in demand for lactic acid, its salts, and its esters has stemmed from their use as platform chemicals for the production of biodegradable polymers and renewable solvents [188,189]. Current methods of lactic acid production are based on the anaerobic

microbial fermentation of glucose using bacteria. The main drawbacks associated with this process are the use of stoichiometric amounts of calcium hydroxide to neutralize the product, the large amounts of energy consumed, and waste generated during the separation of lactic acid from the fermentation broth [190]. Much effort has been devoted to develop efficient chemical synthesis routes to address the drawbacks for biological synthesis route.

For the chemical transformation of monosaccharides, dissolved metal salts have been used as Lewis acid catalysts. Zn(II), Cr(III), Co(II), and Ni(II) salts generated the best improvement in lactic acid yields for transformation of glucose in water at subcritical conditions [191-193]. But, reported lactic acid yields were usually low (<40%) and reaction mechanism was not studied. Thus, the conversion of trioses into lactic acid and lactate derivatives has been a subject of intense investigation in recent years. Trioses, such as dihydroxyacetone (DHA) and glycelaldehyde (GLA), can be obtained via biological or chemical synthetic methods from glycerol, a common by-product from the transesterification of triglycerides used in biodiesel production [194-198]. In view of the interesting results obtained with hexoses, homogeneous Lewis acids have also been investigated for the transformation of these trioses into lactate derivatives. Early reports have shown that transition metal complexes can catalyze this reaction effectively by forming stable Lewis acid–Lewis base complexes in water through chelate substrate binding of the monohydrated triose with Rh or Cr species [199,200]. More recently, lactic acid yields exceeding 90% were achieved starting from DHA using Lewis acid salts containing Al(III) and Cr(III) cationic species[201,202].

The large-scale production of lactate derivatives necessitates the use of heterogeneous catalysts to avoid energy-intensive separation procedures. For reactions of DHA in ethanol, ultrastable zeolite Y materials (a low Si/Al ratio and a high content of extra-framework aluminum) exhibited the highest yields (>95%) toward the desired lactate products [203,204]. It was concluded that both Lewis and Brønsted acidity is required for optimal yield: Brønsted acid sites are needed to convert trioses into pyruvaldehyde, and Lewis acid sites are needed for the intramolecular isomerization of the aldehyde into the lactate. The incorporation of tin into the framework of porous silicates results in highly active and selective catalysts for the production of lactate derivatives from trioses or hexoses [205,206]. Sn–Beta catalysts with high Si/Sn ratios (typically ranging between 90 and 200) quantitatively convert DHA dissolved in methanol into methyl lactate at 353 K in 24 h. Sn–Beta appears to simultaneously activate the carbonyl and hydroxyl groups in the trioses, promoting an intramolecular hydride shift similarly to that observed for MPV reactions catalyzed by Lewis acids [193]. In the presence of water, lactic acid yields of 90% can be obtained, but recycling of the catalyst was proved to be difficult because the lactic acid product carbonizes within the zeolite pores (subsequent reuse requires prior calcination to remove this carbonaceous residue) [164,193]. Sn–Beta can also convert glucose, fructose, and sucrose into alkyl lactates in an alcohol solution in yields ranging from 45 to 60% [206]. These results suggest that Sn–Beta is also active in breaking the hexose into two trioses by way of retro-aldol condensation reactions prior to isomerizing these fragments into the final lactate product.

1-4 Outline of this thesis

The use of solid acids enables the development of environmentally sustainable chemical processes. A number of different types of solid acids have been developed as replacements for homogeneous acids. In this thesis, the synthesis and catalytic activities of carbon solid acids as replacement of H_2SO_4 and water-tolerant solid Lewis acid catalysts was studied. Recently, we have developed carbon solid acid as the novel solid acid; an amorphous carbon consisting of nanosized carbon sheets with large amounts of SO_3H groups. I investigated the catalytic performance of cellulose-derived catalysts in the hydrolysis of cellulose. New type of carbon solid acid was prepared from polyvinyl chloride to improve the catalytic activity in the hydrolysis of cellobiose. I prepared SO_3H-bearing mesoporous carbon by using mesoporous RF resin as a starting material, and examined catalytic performance for hydrophobic reactions, such as α-methylstyrene dimerization. I studied Ta_2O_5 as a water-tolerant Lewis acid catalyst and applied Ta_2O_5 to the production of lactic acid from DHA in water.

Chapter 2

SO_3H-bearing amorphous carbon was prepared by partial carbonization of cellulose followed by sulfonation. The catalytic activity was examined by the acid-catalyzed hydrolysis of β-1,4 glucan, including cellobiose and crystalline cellulose.

Chapter 3

The catalytic performance of various acid catalysts was investigated through the hydrolysis of cellulose into saccharides. The high catalytic performance related to structure of the SO_3H-bearing amorphous carbon was studied.

Chapter 4

Sulfonated amorphous carbon prepared from polyvinyl chloride (PVC) has been studied as a solid acid catalyst. The difference in the structural property and the catalytic activity for the hydrolysis of cellulose between the solid acids prepared from PVC and cellulose were clarified.

Chapter 5

A SO_3H-bearing mesoporous carbon material was prepared by carbonization of resorcinol-formaldehyde resin, followed by sulfonation. The catalytic performance of this carbon solid acid was demonstrated through dimerization of α-methylstyrene (AMS), as the acid-catalyzed reaction using hydrophobic reactants.

Appendix 1

Lewis acidity of Ta_2O_5 in the presence of water was studied. Catalytic performance was examined for lactic acid production from aqueous DHA solution. In addition, H_3PO_4 treatment of Ta_2O_5 was attempted to improve the catalytic performance of the samples.

References

[1] R.A. Sheldon, I. Arends, U. Hanefeld, *Green Chemistry and Catalysis*, Wiley-VCH, Weinheim, **2007**.

[2] K. Tanabe, W.F. Hölderich, *Appl. Catal. A: Gen.* **181** (1999) 399-434.

[3] A. Corma, *Current Opinion in Solid State & Mater. Sci.* **2** (1) 1997, 63-75.

[4] R.A. Sheldon, H. van Bekkun (Eds.), *Fine Chemicals through Heterogeneous Catalysis*, Wiley-VCH, Weiheim, **2001**.

[5] W.F. Hölderich, *Catal. Today* **62** (2000) 115-130.

[6] A. Corma, H. Garcia, *Chem. Rev.* **103** (2003) 4307-.4365

[7] R.A. Sheldon, R.S. Downing, *Appl. Catal. A: Gen.* **189** (1999) 163-183.

[8] A. Mitsutani, *Catal. Today* **73** (2002) 57-63.

[9] A. Corma, *J. Catal.* **216** (2003) 298-312.

[10] A. Corma, *Chem. Rev.* **95** (1995) 559-614.

[11] A. Vaccari, *Catal. Today* **41** (1998) 53-71.

[12] A. Vaccari, *Appl. Clay Sci.* **14** (1999) 161-198.

[13] I.V. Kozhevnikov, *Chem. Rev.* **98** (1998) 171-198

[14] T. Okuhara, *Chem. Rev.* **102** (2002) 3641-3666.

[15] M.A. Harmar, Q. Sun, *Appl. Catal. A: Gen.* **221** (2001) 45-62.

[16] G. Gelbard, *Ind. Eng. Chem. Res.* **44** (2005) 8468-8498.

[17] H. Ichitani, M. Kitamura, *Catal. Today* **73** (2002) 23-28.

[18] H. Ichitani, H. Sato, *Appl. Catal. A: General* **221** (2001) 359-366.

[19] P. Roffia, G. Leofanti, A. Cesana, M. Mantegazza, M. Padovan, G. Petrini, S. Tonti, P. Gervasutti, *Stud. Surf. Sci. Catal.* **55** (1990) 43-50.

[20] G.W. Huber, S. Iborra, A. Corma, *Chem. Rev.* **106** (2006) 4044-4098.

[21] Y. Román-Leshkov, M.E. Davis, *ACS Catal.* **1** (2011) 4566-1580.

[22] O. Sieskind, P. Albrecht, *Tetrahedron Lett.* **34** (1993) 1197-1200.

[23] A. Cornelis, P. Laszlo, *Synlett.* **3** (1994) 155-161.

[24] J.H. Clark, A.P. Kybett, D.J. Macquarrie, S.J. Barlow, *J. Chem. Soc., Chem. Commun.* **1989**, 1353-1354.

[25] S.J. Barlow, T.W. Bastock, J.H. Clark, S.R. Cullen, *J. Chem. Soc., Perkin Trans.* **2** (1994) 411-414.

[26] T.J. Pinnavaia, *Science* **220** (1983) 365-371.

[27] F. Figueras, *Catal. Rev. Sci. Eng.* **30** (1988) 457-499.

[28] J. Sterte, *Catal. Today* **2** (1988) 219-231.

[29] S.L. Suib, *Chem. Rev.* **93** (1993) 803-826.

[30] W.D. Haag, *Stud. Surf. Sci. Catal.* **84** (1994) 1375-1394.

[31] D. Barthomeuf, *Mater. Chem. Phys.* **17** (1987) 49-71.

[32] L.A. Pine, P.J. Maher, W.A. Wachter, *J. Catal.* **85** (1984) 466-476.

[33] H. Ichihashi, M. Ishida, A. Shiga, M. Kitamura, T. Suzuki, K. Suenobu, K. Sugita, *Catal. Surveys Asia* **7** (2003) 261-270.

[34] H. Ichihashi, H. Sato, *Appl. Catal. A: Gen.* **221** (2001) 359-366.

[35] H. Ichihashi, M. Kitamura, *Catal. Today* **73** (2002) 23-28.

[36] H. Sato, *Catal. Rev. Sci. Eng.* **39** (1997) 395-424.

[37] G. Dahlhoff, J.P.M. Niederer, W.F. Hölderich, *Catal. Rev.* **43** (2001) 381-441.

[38] G.P. Heitmann, G. Dahlhoff, W.F. Hölderich, *J. Catal.* **186** (1999) 12-19

[39] H. Ishida, *Catal. Surv. Jpn.* **1** (1997) 241-245.

[40] H. Ishida, Y. Fukuoka, O. Mitsui, M. Kono, *Stud. Surf. Sci. Catal.* **83** (1994) 473-480.

[41] P.B. Venuto, *Microporous Mater.* **2** (1994) 297-411.

[42] G. A. Tsigdinos, *Top. Curr. Chem.* **76** (1978) 1-64.

[43] M. T. Pope, A. Muller, *Angew. Chem., Int. Ed. Engl.* **30** (1991) 34-38.

[44] M. T. Pope, *Heteropoly and Isopoly Oxometalates*; Springer: Berlin, **1983**.

[45] G. M. Maksimov, *Russ. Chem. Rev.* **64** (1995) 445-461.

[46] P. Souchay, *Polyanions et Polycations*; Gauthier-Villars: Paris, **1963**.

[47] P. Souchay, *Ions Mineraux Condenses*; Masson: Paris, **1969**.

[48] T. J. R. Weakley, *Structure and Bonding* **18** (1974) 131-176.

[49] J. F. Keggin, *Proc. R., Soc. Lond. A* **144** (1934) 75-100.

[50] Y. Izumi, R. Hasebe, K. Urabe, *J. Catal.* **84** (1983) 402-409 .

[51] Y. Izumi, K. Urabe, *Chem. Lett.* **1981** 663-666.

[52] M. A. Schwegler, H. van Bekkum, N. A. de Munck, *Appl. Catal.* **74** (1991) 191-204.

[53] T. Baba, Y. Ono, *Appl. Catal.* **22** (1986) 321-324.

[54] S. Tatemastu, T. Hibi, T. Okuhara, M. Misono, *Chem. Lett.* **1984** 865-868.

[55] T. Okuhara, H. Watanabe, T. Nishimura, K. Inumaru, M. Misono, *Chem. Mater.* **12** (2000) 2230-2238.

[56] T. Okuhara, M. Kimura, T. Nakato, *Appl. Catal. A: Gen.* **155** (1997) L9-L13.

[57] M. Kimura, T. Nakato, T. Okuhara, *Appl. Catal. A: Gen.* **165** (1997) 227-240.

[58] T. Okuhara, *Catal. Today* **73** (2002) 153-165.

[59] T. Okuhara, *Appl. Catal.* **222** (2002) 63-77.

[60] T. Okuhara, M. Kimura, T. Nakato, *Chem. Lett.* **1997**, 839-840.

[61] N. Horita, M. Yoshimune, Y. Kamiya, T. Okuhara, *Chem. Lett.* **2005**, 1376-1377.

[62] Z. Chen, T. Izuka, K. Tanabe, *Chem. Lett.* **1984**, 1085-1088.

[63] T. Iizuka, K. Ogasawara, K. Tanabe, *Bull. Chem. Soc. Jpn.* **56** (1983) 2927-2931.

[64] K. Hanaoka, T. Takeuchi, T. Matsuzaki, Y. Sugi, *Catal. Today* **8** (1990) 123-132.

[65] K. Hanaoka, T. Takeuchi, T. Matsuzaki, Y. Sugi, *Catal. Lett.* **5** (1990) 13-16.

[66] K. Ogasawara, T. Iizuka, K. Tanabe, *Chem. Lett.* **1984**, 645-648.

[67] O. Okazaki, H. Harada, *Chem. Lett.* **1988**, 1313-1316.

[68] T. Ushikubo, K. Wada, *Appl. Catal.* **67** (1990) 25-38.

[69] S.D. Jackson, J.S.J. Hargreaves (Eds.), *Metal Oxide Catalysis*, Wiley-VCH, Weiheim, **2009**.

[70] L. Li, Y. Yoshinaga, T. Okuhara, *Phys. Chem. Chem. Phys.* **1** (1999) 4913-4918.

[71] H. Momose, K. Kusumoto, Y. Izumi, Y. Mizutani, *J. Catal.* **77** (1982) 554-557.

[72] M. Hino, S. Takasaki, S. Furuta, H. Matsuhashi, K. Arata, *Catal. Commun.* **7** (2006) 162-165.

[73] M. Hino, S. Takasaki, S. Furuta, H. Matsuhashi, K. Arata, *Appl. Catal. A; Gen.* **321** (2007) 147-154.

[74] K. Arata, *Appl. Catal. A: Gen.* **29** (2004) 187-191.

[75] K. Arata, *Adv. Catal.*, **37** (1990) 165-211.

[76] B.M. Reddy, M.K. Patil, *Chem. Rev.*, **109** (2009) 2185-2208.

[77] X. Song, A. Sayari, *Catal. Rev. Sci. Eng.*, **38** (1996) 329-412.

[78] K. Arata, *Green Chem.*, **11** (2009) 1719-1728.

[79] M. Hino, M. Kurashige, H. Matsuhashi, K. Arata, *Thermochim. Acta*, **441** (2006) 35-41.

[80] K. Segawa, N. Kihara, H. Yamamoto, *J. Mol. Catal.* **74** (1992) 213-221.

[81] T. Armaroli, G. Busca, C. Carlini, M. Giuttari, A.M.R. Galletti, G. Sbrana, *J. Mol. Catal.* **151** (2000) 233-243.

[82] M.A. Harmer, Q. Sun, *Appl. Catal. A: Gen.* **221** (2001) 45-62.

[83] M.A. Harmer, Q. Sun, W.E. Farneth, *J. Am. Chem. Soc.* **118** (1996) 7708-7715.

[84] A. Chakrabarti, M.M. Sharma, *React.Polym.* **20** (1993) 1-45.

[85] G.A. Olah., P.S. Lyer, G.K.S. Prakasn, *Synthesis* **1986**, 513-531.

[86] H.J. Panneman, A.A.C.M. Beenackers, *Ind. Eng. Chem. Res.* **34** (1995) 4318-4325.

[87] M.M. Sharma, *React. Funct. Polym.* **26** (1995) 3-23.

[88] A. Chakrabarti, M.M. Sharma, *React. Funct. Polym.* **20** (1993) 1-45.

[89] M.A. Harmer, Q. Sun, A.J. Vega, W.E. Farneth, A. Heidekum, W.F. Hoelderoch, *Green Chem.* 2 (2000) 7-14.

[90] W. F. Hoelderich, *Stud. Surf. Sci. Catal.* **75** (1993) 127-163.

[91] K. Okuyama, X. Chen, K. Takata, D. Odawara, T. Suzuki, S. Nakata, T. Okuhara, *Appl. Catal. A: Gen.* **190** (2000) 253-260.

[92] Z. Hou, T. Okuhara, *Appl. Catal. A: Gen.* **216** (2001) 147-155.

[93] P. Judenstein, C. Sanchez, *J. Mater. Chem.* **6** (1996) 511-52

[94] U. Schubert, N. Hüsing, A. Lorenz, *Chem. Mater.* **7** (1995) 2010-2027.

[95] K. Moller, T. Bein, *Chem. Mater.* **10** (1998) 2950-2963.

[96] J.H. Clark, D. Macquarrie, *Chem. Soc. Rev.* **1996**, 303-310.

[97] C.T. Kresge, M.E. Leonowicz, W.J. Roth, J.C. Varturi, J.S. Beck, *Nature* **359** (1992) 710-712.

[98] J.S. Beck, J.C. Varturi, W.J. Roth, M.E. Leonowicz, C.T. Kresge, K.D. Schmitt, C.T. Chu, D.H. Olson, E.W. Sheppard, S.B. McCullen, J.B. Higgins, J.L. Schlenker, *J.Am. Chem. Soc.* **114** (1992) 10834-10843.

[99] A. Corma, *Chem. Rev.* **97** (1997) 2373-2419.

[100] A.Corma, *Top. Catal.* **4** (1997) 249-260.

[101] J.S. Beck, J.C. Varturi, *Current opinion in solid state & Material Science* **1** (1996) 79-87.

[102] N.K. Raman, M.T. Anderson, C.J. Brinker, *Chem. Mater.* **8** (1996) 1682-1701.

[103] U. Cieala, F. Schüth, *Microporous Mesoporous Mater.* **27** (1999) 131-149.

[104] W.M.V. Rhijn, D.E. DeVos, B.F. Sels, W.D. Bossaert, P.A. Jacobs, *Chem. Commun.* **1998**, 317-318.

[105] W.M.V. Rhijn, D.E. DeVos, W.D. Bossaert, J. Bullen, B. Wouters, P. Grobet, P.A. Jacobs, *Stud. Surf. Sci. Catal.* **117** (1998) 183-190.

[106] M.H. Lim, C.F. Blanford, A. Stein, *Chem. Mater.* **10** (1998) 467-470.

[107] L. Mersier, T.J. Pinnavais, *Adv. Mater.* **9** (1997) 500-503

[108] L. Mersier, T.J. Pinnavais, *Environ. Sci. Technol.* **32** (1998) 2749-2754.

[109] S.L. Burkett, S.D. Sims, S. Mann, *Chem. Commun.* **1996**, 1367-1368.

[110] D. Macquarrie, *Chem. Commun.* **1996**, 1961-1962.

[111] C.E. Fowler, S.L. Burkett, S. Mann, *Chem. Commun.* **1997**, 1769-1770.

[112] R. Richer, L. Mercier, *Chem. Commun.* **1998**, 1775-1776.

[113] A. Sayari, S. Hamoudi, *Chem. Mater.* **13** (2001) 3151-3168.

[114] D.W. Bossaert, D.E. De Vos, W.M.V. Rhijn, J. Bullen, P.J. Grobet, P.A. Jacobs, *J. Catal.* **182** (1999) 156-164.

[115] I. Diaz, C. Marquez-Alvarez, F. Mohino, J. Perez-Pariente, E. Sastre, *J. Catal.* **193** (2000) 295-302.

[116] D. Das, J.F. Lee, S. Cheng, *Chem. Commun* **2001**, 2178-2179.

[117] M. Hara, T. Yoshida, A. Takagaki, T. Takata, J.N. Kondo, S. Hayashi, K. Domen, *Angew. Chem. Int. Ed.* **43** (2004) 2955-2958.

[118] M. Toda, A. Takagaki, M. Okamura, J.N. Kondo, S. Hayashi, K. Domen, M. Hara, *Nature* **438** (2005) 178.

[119] A. Takagaki, M. Toda, M. Okamura, J.N. Kondo, K. Domen, S. Hayashi, M. Hara, *Catal. Today* **116** (2006) 157-161.

[120] M. Okamura, A. Takagaki, M. Toda, J.N. Kondo, T. Tatsumi, K. Domen, M. Hara, S. Hayashi, *Chem. Mater.* **18** (2006) 3039-3045.

[121] K. Nakajima, M. Okamura, J.N. Kondo, K. Domen, T. Tatsumi, S. Hayashi, M. Hara, *Chem. Mater.* **21** (2009) 186-193.

[122] V.L. Budarin, J.H. Clark, R. Luque, D.J. Macquarrie *Chem.Commun.* **2007**, 634-636.

[123] K. Milkowski, J.H. Clark, S. Doi, *Green Chem.* **6** (2004) 189-190.

[124] V. Budarin, J.H. Clark, F.E.I. Deswarte, J.J.E.Hardy, A.J. Hunt, F.M. Kerton, *Chem.Commun.* **2005**, 2903-2905.

[125] X. Wang, R. Liu, M.M. Waje, Z. Chen, Y. Yan, K.N. Bozhilov, P. Feng, *Chem. Mater.* **19** (2007) 2395-2397.

[126] H. Yamamoto, Ed.; *Lewis Acids in Organic Synthesis*, Wiley-VCH: Weiheim, **2000**.

[127] R.D. Howells, J.C. McCown, *Chem. Rev.* **77** (1977) 69-92.

[128] S. Kobayashi, *Chem. Lett.* **1991**, 2187-2190.

[129] S. Kobayashi, K. Manabe, *Acc. Chem. Res.* **35** (2002) 209-217.

[130] S. Kobayashi, M. Sugiura, H. Kitagawa, W.W.L. Lam, *Chem. Rev.* **102** (2002) 2227-2302.

[131] S. Kobayashi, *Synlett* **1994**, 689-701.

[132] S. Kobayashi, M. Araki, H. Ishitani, S. Nagayama, I. Hachiya, *Synlett* **1995**, 233-234.

[133] S. Kobayashi, H. Ishitani, S. Nagayama, *Chem. Lett.* **1995**, 423-424.

[134] S. Kobayashi, H. Ishitani, S. Nagayama, *Synyhesis*, **1995**, 1190-1194.

[135] S. Kobayashi, T. Wakabayashi, *Tetrahedron Lett.* **39** (1998) 5389-5392.

[136] S. Kobayashi, S. Nagayama, S. *J. Org. Chem.* **61** (1996) 2256-2257.

[137] M. Manabe, Y. Mori, T. Wakabayashi, S. Nagayama, S. Kobayashi, *J. Am. Chem. Soc.* **122** (2000) 7202-7207.

[138] M. Taramasso, G. Perego, B. Notari, US Patent 4,410,501; 1983.

[139] C. Perego, A. Carati, P. Ingallina, M.A. Mantegazza, G. Bellussi, *Appl. Catal., A: Gen.* **221** (2001) 63-72.

[140] B. Notari, *Catal. Today* **18** (1993) 163-172.

[141] R.A. Sheldon, M. Wallau, I.W.C.E. Arends, U. Schuchardt, *Acc. Chem. Res.* **31** (1998) 485-493.

[142] D.R.C. Huybrechts, L.D. Bruycker, P. A. Jacobs, *Nature* **345** (1990) 240-242.

[143] N.K. Mal, A.V. Ramaswamy, *Chem. Commun.* **1997**, 425-426.

[144] Y. Zhu, G. Chuah, S. Jaenicke, *J. Catal.* **227** (2004) 1-10.

[145] A. Corma, F.X. Llabrès i Xamena, C. Prestipino, M. Renz, S. Valencia, *J. Phys. Chem. C* **113** (2009)

11306-11315.

[146] A. Corma, M.T. Navarro, L. Nemeth, M. Renz, *Chem. Commun.* **2001**, 2190-2191.

[147] A. Corma, M.T. Navarro, M. Renz, *J. Catal.* **219** (2003) 242-246.

[148] A. Corma, M. Renz, *Chem. Commun.* **2004**, 550-551.

[149] M. Boronat, P. Concepcion, A. Corma, M. Renz, *Catal. Today* **121** (2007) 39-44.

[150] A. Corma, M.E. Domine, S. Valencia, *J. Catal.* **215** (2003) 294-304.

[151] M. Renz, T. Blasco, A. Corma, V. Fornes, R. Jensen, L. Nemeth, *Chem. Eur. J.* **8** (2002) 4708-4717.

[152] M. Moliner, Y. Román-Leshkov, M.E. Davis, *Proc. Nat. Acad. Sci.* **107** (2010) 6164-6168.

[153] Y. Román-Leshk, M. Moliner, J.A. Labinger, M.E. Davis, *Angew. Chem., Int. Ed.* **49** (2010) 8954-8957.

[154] F.W. Linchtenthaler, *Carbohydr. Res.* **313** (1998) 69-89.

[155] H. Danner, R. Braun, *Chem. Soc. Rev.* **28** (1999) 395-405.

[156] A. Corma, S. Iborra, A. Velty, *Chem. Rev.* **107** (2007) 2411-2502.

[157] C. H. Christensen, J. Rass-Hansen, C. C. Marsden,E. Taarning, K. Egeblad, *ChemSusChem* **1** (2008) 283-289.

[158] J.N. Chheda, G.W. Huber, J.A. Dumesic, *Angew. Chem. Int. Ed.* **46** (2007) 7164-7183.

[159] O. Bobleter in *Polysaccharides*, 2nd ed. (Ed.: S. Dumitriu), Marcel Dekker, New York, **2005**, pp. 893-937.

[160] A. Takagaki, C. Tagusagawa, K. Domen, *Chem. Commun.* **2008**, 5363-5365.

[161] K. Shimizu, H. Furukawa, N. Kobayashi, Y. Itaya, A. Satsuma, *Green Chem.* **11** (2009) 1627-1632.

[162] S. Van de Vyver, L. Peng, J. Geboers, H. Schepers, F. de Clippel, C. J. Gommes, B. Goderis, P. A. Jacobs, B. F. Sels, *Green Chem.* **12** (2010) 1560-1563.

[163] A. Takagaki, N. Nishimura, S. Nichimura, K.Ebitani, *Catal. Lett.* **40** (2011) 1195-1197.

[164] Y. Román-Leshkov, M.E. Davis, *ACS Catal.* **1** (2011) 1566-1580.

[165] B. Kamm, M. Kamm,M. Schmidt, T. Hirth, M. Schulze, in: B. Kamm, P.R. Gruber, M. Kamm (Eds.), *Biorefineries: Industrial Processes and Products*, 2, Wiley, Weinheim, Germany, **2006**, pp. 97–149.

[166] J. Lewkowski, *Arkivoc* **1** (2001) 17–54.

[167] X. Tong, Y. Ma, Y. Li, *Appl. Catal. A: Gen.* **385** (2010) 1-13.

[168] X. Qi, M. Watanabe, T.M. Aida, R.L. Smith Jr., *Green Chem.* **10** (2008) 799–805.

[169] X. Qi, M. Watanabe, T.M. Aida, R.L. Smith Jr., *Ind. Eng. Chem. Res.* **47** (2008) 9234–9239.

[170] C. Moreau, R. Durand, S. Razigade, J. Duhamet, P. Faugeras, P. Rivalier, P. Ros, G. Avignon, *Appl. Catal. A: Gen.* **145** (1996) 211–224.

[171] M. Watanabe, Y. Aizawa, T. Iida, R. Nishimura, H. Inomata, *Appl. Catal. A: Gen.* **295** (2005) 150–156.

[172] C. Carlini, M. Giuttari, A.M. Raspolli Galletti, G. Sbrana, T. Armaroli, G. Busca, *Appl. Catal. A: Gen.* **183** (1999) 295–302.

[173] P. Carniti, A. Gervasini, S. Biella, A. Auroux, *Catal. Today* **118** (2006) 373–378.

[174] C. Carlini, P. Patrono, A.M.R. Galletti, G. Sbrana, *Appl. Catal. A: Gen.* **275** (2004) 111–118.

[175] F. Benvenuti, C. Carlini, P. Patrono, A.M. Raspolli Galletti, G. Sbrana, M.A. Massucci, P. Galli, *Appl. Catal. A: Gen.* **193** (2000) 147–153.

[176] L. Cottier, G. Descotes, *Trends Heterocycl. Chem.* **2** (1991) 233-248.

[177] Takagaki, A.; Ohara, M.; Nishimura, S.; Ebitani, K. *Chem. Commun.* **2009**, 6276-6278.

[178] Ohara, M.; Takagaki, A.; Nishimura, S.; Ebitani, K. *Appl. Catal., A: Gen.* **383** (2010) 149-155.

[179] Nikolla, E.; Román-Leshkov, Y.; Moliner, M.; Davis, M. E. *ACS Catal.* **2011**, 408-410.

[180] K.J.Zeitsch, *The Chemistry and Technology of Furfural and Its Many By-Products*, first ed., sugar series, vol. 13, Elsevier, Amsterdam, **2000**.

[181] Y.L. Zhu, H.W. Xiang, Y.W. Li, H. Jiao, G.S. Wu, B. Zhong, G.Q. Guo, New J. Chem. **27** (2003) 208-210.

[182] A. Gandini, M.N. Belgacem, *Prog. Polym. Sci.* **22** (1997) 1203-1379.

[183] C. Moreau, R. Durand, D. Peyron, J. Duhamet, P. Rivalier, *Ind. Crops Prod.* **7** (1998) 95-99.

[184] A.S. Dias, M. Pillinger, A.A. Valente *Appl. Catal. A: Gen.* **285** (2005) 126-131.

[185] A.S. Dias, M. Pillinger, A.A. Valente *J. Catal.* **229** (2005) 414-423.

[186] A.S. Dias, S. Lima, P. Brandao, M. Pillinger, J. Ocha, A.A. Valente *Catal. Lett.* **108** (2006) 179-186.

[187] T. Ooi, T. Miura, K. Maruoka, *Angew. Chem., Int. Ed.* **37** (1998) 2347-2349.

[188] Datta, R. Henry, M. *J. Chem. Technol. Biotechnol.* **81**(2006) 1119-1129.

[189] A. Takasu, Y. Narukawa, T. Hirabayashi, *J. Polym. Sci., Part A:Polym. Chem.* **44** (2006) 5247-5253.

[190] K.L. Wasewar, A.A. Yawalkar, J.A. Moulijn, V.G. Pangarkar, *Ind. Eng. Chem. Res.* **43** (2004) 5969-5982.

[191] L. Kong, G.Li, H. Wang, W. He, F. Ling *J. Chem. Technol. Biotechnol.* **83** (2008) 383-388.

[192] M. Bicker, S. Endres, L. Ott, H. Vogel *J. Mol. Catal. A: Chem.***239** (2005) 151-157.

[193] E. Taarning, S. Saravanamurugan, M. Spangsberg Holm, J. Xiong, R.M.West, C.H. Christensen, *ChemSusChem* **2** (2009) 625-627.

[194] H. Kimura, K. Tsuto, T. Wakisaka, Y. Kazumi, Y. Inaya, *Appl. Catal., A: Gen.* **96** (1993) 217-228.

[195] R. Ciriminna, G. Palmisano, C.D. Pina, M. Rossi, M. Pagliaro, *Tetrahedron Lett.* 47 (2006) 6993-6995.

[196] S. Demirel, K. Lehnert, M. Lucas, P. Claus, *Appl. Catal., B: environ.* **70** (2007) 637-643.

[197] R.M. Painter, D.M. Pearson, R.M. Waymouth, *Angew. Chem., Int. Ed.* **49** (2010) 9456-9459.

[198] C. Gätgens, U. Degner, S. Bringer-Meyer, U. Herrmann, *Appl. Microbiol. Biotechnol.* **76** (2007) 553-559.

[199] J. Eriksen, O. Mønsted, L. Mønsted, *Transition Met. Chem.* **23** (1998) 783-787.

[200] J.E. Bang, L. Monsted, O. Monsted, *Acta Chem. Scand.* **48** (1994) 12-19.

[201] C. Rasrendra, I. Makertihartha, S. Adisasmito, H. Heeres, *Top. Catal.* **53** (2010) 1241-1247.

[202] C.B. Rasrendra, B.A. Fachri, I.G.B.N. Makertihartha, S. Adisasmito, H.J. Heeres, *ChemSusChem* **4** (2011) 768-777.

[203] R.M. West, M.S. Holm, S. Saravanamurugan, J. Xiong, Z. Beversdorf, E. Taarning, C.H. Christensen, *J. Catal.* **269** (2010) 122-130.

[204] P.P. Pescarmona, K.P.F. Janssen, C. Delaet, C. Stroobants, K. Houthoofd, A. Philippaerts, C. De Jonghe, J.S. Paul, P. A. Jacobs, B.F. Sels, *Green Chem.* **12** (2010) 1083-1089.

[205] E. Taarning, S. Saravanamurugan, M.S. Holm, J. Xiong, R.M. West, C.H. Christensen, *ChemSusChem* **2** (2009) 625-627.

[206] M.S. Holm, S. Saravanamurugan, E. Taarning, *Science* **328** (2010) 602-605.

Chapter 2

Synthesis and Acid Catalysis of Cellulose-derived Carbon-based Solid Acid

2-1 Abstract

SO_3H-bearing amorphous carbon, prepared by partial carbonization of cellulose followed by sulfonation in fuming H_2SO_4, was applied as a solid catalyst for the acid-catalyzed hydrolysis of β-1,4 glucan, including cellobiose and crystalline cellulose. Structural analyses revealed that the resulting carbon material consists of graphene sheets with 1.5 mmol g^{-1} of SO_3H groups, 0.4 mmol g^{-1} of COOH, and 5.6 mmol g^{-1} of phenolic OH groups. The carbon catalyst showed high catalytic activity for the hydrolysis of β-1,4 glycosidic bonds in both cellobiose and crystalline cellulose. Pure crystalline cellulose was not hydrolyzed by conventional strong solid Brønsted acid catalysts such as niobic acid, Nafion® NR-50, and Amberlyst-15, whereas the carbon catalyst efficiently hydrolyzes cellulose into water-soluble saccharides. The catalytic performance of the carbon catalyst is due to the large adsorption capacity for hydrophilic reactants and the adsorption ability of β-1,4 glucan, which is not adsorbed to other solid acids.

2-2 Introduction

Sulfuric acid is one of the most popular acid catalysts for practical chemical processes and is widely used in the production of industrially important chemicals. Such homogeneous acids generally require special processing in the form of neutralization, which involves energy-inefficient catalyst separation from products and results in the formation of a large amount of sulfate wastes [1-4]. The development of environmentally sustainable chemical processes has stimulated the use of solid acid catalysts, because solid acids can be easily separated from the reaction matrix by simple filtration or decantation for repeated use. Replacing conventional homogeneous acids with heterogeneous counterparts, such as silica-alumina [5], zeolites [6-8], niobic acid [9,10], and strong ion-exchangeable resins [11-13], is a most promising solution to this problem; however, the catalytic activity and stability of these acids are much lower than those of homogeneous acids. Therefore, there has been increasing demand for the development of stable and highly active solid

acid catalysts [14-17].

Recently, we have developed novel solid acid materials referred to as carbon-based solid acids that contain nano-sized graphene sheets (ca. 1.5 nm) with high densities of sulfonic acid groups in the amorphous carbon, which function as efficient and reusable solid acid catalysts for industrially important chemical reactions such as hydration, hydrolysis, and esterification: the catalytic activity of the carbon-based solid acids in these reactions is comparable to that of sulfuric acid [18-22]. These catalysts can be prepared by incomplete carbonization of sulfopolycyclic aromatic hydrocarbons [18] or sulfonation of incompletely carbonized natural organic materials containing D-glucose units [19-22]. These D-glucose-derived carbon-based solid acids can incorporate large amounts of hydrophilic molecules, including water, into the carbon bulk, due to the presence of hydrophilic functional groups such as -SO_3H, -COOH, and phenolic -OH groups on the flexible carbon sheets [19-21]. In corporation of hydrophilic molecules provides good access by reactants to the SO_3H groups, which gives rise to high catalytic performance, despite the low surface area (ca. 2 m^2 g^{-1}) [18-22]. The conversion of cellulose into useful saccharides is an attractive route to the environmentally benign production of chemicals, including ethanol [23,24]. Sulfuric acid can function as an effective catalyst for the hydrolysis of cellulose into water-soluble saccharides. However, this catalyst requires a special processing in the form of neutralization, involving costly and inefficient catalyst separation. This results in large energy consumption [25-27]. Recently, we found that amorphous carbon bearing -SO_3H, -COOH, and phenolic -OH groups, prepared by sulfonation of partially carbonized cellulose, can catalyze the hydrolysis of cellulose [22]. The particulate catalyst can be readily separated from the aqueous solution containing saccharides, allowing for the repeated reuse without minimum energy consumption. The reaction does not proceed in the tested conventional strong solid Brønsted acid catalysts such as niobic acid, H-mordenite, Nafion NR-50 and Amberlyst-15. While the carbon catalyst can function as an active catalyst for the hydrolysis of cellulose, the details of the structure and acid catalysis of the cellulose-derived carbon catalyst have not yet been cleared. In this study, the structure and acid catalysis of the carbon-based solid acid have been studied through structural analyses and the hydrolysis of cellobiose and cellulose.

2-3 Experimental

Preparation of the carbon-based solid acid

The carbon-based solid acid was prepared by sulfonation of incompletely carbonized cellulose. 500 g of microcrystalline cellulose powder was heated for 1 h at 673 K under N_2 flow to obtain amorphous carbon, which was then ground to a powder. The powder (5 g) was then boiled in 150 mL of fuming sulfuric acid (15 wt% SO_3) at 353-393 K under N_2 flow. After heating for 10 h and then cooling in an ice bath, 1000 mL of distilled water was added to the mixture to form a black precipitate. The precipitate was washed repeatedly in hot distilled water at 373 K until sulfate ions were not detected in the wash water.

Characterization

Structural information for the prepared carbon material was obtained by powder X-ray diffraction (XRD; Ultima IV, RIGAKU), Raman spectroscopy (NRS-3100, JASCO), and ^{13}C cross-polarization (CP) magic angle spinning (MAS) nuclear magnetic resonance (NMR). ^{13}C CP/MAS NMR spectra were measured at room temperature using a Bruker ASX-200 spectrometer at a Lamor frequency of 50.3 MHz. A Bruker MAS probehead was used with a 7mmzirconia rotor. The spinning rate of the sample was 4.0 kHz. The frequency of the spectra is expressed with respect to pure tetramethylsilane. Glycine was used as a second reference material, with a carbonyl signal set at 176.48 ppm. The Brunauer-Emmet-Teller (BET) surface areas and water vapor adsorption isotherms for the samples were measured using a surface area analyzer (NOVA-4200e, QUANTACHROME) and volumetric absorption equipment (AUTOSORB MP/VP, QUANTACHROME), respectively. The amount of functional groups bonded to the carbon-based solid acid was estimated by elemental analysis (vario MICRO cube, ELEMENTAR) and cation-exchange analysis. According to X-ray photoelectron spectroscopic (XPS) analysis, all S atoms in the carbon material, which possesses SO_3H, COOH, and phenolic OH, is expected to be confined to SO_3H groups [19-22]. The densities of SO_3H groups were thus estimated based on the sulfur content determined from sample compositions obtained by elemental analysis. The total SO_3H + COOH and SO_3H + COOH + OH contents were estimated from the exchange of Na^+ in aqueous NaCl and NaOH solutions, respectively, to afford the proportions of each functional group [22].

Hydrolysis of cellobiose

Hydrolysis of cellobiose was carried out at 373 K in cellobiose solution (cellobiose, 0.1 g; water, 10 mol) over 0.2 g of carbon catalyst. Niobic acid (Nb_2O_5•nH_2O, CBMM), Nafion® NR50 (perfluorosulfonated ionomer, Aldrich), and Amberlyst-15 (polystyrene-based cation-exchangeable resin with SO_3H, Aldrich) catalysts (0.2 g) were used for comparison. The liquid phase during reaction was analyzed by liquid chromatography (LC; LC-2000 plus, JASCO).

Hydrolysis of cellulose

The hydrolysis of pure microcrystalline cellulose (Avicel) was typically carried out in a Pyrex reactor (catalyst, 0.300 g; cellulose, 0.025 g; distilled water, 0.700 g) at 373 K. The catalysts tested for hydrolysis of cellulose were sulfuric acid (H_2SO_4; 96%, KANTO Chemicals), niobic acid, Nafion® NR50, Amberlyst-15, and the carbon catalyst. After the reaction, an aliquot of the supernatant solution was decanted and analyzed. The yields of glucose and water-soluble β-1,4 glucan were determined by LC, and the enzymatic hydrolysis of water-soluble β-1,4 glucan using cellulase, respectively. The amount of glucose produced in the collected supernatant solution was estimated by LC. 0.2 g of crude cellulose obtained from Trichoderma viride (Wako Pure Chemical industries) was then added to the collected supernatant solution, and the solution was warmed for 48 h at 313 K in order to hydrolyze the water-soluble β-1,4 glucan in the solution into glucose. After

the enzymatic hydrolysis, glucose produced by hydrolysis of β-1,4 glucan was also analyzed by LC. Cellulose conversion was obtained using the following equations [22].

Cellulose conversion (%) = 100(B + C)/A.

A: total amount (mol) of glucose monomer in cellulose

B: amount (mol) of glucose produced by acid-catalyzed hydrolysis

C: total amount (mol) of glucose monomer in water-soluble β-1,4 glucan produced by acid-hydrolyzed hydrolysis.

2-4 Results and discussion

Characterization of carbon materials

Fig. 2-1 shows XRD patterns and Raman spectra for the carbonized cellulose before and after sulfonation. The XRD patterns in Fig. 2-1(A) exhibit a weak and broad C(002) diffraction peak ($2\theta = 10\text{-}30^{o}$) attributed to amorphous carbon. This indicates that both the carbon precursor and carbon catalyst are composed of aromatic carbon sheets oriented in a considerably random fashion [28]. The Raman spectra (Fig. 2-1(B)) display two broad signals assigned to the D-band (ca. 1400 cm^{-1}, A_{1g} D breathing mode) and G-band (ca. 1590 cm^{-1}, E_{2g} G mode). The intensity ratio of the D- and G-bands for these samples is nearly equal, indicating that there is no significant difference in the average sizes of graphene among these materials. The average size of graphene was estimated to be approximately 1.2 nm [28]. Fig. 2-2 shows ^{13}C CP/MAS NMR spectra for carbonized cellulose before and after sulfonation. Signals at 130 and 155 ppm with spinning sidebands attributed to polycyclic aromatic carbon atoms and phenolic OH groups are observed in these spectra, indicating that the carbon frameworks of these materials consist mainly of sp^2-derived carbon sheets with phenolic OH groups. The broad signal for aliphatic hydrocarbon moieties (15 ppm) observed for carbonized cellulose in Fig. 2-2(a) disappeared and a weak signal at 180 ppm, assigned to -COOH groups, appears after sulfonation (Fig. 2-2(b)). This suggests that the aliphatic hydrocarbons were decomposed and/or carbonized by the strong oxidative and dehydrating properties of fuming H_2SO_4 when heated. The formation of -COOH groups in the carbon catalyst can probably be attributed to the partial oxidation of graphene sheets by H_2SO_4. The peak due to aromatic carbon bonded to the SO_3H group (Ar-SO_3H, ca. 140 ppm) is not observed in the spectrum (Fig. 2-2(b)), because broad peaks due to aromatic carbon atoms (130 ppm) and phenolic OH groups (155 ppm) completely obscure the peak. The introduction of sulfonic acid groups was directly confirmed by XPS analysis. The XPS spectra for carbon materials after sulfonation exhibit a single S2p peak attributable to SO_3H groups. Fig. 2-3 shows S2p XPS spectra for carbonized cellulose before and after sulfonation. Although no signal is observed in the spectrum for carbonized cellulose (Fig. 2-3(a)), a single peak at 168 eV assigned to the SO_3H groups is clearly observed in the spectrum for sulfonated carbon, indicating that sulfonation of amorphous carbon was successfully achieved in fuming H_2SO_4 to form sulfonic acid groups, and all sulfur in the carbon catalyst is contained in the SO_3H groups. From the elemental analysis and cation-exchange experiments, the amounts of SO_3H, COOH, and phenolic OH groups bonded to the graphene were estimated to be 1.5, 0.4, and 5.4 mmol g^{-1},

respectively [22]. The proposed carbon structure is schematically illustrated in Fig. 2-4. The prepared material is amorphous carbon consisting of SO_3H-, COOH-, and phenolic OH bearing graphene sheets in a considerably random fashion. The carbon catalyst possesses a high density of almost neutral phenolic OH groups in addition to Brønsted acid sites (SO_3H and COOH), which is distinct from conventional solid acids that have single functional groups, such as sulfonated resins.

One of the important features of the carbon catalyst is that it can adsorb large amounts of hydrophilic molecules. A carbon catalyst prepared from D-glucose was reported to have a high density of effective Brønsted acid sites and exhibited high catalytic performance for acid-catalyzed reactions, despite the low surface area (2 m^2 g^{-1}) [19-21]. Fig. 2-5 shows the H_2O vapor adsorption-desorption isotherm of the carbon catalyst at 298 K. Although the carbon catalyst prepared from cellulose also has a low surface area (2-3 m^2 g^{-1}), the amount of adsorbed H_2O at 1.5 kPa is much smaller than that at saturated water vapor pressure (ca. 3 kPa) exceeds 0.01 mol g^{-1}. Assuming that the adsorption cross sectional area of H_2O is 0.125 nm^2, the effective surface area of the carbon catalyst is estimated to exceed over 560 m^2 g^{-1}, which means that the carbon catalyst can incorporate large amounts of water into the carbon bulk, due to the high density of hydrophilic functional groups bound to the flexible nanographene sheets. This provides good access by reactants in solution to the SO_3H groups in the carbon material, resulting in high catalytic performance, despite the low surface area [22].

Hydrolysis of cellobiose by solid acid catalysts

Fig. 2-6 shows time courses for D-glucose formation from cellobiose over the carbon catalyst. For comparison, the results for Nafion® resin (NR50), Amberlyst-15, and niobic acid are included. Nafion® NR50 and Amberlyst-15 are polymer-based strong solid acids with high densities of SO_3H, and very high activity for a variety of reactions [11-13]. Niobic acid is a typical inorganic oxide strong solid acid that is widely used in industrial acid-catalyzed reactions [9,10]. Although the catalytic activity of niobic acid is moderate, the SO_3Hbearing solid acid catalysts exhibit high catalytic activity for this reaction. The catalytic activity for the carbon catalyst is approximately twice as high as those of Amberlyst-15 and Nafion NR-50. Therefore, the difference in the catalytic properties of sulfonic acid-bearing catalysts for this reaction can be adequately explained as not being due to acid amount or acid strength. Catalysis over the carbon catalyst with SO_3H, COOH, and phenolic OH was thus further investigated by examining the adsorption of cellobiose on each of the solid acid catalysts used in this study [29]. 0.1 g of each solid acid was added to 2 cm^3 (cellobiose, 3 mol) of aqueous cellobiose solution (1.5 mmol L^{-1}) and then stirred at room temperature. Cellobiose was not hydrolyzed into glucose at room temperature under the experimental conditions, and the amount of adsorbed cellobiose was estimated by LC of the supernatant solution. The conventional solid acids, such as Nafion, and Amberlyst-15, did not adsorb cellobiose in water even after stirring for 24 h, whereas the carbon catalyst adsorbed 24% of the cellobiose in just 3 h. Cellobiose adsorption reached a plateau at 5 h, with adsorption of 26% (0.8 mol) of the cellobiose dissolved in the solution, which suggests that the carbon material has a stronger affinity for β-1,4 glucan than the other solid acids. It should be pointed out that the carbon

catalyst cannot adsorb D-glucose at all, suggesting that the glycosidic bond in β-1,4 glucan participates in adsorption on the carbon catalyst. The ability to adsorb β-1,4 glucan may be attributed to the phenolic OH groups bonded to the graphene sheets. In the cellobiose adsorption experiment for the COOH-containing (Amberlite IRC-50 (Aldrich)) and SO_3H-containing (Amberlyst-15) resins, cellobiose was not adsorbed to the resins, indicating that these functional groups do not adsorb cellobiose. With regard to the stronger affinity for β-1,4 glucan, the large surface area of the carbon catalyst in a water medium can enhance the incorporation of cellobiose, providing good access by reactants to the SO_3H groups in the carbon material and resulting in high catalytic activity.

The results for the carbon catalyst reusability experiment are shown in Fig. 2-7. Judging from statistics, the experimental error in glucose yield was estimated to be 3% yield [30]. As a result, there is no significant difference in activity among the catalyst reuse experiments. In addition, no decrease in activity and SO_3H density is observed even after 4 reuses for the hydrolysis of cellobiose by the carbon material [29]. These results indicate that SO_3H groups are tightly bonded to the graphene sheets, and thus the carbon catalyst can function as a stable and highly active solid acid for the hydrolysis of β-1,4 glycosidic bond.

Hydrolysis of cellulose by solid acid catalysts

The performance of various acid catalysts and sulfuric acid for the hydrolysis of pure microcrystalline cellulose powder was examined at 373 K; the time courses of cellulose conversion are shown in Fig. 2-8. Cellulose could not be hydrolyzed into glucose or water-soluble β-1,4 glucan using conventional solid acid catalysts such as niobic acid, Amberlyst-15, and Nafion® NR-50. However, the carbon catalyst exhibited remarkable performance for the hydrolysis reaction, with catalytic activity comparable to that of sulfuric acid. All cellulose was converted into water-soluble saccharides over the carbon catalyst within 6 h, and the catalyst could be readily separated by decantation from the solution containing dissolved saccharides after the reaction. Fig. 2-9 shows the product distribution for the reaction, as determined by LC. While the conventional solid strong Brønsted acids of niobic acid, Nafion® NR-50, and Amberlyst-15 did not produce any water-soluble saccharides, the carbon catalyst hydrolyzed cellulose into water-soluble oligosaccharides and D-glucose, as did sulfuric acid. The water-soluble oligosaccharides produced in this reaction were analyzed by matrix-assisted laser desorption/ionization-time-of-flight-mass spectrometry (MALDI-TOF-MS) of the reaction solution after 3 h in the presence of the carbon catalyst. Large signals appeared at m/z = 162 intervals, which is the mass number of the glucose monomer ($-(-O-C_6H_{10}O_4-)_n-$) in - glucan, indicating that the water-soluble hydrolysis product from cellulose was β-1,4 glucan (results not shown). The β-1,4 glucan component was estimated to be $C_6H_{11}O_5-(-O-C_6H_{10}O_4-)_{2\sim10}-O-C_6H_{11}O_5$ by MALDI-TOF-MS. The results indicate that the hydrolysis of cellulose on the carbon material proceeds as well as that on sulfuric acid: H^+ attacks hydrogen and β-1,4 glycosidic bonds in solid crystalline cellulose to form water-soluble β-1,4 glucan, followed by hydrolysis of the β-1,4 glycosidic bonds in β-1,4 glucan to form glucose.

Therefore, efficient conversion of cellulose into glucose using a solid acid catalyst requires strong interaction between the solid acid and β-1,4 glucan (solid cellulose and water-soluble β-1,4 glucan), because the Brønsted acid sites of the solid acid cannot approach the cellulose surface without such interaction. This is distinct from hydrolysis in the homogeneous sulfuric acid system. The SO_3H-bearing carbon material, which is capable of adsorbing β-1,4 glucan, can thus be expected to have much higher activity for hydrolytic catalysis than the other solid acids examined in this study.

2-5 Conclusion

The sulfonation of carbon material prepared by low temperature carbonization of cellulose resulted in a highly active, stable solid acid catalyst as a replacement for sulfuric acid. The carbon catalyst, consisting of polycyclic aromatic carbon with SO-H, COOH, and phenolic OH, was demonstrated to function as a highly active catalyst for the direct hydrolysis of β-1,4 glucan in solid cellulose, despite the low surface area of the catalyst. The high catalytic activity for the reaction can be attributed to the ability to adsorb β-1,4 glucan and the large effective surface area of the catalyst in water.

References and notes

[1] P.T. Anastas, M.M. Kirchhhoff, *Acc. Chem. Res.* **35** (2002) 686.
[2] J.M. DeSimone, *Science* **297** (2002) 799.
[3] B. Harton, *Nature* **400** (1999) 797.
[4] P.T. Anastas, J.B. Zimmermann, *Environ. Sci. Technol.* **37** (2003) 94A.
[5] J.H.D. Boer, W.J. Visseren, *Catal. Rev.* **5** (1972) 55.
[6] S. Namba, N. Hosonuma, T. Yashima, *J. Catal* **72** (1981) 16.
[7] H. Ishida, *Catal. Surv. Jpn.* **1** (1997) 241.
[8] K. Eguchi, T. Tokiai, H. Arai, *Appl. Catal*. **34** (1987) 275.
[9] I. Nowak, M. Ziolek, *Chem. Rev.* **99** (1999) 3603.
[10] K. Tanabe, S. Okazaki, *Appl. Catal.* **133** (1995) 191.
[11] G.A. Olah, P.S. Lyer, G.K.S. Prakasn, *Synthesis* (1986) 513.
[12] M.M. Sharma, *React. Polym.* (1995) 1.
[13] A. Chakrabati, M.M. Sharma, *React. Polym.* (1993) 1.
[14] J.H. Clark, *Acc. Chem. Res.* **35** (2002) 791.
[15] M. Misono, C.R. *Acad. Sci. Ser. IIc* **3** (2000) 471.
[16] T. Okuhara, *Chem. Rev.* **102** (2002) 3641.
[17] K. Smith, G.A. El-Hiti, A. Gamal, A.J. Jayne, K. Butters, *Org. Biomol. Chem.* **1** (2003) 1560.
[18] M. Hara, T. Yoshida, A. Takagaki, T. Takata, J.N. Kondo, K. Domen, S. Hayashi, *Angew. Chem. Int. Ed.* **43** (2004) 2955.
[19] M. Toda, A. Takagaki, M. Okamura, J.N. Kondo, S. Hayashi, K. Domen, M. Hara, *Nature* **438** (2005) 178.
[20] M. Okamura, A. Takagaki, M. Toda, J.N. Kondo, T. Tatsumi, K. Domen, M. Hara, S. Hayashi, *Chem. Mater.* **18** (2006) 3039.
[21] A. Takagaki, M. Toda, M. Okamura, J.N. Kondo, S. Hayashi, K. Domen, M. Hara, *Catal. Today* **116** (2006) 157.
[22] S. Suganuma, K. Nakajima, M. Kitano, D. Yamaguchi, H. Kato, S. Hayashi, M. Hara, *J. Am. Chem. Soc.* **130** (2008) 12787.
[23] A.J. Ragauskas, C.K. Williams, B.H. Davison, G. Britovsek, J. Cairney, C.A. Eckert, W.J. Frederick, J.P. Hallett, D.J. Leak, C.L. Liotta, J.R. Mielenz, R. Murphy, R. Templer, T. Tschaplinski, *Science* **311** (2006) 484.
[24] B. Hahn-Haegerdal, M. Galbe, M.F. Gorwa-Grauslund, G. Liden, G. Zacchi, *Trends Biotechnol.* **24** (2006) 549.
[25] E.C. Sherrard, F.W. Kressman, *Ind. Eng. Chem.* **37** (1945) 5.
[26] W.L. Faith, *Ind. Eng. Chem.* **37** (1945) 9.
[27] E.E. Harris, E. Beglinger, *Ind. Eng. Chem.* **38** (1946) 890.
[28] A.C. Ferrari, J. Robertson, *Phys. Rev. B* **61** (2000) 14095.
[29] M. Kitano, D. Yamaguchi, S. Suganuma, K. Nakajima, H. Kato, S. Hayashi, M. Hara, *Langmuir* **25** (2009) 5068.

[30] D. Yamaguchi, M. Kitano, S. Suganuma, K. Nakajima, H. Kato, M. Hara, *J. Phys. Chem. C* **113** (2009) 3181.

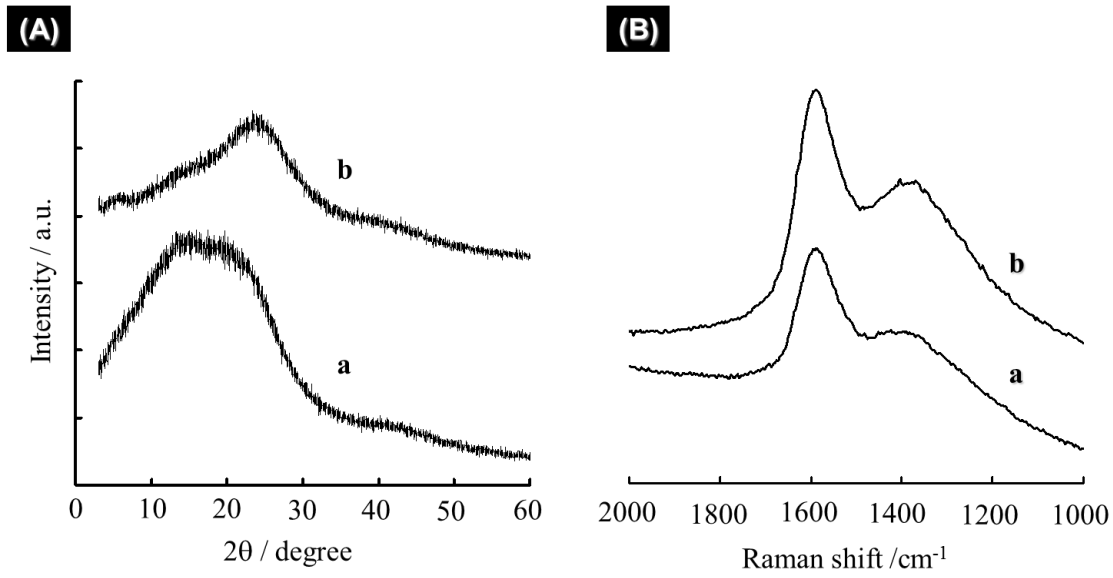

Figure2-1. XRD patterns (A) and Raman spectra (B) for carbonized cellulose (a) before and (b) after sulfonation.

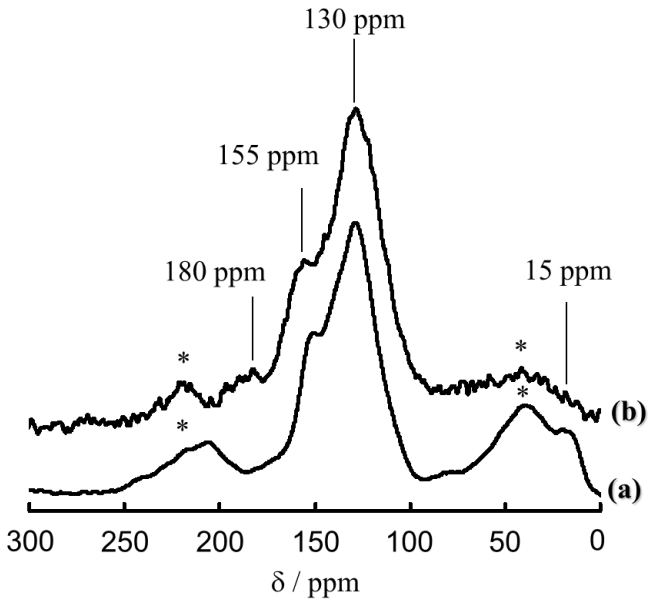

Figure 2-2. ^{13}C CP/MAS NMR spectra for carbonized cellulose (a) before and (b) after sulfonation. * is denoted as spinning sidebands

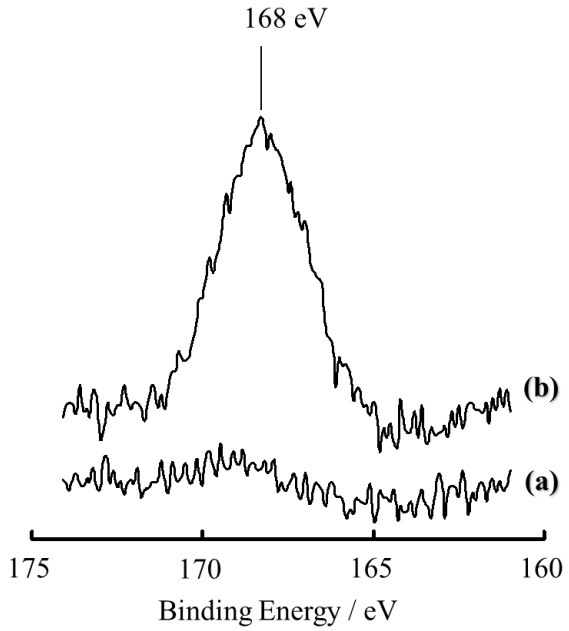

Figure 2-3. S2p XPS spectra for carbonized cellulose (A) before and (B) after sulfonation.

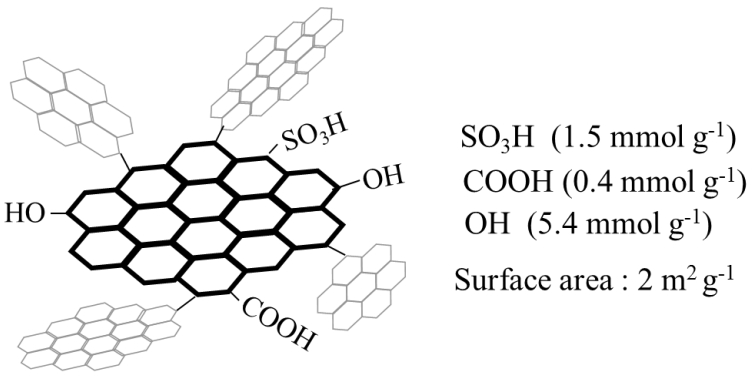

Figure 2-4. The proposed structure of sugar catalyst prepared from cellulose.

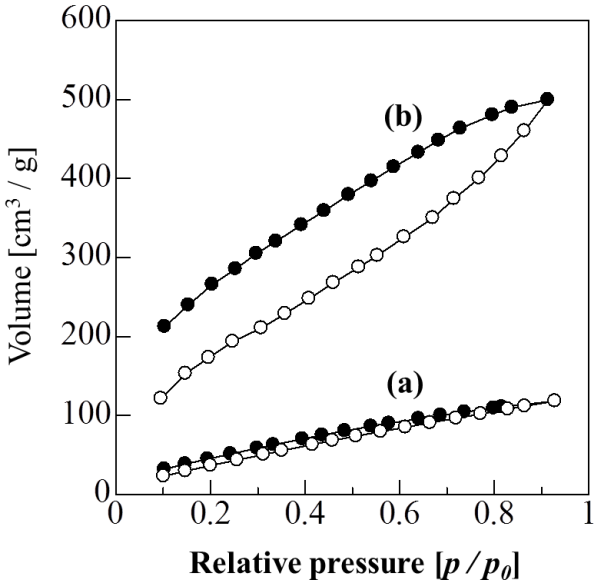

Figure 2-5. H_2O adsorption-desorption isotherms (298 K) for carbonized cellulose (a) before and (b) after sulfonation. ○ and ● denote adsorption and desorption points, respectively.

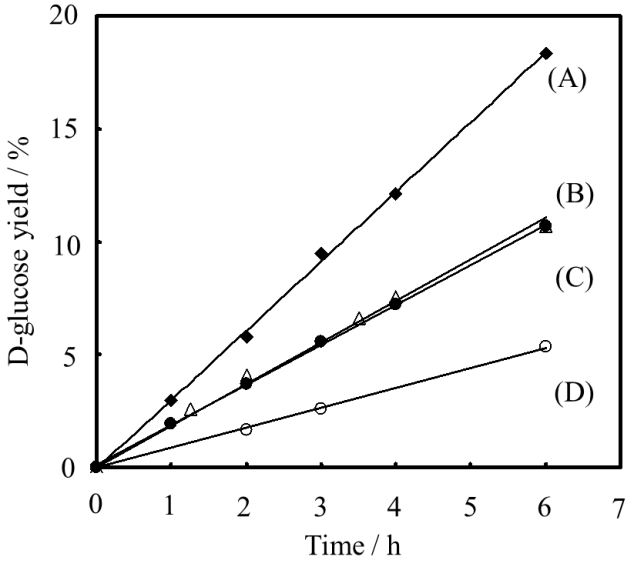

Figure 2-6. Time courses of D-glucose formation from cellobiose over various solid acid catalysts at 373 K: (A) carbon-based solid acid, (B) Nafion NR50, (C) Amberlyst-15, and (D) niobic acid. Reactants : catalyst, 0.2 g; cellobiose, 0.1 g; and water, 10 ml.

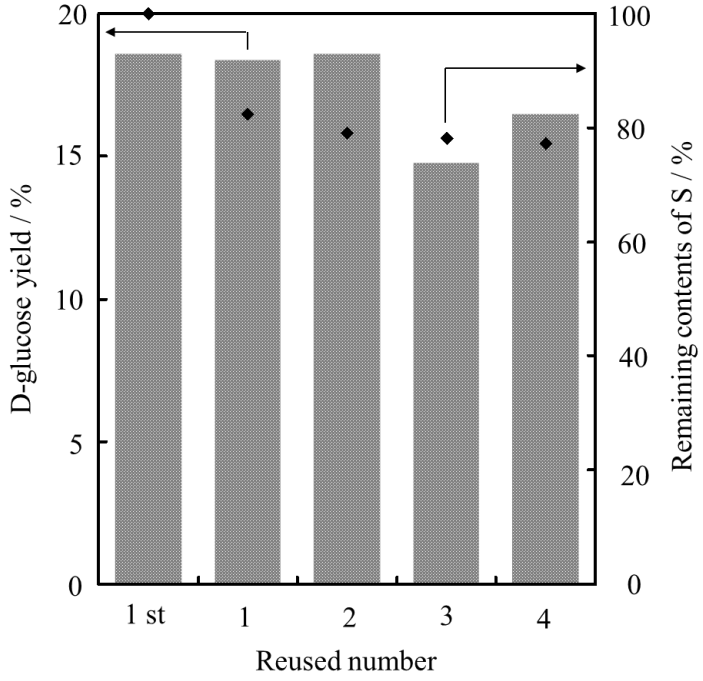

Figure 2-7. Catalytic activity of reused carbon-based solid acid for hydrolysis of cellobiose and the remaining S contents of the catalyst after reactions.

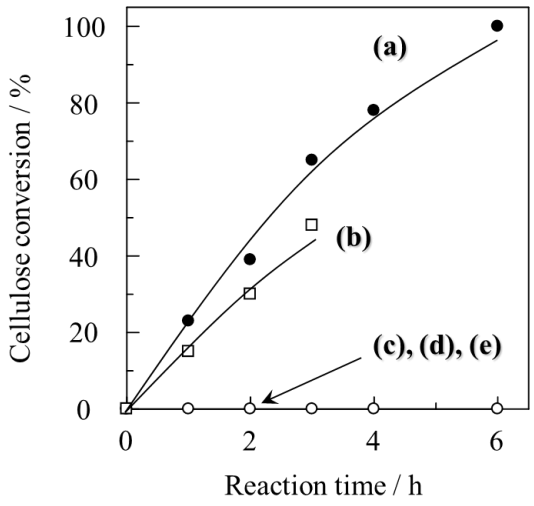

Figure 2-8. Time courses of cellulose conversion in hydrolysis (catalyst, 0.300 g; cellulosic reactant, 0.025 g; water, 0.700 g; reaction temperature, 373 K) of pure crystalline cellulose using (a) carbon material, (b) sulfuric acid, (c) niobic acid (Nb_2O_5•nH_2O), (d) Nafion NR-50, and (e) Amberlyst-15.

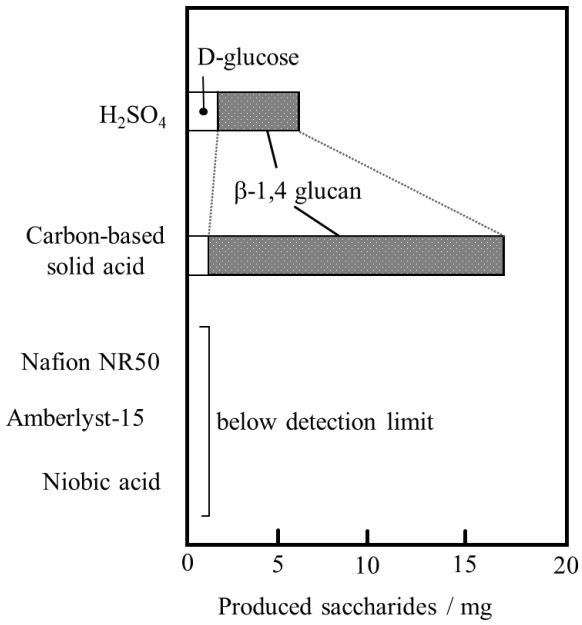

Figure 2-9. Product distribution in the hydrolysis of pure crystalline cellulose over various solid acids and sulfuric acid at 373 K. Reaction condition: catalyst; 0.300g, cellulose; 0.025 g, water; 0.7 g, reaction time; 3 h.

Chapter 3

Hydrolysis of Cellulose by Amorphous Carbon Bearing SO_3H, COOH, and OH Groups

3-1 Abstract

The hydrolysis of cellulose into saccharides using a range of solid catalysts is investigated for potential application in the environmentally benign saccharification of cellulose. Crystalline pure cellulose is not hydrolyzed by conventional strong solid Brønsted acid catalysts such as niobic acid, H-mordenite, Nafion and Amberlyst-15, whereas amorphous carbon bearing SO_3H, COOH, and OH function as an efficient catalyst for the reaction. The apparent activation energy for the hydrolysis of cellulose into glucose using the carbon catalyst is estimated to be 110 kJ mol^{-1}, smaller than that for sulfuric acid under optimal conditions (170 kJ mol^{-1}). The carbon catalyst can be readily separated from the saccharide solution after reaction for reuse in the reaction without loss of activity. The catalytic performance of the carbon catalyst is attributed to the ability of the material to adsorb β-1,4 glucan, which does not adsorb to other solid acids.

3-2 Introduction

A range of industrially important chemicals can be produced from sugars, including ethanol, hydrocarbons, and the starting materials for polymers [1,2]. Among this fundamental group of biological compounds, cellulose is an abundant source of sugars in the form of saccharide polymers linked by β-1,4 glycosidic bonds. As cellulose is a key component of grasses and agricultural and wood waste, the conversion of such vegetable matter into useful sugars (saccharides) is of interest as a means of producing cellulosic ethanol fuel and a range of industrially important chemicals.1-8 Cellulose, a water-insoluble long-chain β-1,4 glucan, is converted to saccharides by hydrolysis of the β-1,4 glycosidic bonds, and substantial effort has been devoted to the development of appropriate hydrolysis schemes, including catalysis using mineral acids [3-5], enzyme-driven reactions [6], the use of supercritical water [7], and solid catalysts for hydrogenolysis [8]. The sulfuric acid catalyzed hydrolysis of cellulose has received considerable attention and has been implemented on relatively large scales [3-5]. However, while sulfuric acid is inexpensive and acts

as a highly active catalyst for this reaction, its use is wasteful and energy-inefficient, requiring separation, recycling, and treatment of the waste sulfuric acid.

The move toward more environmentally sustainable approaches to chemical processes has stimulated the use of recyclable solid acids as replacements for the unrecyclable liquid acid catalysts such as sulfuric acid [9-12]. Any solid Brønsted acid catalyst that is as effective as sulfuric acid in hydrolyzing cellulose is potentially applicable for the efficient conversion of cellulose, and particulate catalysts can be readily separated from the water-soluble saccharides following the reaction, allowing for repeated reuse of the catalyst with low energy consumption. In this study, the hydrolysis of cellulose using solid acid catalysts, including amorphous carbon with a high density of sulfonic acid groups (SO_3H), was examined for potential application in the environmentally benign saccharification of cellulose. The amorphous carbon is a solid Brønsted acid catalyst consisting of flexible polycyclic carbon sheets with SO_3H, COOH, and phenolic hydroxyl (OH) groups in a three-dimensional network that can be readily prepared by partial carbonization of natural organic compounds, such as sugar, cellulose and starch, followed by sulfonation of the resulting amorphous carbon [13-15]. The carbon material can incorporate large amounts of hydrophilic molecules, including water, into the carbon bulk, due to the high density of the hydrophilic functional groups bound to the flexible carbon sheets. This incorporation provides good access by reactants in solution to the SO_3H groups in the carbon material, which gives rise to high catalytic performance for acid-catalyzed reactions in the presence of water such as esterification and hydration, despite the small surface area (2 $m^2 \cdot g^{-1}$) [14]. However, the details of the carbon structure, including graphene size and functional groups other than SO_3H, and catalysis-related structure remain to be clarified.

3-3 Experimental

Preparation of Carbon Material Bearing SO_3H Groups.

The carbon material with SO_3H groups was prepared from microcrystalline cellulose powder (Avicel, MERCK; particle size, 20-100 μm; crystallinity, 80%; degree of polymerization, 200-300). The starting material (20 g) was heated for 5 h at 723 K under N_2 flow to produce a black solid, which was then ground to a powder. The powder (7 g) was then boiled in 150 cm3 of fuming sulfuric acid (15 wt% SO_3) at 353 K under N_2. After heating for 10 h and then cooling to room temperature, the suspension was filtered to yield a black precipitate, which was washed repeatedly with hot distilled water (>353 K, 1000 cm^3) until impurities such as sulfate ions were no longer detected in the wash water. As only a small amount of the excess fuming sulfuric acid is consumed in the reaction, the sulfuric acid recovered after filtration of the powder can be reused for repeated sulfonation of the carbon material. The densities of the functional groups in the carbon material are mainly dominated by the degree of carbonization in the carbon material before sulfonation [14], and the degree of carbonization can be controlled with good reproducibility, resulting in the preparation of the reproducible carbon material.

Characterization

Structural information for the prepared carbon material was obtained by scanning electron microscopy (SEM, S-5200, Hitachi), powder X-ray diffraction (XRD, RINT 2100 diffractometer, RIGAKU), Raman spectroscopy (NRS-2100, JASCO), Fourier transform infrared spectroscopy (FTIR, FT/IR-6100, JASCO), ^{13}C cross-polarization (CP) magic angle spinning (MAS) nuclear magnetic resonance (NMR), ^{31}P MAS NMR, and gas adsorption analysis. The FTIR spectrum for the carbon material was obtained by using a KBr pellet containing the prepared carbon powder. ^{13}C CP/MAS NMR spectra were measured at room temperature using a Bruker ASX-200 spectrometer at a Larmor frequency of 50.3 MHz. A Bruker MAS probehead was used with a 7 mm zirconia rotor. The spinning rate of the sample was 4.0 kHz. The frequency of the spectra is expressed with respect to neat tetramethylsilane. Experimentally, glycine was used as a second reference material, whose carbonyl signal was set at 176.48 ppm. The acid strength of the carbon material was examined by colorproducing reagents and ^{31}P MAS NMR measurement, using trimethylphosphine oxide (TMPO) as a probe molecule [14]. The Brunauer-Emmett-Teller (BET) surface areas and water vapor adsorption isotherms for the samples were measured by NOVA-4200e (QUANTACHROME) and AUTOSORB MP/VP (QUANTACHROME), respectively.

The amount of the functional groups bonded to the carbon material was estimated by elemental analysis (vario MICRO cube, ELEMENTAL) and cation-exchange analysis. According to X-ray photoelectron spectroscopy (XPS) analysis, all sulfur in the carbon material, which possesses SO_3H, COOH, and phenolic OH, is expected to be confined to SO_3H groups [14]. The densities of SO_3H groups were thus estimated based on the sulfur content determined from sample compositions obtained by elemental analysis. The total SO_3H + COOH and SO_3H + COOH + OH contents were estimated from the exchange of Na^+ in aqueous NaCl and NaOH solutions, respectively, to afford the proportions of each functional group.

Hydrolysis of Cellulose

The hydrolysis of pure microcrystalline cellulose (Avicel; particle size, 20-100 μm; crystallinity, 80%; degree of polymerization, 200-300) and eucalyptus flakes (width, 0.5-1.5 mm; thickness, 0.1-0.5 mm; length, 0.5-5.0 mm) was carried out in a Pyrex reactor (catalyst, 0.300 g; cellulose reactant, 0.025 g; distilled water, 0.700 g) at 373 K. The catalysts tested were sulfuric acid (H_2SO_4 (96%), KANTO chemical), niobic acid ($Nb_2O_5 \cdot nH_2O$, CBMM), H-mordenite (reference catalyst, The Catalysis Society of Japan), Nafion NR50 (perfluorosulfonated ionomer, Aldrich), Amberlyst-15 (polystyrene-based cationexchangeable resin with SO_3H, Aldrich), and the carbon material prepared from cellulose. In sulfuric acid reactions, 0.320 g of 96% sulfuric acid (net 0.307 g) was used as the catalyst. The Pyrex test tube reactor containing the catalyst and reactant was sealed using a Swagelok tube fitting (reactor volume, 3.5 cm^3) prior to reaction and then placed in boiling water or an oil bath. The mixture was stirred by a stir bar in the reactor during reaction. After the reaction, an aliquot of the supernatant solution, readily obtained by decantation, was analyzed by liquid and gel permeation chromatography (LC-2000 plus, JASCO) and matrix-assisted

laser desorption/ionization time-of-flight mass spectrometry (MALDI-TOF-MASS, AXIMA-TOF2, SHIMAZU). In the sulfuric acid reactions, the reacted solution was neutralized with aqueous $CaCl_2$ solution, the $CaSO_4$ precipitate was removed by centrifugation, and the supernatant solution was analyzed.

In hydrolysis products of cellulose, the amounts of glucose and short-chain β-1,4 glucan such as cellobiose-cellotetraose can be readily estimated by liquid chromatography (LC). While water-soluble β-1,4 glucan longer than cellopentose-cellohexose can be detected by gel permeation chromatography (GPC) and MALDITOF-MASS, it is difficult to estimate the amount of each long-chainβ-1,4 glucan solved in solution by using these methods. In this study, the yields of glucose and water-soluble β-1,4 glucan were obtained by LC and the enzymatic hydrolysis of water-soluble β-1,4 glucan using cellulase. After hydrolysis, the solid sample (catalyst and residual cellulosic reactants) was rinsed 5 times in 2 cm^3 of distilled water added directly to the reactor. During each rinse, the suspension was stirred vigorously for 30 min and then centrifuged to collect the solid and the supernatant solution. The amount of produced glucose in the collected supernatant solution was estimated by LC. 0.2 g of crude cellulase obtained from Trichoderma Viride (Wako Pure Chemical Industries) was then added to the collected supernatant solution, and the solution was warmed in order to hydrolyze polysaccharides (water-soluble β-1,4 glucan) in the solution into monosaccharides (glucose) for 48 h at 313 K. After the enzymatic hydrolysis, glucose produced by the hydrolysis of water-soluble β-1,4 glucan was also analyzed by LC. Cellulose conversion as well as glucose and β-1,4 glucan yields were obtained by using the following equations.

Cellulose conversion (%)=100(B+C)／A

Glucose yield (%)=100B／A

Total β-1,4 glucan (%)=100C／A

A: total amount (mol) of glucose monomer in cellulose.

B: amount (mol) of glucose produced by acid-catalyzed hydrolysis.

C: total amount (mol) of glucose monomer in water-soluble β-1,4 glucan produced by acid-catalyzed hydrolysis

3-4 Results and discussion

Structure of the Prepared Carbon Material

The particle size and surface area of the black powder obtained by sulfonation of partial carbonized cellulose were estimated to be 10-40 μm and 2 $m^2\ g^{-1}$, respectively by SEM and BET measurements. Figure 3-1 shows the XRD pattern and Raman spectrum for the prepared sample. The XRD pattern exhibiting two broad but weak diffraction peaks at 2θ angles of 10°-30° and 35°-50° is attributable to amorphous carbon composed of aromatic carbon sheets oriented in a considerably random fashion [16]. In the Raman spectrum, the intensity ratio of the D band (1350 cm^{-1}, A_{1g} D breathing mode) to the G band (1580 cm^{-1}, E_{2g} G mode) for the carbon material is 0.81, indicating that the average graphene size in the amorphous carbon is ca. 1 nm [17]. The FT-IR and

^{13}C CP/MAS NMR spectra for the carbon material are shown in Figure 3-2. The vibration bands at 1040 (SO_3^- stretching) and 1377 cm^{-1} (O=S=O stretching in SO_3H) in the FT-IR spectrum indicate that the resulting material possesses SO_3H groups. The broadband at 2300-2700 cm^{-1} can be assigned to an overtone (Fermi resonance) of the bending mode of -OH· · ·O= linked by a strong hydrogen bond, as seen in strong liquid Brønsted acids such as CF_3SO_3H [18], suggesting that some SO_3H groups are interacted with SO_3H, COOH, or phenolic OH groups in close proximity. The chemical shifts at 130, 155, and 180 ppm in the NMR spectrum are attributable to polycyclic aromatic carbon atoms, phenolic OH, and COOH groups, respectively [16,19]. The peak due to aromatic carbon with SO_3H groups (Ar-SO_3H, ca. 140 ppm) is not observed in the spectrum. The resonance derived from Ar-SO_3H is not distinguished in the spectra of SO_3H-bearing amorphous carbon samples, because broad peaks due to aromatic carbon atoms (130 ppm) and OH groups (155 ppm) obscure the peak. Elemental analysis and cation-exchange experiment revealed that the sample composition is $CH_{0.622}O_{0.540}S_{0.048}$ and that the amounts of SO_3H, COOH, and phenolic OH groups bonded to the graphene are 1.9, 0.4, and 2.0 mmol g-1, respectively.

The schematic carbon structure proposed on the basis of these results is shown in Figure 3-3. The prepared material is amorphous carbon consisting of SO_3H-, COOH-, and phenolic OH-bearing nanographene sheets in a considerably random fashion. If the carbon material is composed of uniform functionalized graphene sheets, each graphene sheet is expected to bind SO_3H and phenolic OH. The carbon material possesses a high density of almost neutral phenolic OH in addition to Brønsted acid sites (SO_3H and COOH). This is distinct from conventional solid acids with single functional groups.

Hydrolysis of Cellulose by Acid Catalysts

The performance of various acid catalysts was examined through the hydrolysis of pure microcrystalline cellulose powder (Avicel) at 373 K. The same amount of catalyst was used in all cases (0.3 g). The results, including acid density, maximum acidity (Hammet function; H_0), and surface area of the tested catalysts, are summarized in Table 3-1. The catalysts tested were sulfuric acid (H_2SO_4), niobic acid ($Nb_2O_5 \cdot nH_2O$), H-mordenite (zeolite), Nafion NR50 (perfluorosulfonated ionomer), Amberlyst-15 (polystyrene-based cation-exchangeable resin with SO_3H), and the carbon material prepared from cellulose. Niobic acid and H-mordenite are typical strong inorganic solid Brønsted acids that are widely used in industrial acid-catalyzed reactions, while Nafion and Amberlyst-15 are strong polymer-based solid acids with high SO_3H density and very high activity for a range of reactions [9-12,20].

As shown in Table 3-1, neither cellulose could be hydrolyzed into glucose nor water-soluble β-1,4 glucan using conventional solid acid catalysts such as niobic acid, H-mordenite, Nafion, or Amberlyst-15, whereas the carbon material exhibited remarkable hydrolysis performance for the reaction. After reaction for 3 h, the white cellulose powder could no longer be observed in suspension, and of the 25 mg of cellulose powder (total glucose monomer; 154 μmol) added to the reaction, 68% was hydrolyzed into glucose (6 μmol, yield; 4%) and water-soluble β-1,4 glucan (total glucose monomer; 98 μmol, yield; 64%). Figure 3-4 shows the MALDI-TOF-MASS

spectrum for the reaction solution after 3 h in the presence of the carbon material. The large signals appear at m/z) 162 intervals that is the mass number of glucose monomer (-(-O-$C_6H_{10}O_4$-)$_n$-) in β-1,4 glucan, meaning that β-1,4 glucan as the hydrolysis products of cellulose is solved in water. Theβ-1,4 glucan component was estimated to be $C_6H_{11}O_5$-(-O-$C_6H_{10}O_4$-)$_{2\text{-}10}$-O-$C_6H_{11}O_5$ by MALDI-TOFMASS. Under the present reaction conditions, short β-1,4 glucans, such as cellobiose and cellotriose, 5-hydroxymethylfurfural, and levulinic acid (byproduct formed by the decomposition of glucose) [21], were not observed in the aqueous solution after reaction. 0.3 g of H_2SO_4 (corresponding to 30 wt% H_2SO_4 solution) also has a high hydrolysis activity, and the yields of glucose and water-soluble β-1,4 glucan at 3 h reach 10 and 38%, respectively (Table 3-1). Dilute H_2SO_4 solution (H_2SO_4, 0.030 g; distilled water, 0.700 g (corresponding to 4.1 wt% H_2SO_4 solution); cellulose, 0.025 g; reaction temperature, 373 K), however, reduced the yields of glucose and water-soluble β-1,4 glucan to 2 and 4%, respectively. Because a dilute sulfuric acid system exhibits high catalytic performance for cellulose saccharification at temperatures above 423-453 K [22], efficient hydrolysis does not proceed in dilute sulfuric acid at 373 K. Figure 3-5 correlates the conversion of cellulose into water-soluble saccharides (glucose and water-soluble β-1,4 glucan) and reaction time over the carbon material with the data for H_2SO_4 under the reaction conditions indicated in Table 3-1. In the case of the carbon material, all cellulose was converted into water-soluble saccharides within 6 h, and the carbon material could be readily separated from the solution containing dissolved saccharides after the reaction by simple decantation. The recovery of the carbon catalyst was 99.4-99.6%. The results for the reuse experiment of the sample are shown in Figure 3-6 [23]. No decrease in activity was observed even after 25 reuses of the sample (total reaction time, 150 h). A total of 0.625 g of cellulose was successfully hydrolyzed in this manner. Elemental analyses of the carbon material and ion chromatography revealed that 6 μmol of SO_3H groups (ca. 1%) were eluted as H_2SO_4 (corresponding to 0.08 wt% sulfuric acid solution) from the carbon material at the first reaction and leaching of SO_3H groups was not detected in the subsequent reactions. The carbon material exhibited a higher hydrolysis activity for the reaction under optimal reaction conditions in a large reaction vessel. The hydrolysis of pure crystalline cellulose into glucose in the presence of the carbon material was remarkably promoted with increases in the amount of cellulose and decreases in the amount of distilled water. Figure 3-7 shows the hydrolysis of cellulose into water-soluble β-1,4 glucan and glucose using the carbon material at 373 K (carbon material, 1.00 g (SO_3H, 1.9 mmol g-1); pure crystalline cellulose, 3.00 g; distilled water, 0.70 g). Distilled water was successively added to the reaction vessel at the rate 3 mg h^{-1} through a microfeeder to compensate for water consumed by the hydrolysis of cellulose. The amounts of glucose and water-soluble β-1,4 glucan produced by the hydrolysis of cellulose increase in proportion to reaction time. The rate of glucose formation per weight reaches 110 μmol h^{-1} g^{-1} that is much larger than that of the carbon material under the reaction conditions indicated in Table 3-1 (ca. 7 μmol h^{-1} g^{-1}), and the turnover number of the effective acid sites (SO_3H, 1.9 mmol g^{-1}) for glucose formation is 1.6 at 27 h. In Figure 3-7, the glucose formation exceeds the formation of water-soluble β-1,4 glucan, in contrast to the reaction in Table 3-1, meaning that produced water-soluble β-1,4 glucan is efficiently hydrolyzed into glucose under the reaction conditions. This

is attributable to an increase in acidity of the SO_3H groups on the carbon material with a decrease in the amount of water. The rates of glucose and water-soluble β-1,4 glucan formation in the presence of sulfuric acid were 85 and 130% those of the carbon material, respectively, under the same reaction conditions indicated in Figure 3-7. The apparent activation energy for the hydrolysis of cellulose into glucose in the presence of the carbon material is estimated to be 110 kJ mol^{-1} at 343-373 K (Figure 3-8). This is smaller than that of the reaction under optimal conditions using sulfuric acid as a catalyst (170 kJ mol^{-1}) [22]. As expected from the Arrhenius plots in Figure 3-8, the formation rates of glucose and water-soluble β-1,4 glucan on the carbon material increased exponentially with increasing reaction temperature at 333-393 K. However, reaction temperatures above 373 K resulted in the formation of byproduct such as levoglucosan (intramolecular dehydration of glucose), maltose, cellobiose (intermolecular dehydration between glucose molecules), levulinic, and formic acids (decomposition of glucose). These results indicate that the efficient catalytic hydrolysis of cellulose appears to proceed at the interface between the carbon material and the highly crystallized cellulose in the presence of water.

The carbon material was also tested as a catalyst for the conversion of dried Eucalyptus flakes (country of origin; Australia) as a natural lignocellulosic substrate. The time course of conversion of cellulose and hemicellulose into water-soluble saccharides (poly- and monosaccharides) using the carbon catalyst and H_2SO_4 is shown in Figure 3-5 [24]. The carbon material exhibited high catalytic performance for the decomposition of the natural substrate, and all cellulosic materials were converted into water-soluble saccharides within 3 h at 373 K. Under all reaction conditions, the insoluble product was produced at yields of 25-33 wt% attributable to lignin [25]. As the sedimentation rates of thin lignin and dense carbon particles differ substantially, separation of the catalyst and lignin could be readily performed by decantation.

Catalysis and Structure of Carbon Material Bearing SO_3H, COOH, and OH

The enhanced hydrolytic catalysis of the carbon material cannot be adequately explained as being due solely to factors such as surface area or acid strength, as other acid catalysts with a similar or higher surface area and acidity do not hydrolyze cellulose (Table 3-1). The catalysis of amorphous carbon with SO_3H, COOH, and OH was thus further investigated by examining the adsorption of cellobiose, a short β-1,4 glucan, on each of the solid acid catalysts considered in this study. In the experiment, 0.1 g of each solid acid was added to 2 cm^3 (cellobiose, 3 μmol) of aqueous cellobiose solution (1.5 mmol dm^{-3}) and then stirred at room temperature. Cellobiose was not hydrolyzed into glucose at room temperature under the experimental conditions, and the amount of adsorbed cellobiose was estimated by LC of the supernatant solution. The conventional solid acids such as H-mordenite, Nafion, and Amberlyst- 15 did not adsorb cellobiose in water even after stirring for 24 h, whereas the carbon material adsorbed 24% of the cellobiose in just 3 h. The cellobiose adsorption reached a plateau at 5 h, reaching adsorption of 26% (0.8 μmol) of the cellobiose solved in the solution. This suggests that the carbon material has a stronger affinity for β-1,4 glucan, including cellulose, than the other solid acids. It was confirmed by soaking cellulose filter papers in solid acid-water suspensions that only SO_3H-bearing carbon particles attach to the

cellulose in the tested solid acids (Figure 3-9). The hydrolysis of cellulose into glucose using Brønsted acids involves two stages: H^+ attack of hydrogen and β-1,4 glycosidic bonds in solid crystalline cellulose to form water-soluble β-1,4 glucan, followed by hydrolysis of the β-1,4 glycosidic bonds in the β-1,4 glucan to form glucose. Efficient conversion of cellulose into glucose using a solid acid catalyst therefore requires a strong interaction between the solid acid and β-1,4 glucan (solid cellulose and water-soluble β-1,4 glucan) because the Brønsted acid sites of the solid acid cannot approach the cellulose surface without such an interaction. This is distinct from the hydrolysis in a homogeneous sulfuric acid system. The SO_3H-bearing carbon material, which is capable of adsorbing β-1,4 glucan, can thus be expected to have much higher activity for hydrolytic catalysis than the other solid acids examined in this study. It should be noted that the carbon material cannot adsorb glucose as a monomer of cellobiose at all. This suggests that the glycosidic bond in β-1,4 glucan participates in the adsorption on the carbon material. The ability to adsorb β-1,4 glucan may be attributable to phenolic OH groups bonded to the graphene sheets. In the cellobiose adsorption experiment of Amberlite IRC-50 (Aldrich), a cation-exchangeable resin with COOH, the resin did not adsorb cellobiose as well as Amberlyst-15 with SO_3H groups: these functional groups do not adsorb cellobiose. On the other hand, neutral OH groups can be linked by strong hydrogen bonds to oxygen atoms in glycosidic bonds. Cellulose is a water-insoluble β-1,4 glucan aggregate formed by the strong hydrogen bond between OH groups in glucose monomers and oxygen atoms in glycosidic bonds among β-1,4 glucan chains.

Although the carbon material has a small surface area (2 $m^2\ g^{-1}$) and the effective Brønsted acid density in the carbon is only 1/10 that of sulfuric acid, the carbon is shown to be as effective as sulfuric acid in hydrolyzing cellulose. Figure 3-10 shows the H_2O vapor adsorption-desorption isotherm of the carbon material at 298 K. The amount of adsorbed H_2O at 1.5 kPa that is much smaller than that at saturated water vapor pressure (ca. 3 kPa) exceeds 0.01 mol g^{-1}. Assuming that the adsorption cross section area of H_2O is 0.125 nm^2, the effective surface area of the carbon material is estimated to exceed 560 $m^2\ g^{-1}$ at the water vapor pressure. This means that the carbon material can incorporate large amounts of water into the carbon bulk, due to the high density of the hydrophilic functional groups bound to the flexible nanographene sheets. This incorporation provides good access by reactants in solution to the SO_3H groups in the carbon material, which gives rise to high catalytic performance, despite the small surface area [14]. As a result, the effective surface area of the carbon material in the hydrolysis reaction requiring water is much larger than the BET surface area measured after dehydration. In general, large molecules with large excluded volumes such as cellobiose are not densely adsorbed on surfaces. However, if only the carbon surface is covered with cellobiose molecules (adsorption cross section area; ca. 0.9 nm^2) [25] without vacancy in the above cellobiose adsorption experiment, the carbon material has to have a surface area above 4 $m^2\ g^{-1}$ at least, indicating that the carbon material can incorporate even large molecules such cellobiose into the bulk in the presence of water.

One possible explanation for the high hydrolysis performance of the carbon material that has a much smaller Brønsted acid density than sulfuric acid is SO_3H groups tolerable to hydration. In the same catalyst weight, sulfuric acid always exhibits higher catalytic activity for esterification [14,15],

an acid-catalyzed reaction in the presence of small amount of water, than the SO_3H-bearing amorphous carbon: the turnover frequency (TOF) of the effective acid sites in the carbon material is about 3 times that of sulfuric acid at most. On the other hand, the carbon material is as effective as sulfuric acid in acid-catalyzed reactions in a large quantity of water such as the hydrolysis of cyclohexyl acetate, and the TOF exceeds 10 times that of sulfuric acid [15]. Sulfuric acid is subject to hydration by many H_2O molecules, resulting in a decrease in catalytic activity for the acid-catalyzed reactions in water such as hydrolysis because of a decrease in acidity by hydration. These results therefore suggest that the carbon material has SO_3H groups tolerable to hydration compared with sulfuric acid. The FTIR spectrum for the carbon material shown in Figure 3-2 was measured by using the carbon material exposed to the saturated water vapor at room temperature. Although the carbon sample incorporates a large quantity of water in to the carbon bulk as expected from the water adsorption-desorption isotherm in Figure 3-10, the broadband at 2300-2700 cm^{-1} assignable to the strong hydrogen bond between SO_3H groups is nevertheless observed. This is also indicative of hydration-tolerant SO_3H groups in the carbon material. The hydrophobic graphene sheets may prevent complete hydration of the SO_3H groups. The details of the SO_3H groups are currently under investigation.

3-5 Conclusion

Amorphous carbon bearing SO_3H, OH, and COOH groups was demonstrated to function as a highly active catalyst for the direct hydrolysis of solid cellulose, despite the small surface area and small effective acid density. The high catalytic activity for the reaction can be attributed to the ability to adsorb β-1,4 glucan, the large effective surface area in water, and SO_3H groups tolerable to hydration in the carbon material.

References and notes

[1] A.J. Ragauskas, C.K. Williams, B.H. Davison, G. Britovsek, J. Cairney, C.A. Eckert, W.J. Frederick, J.P. Hallett, D.J. Leak, C.L. Liotta, J.R. Mielenz, R. Murphy, R. Templer, T. Tschaplinski, *Science* **311** (2006) 484–489.

[2] B. Hahn-Haegerdal, M. Galbe, M.F. Gorwa-Grauslund, G. Liden, G. Zacchi, *Trends Biotechnol.* **24** (2006) 549–556.

[3] E.C. Sherrard, F.W. Kressman, *Ind. Eng. Chem.* **37** (1945) 5–8.

[4] W.L. Faith, *Ind. Eng. Chem.* **37 (**1945) 9–11.

[5] E.E. Harris, E. Beglinger, *Ind. Eng. Chem.* **38** (1946) 890–895.

[6] Y.P. Zhang, L.R. Lynd, *Biotechnol. Bioeng.* **88** (2004) 797–824.

[7] M. Sasaki, Z. Fang, Y. Fukushima, T. Adschiri, K. Arai, *Ind. Eng. Chem. Res.* **39** (2000) 2883–2890.

[8] A. Fukuoka, L.P. Dhepe, *Angew. Chem., Int. Ed.* **45** (2006) 5161–5163.

[9] M. Misono, *C. R. Acad. Sci., Ser. IIc: Chim.* **3** (2000) 471–475.

[10] J.H. Clark, *Acc. Chem. Res.* **35** (2002) 791–797.

[11] T. Okuhara, *Chem. ReV.* **102** (2002) 3641–3666.

[12] K. Smith, E. Hiti, A. Gamal, A.J. Jayne, M. Butters, *Org. Biomol. Chem.* **1** (2003) 1560–1564.

[13] M. Toda, A. Takagaki, M. Okamura, J.N. Kondo, S. Hayashi, K. Domen, M. Hara, *Nature* **438** (2005) 178–178.

[14] M. Okamura, A. Takagaki, M. Toda, J.N. Kondo, T. Tatsumi, K. Domen, M. Hara, S. Hayashi, *Chem. Mater.* **18** (2006) 3039–3045.

[15] M. Hara, T. Yoshida, A. Takagaki, Y. Takata, J.N. Kondo, K. Domen, S. Hayashi, *Angew. Chem., Int. Ed.* **43** (2004) 2955–2958.

[16] N. Tsubouchi, K. Xu, Y. Ohtsuka, *Energy Fuels* **17** (2003) 1119–1125.

[17] A.C. Ferrari, J. Robertson, *Phys. ReV. B* **61** (2000) 14095–14107.

[18] R. Buzzoni, S. Bordiga, G. Ricchiardi, G. Spoto, A.J. Zecchina, *Phys. Chem.* **99** (1995) 11937–11951.

[19] R.M. Silverstien, G.C. Bassler, T.C. Morrill, *Spectrometric identification of organic compound*, 5th ed.; John Wiley & Sons: Indianapolis, (1991) pp 218-232.

[20] G.A. Olah, P.S. Iyer, G.K.S. Prakash, *Synthesis* **7** (1986) 513–531.

[21] M.J. Taherzadeh, C. Nikalasson, G. Liden, *Chem. Eng. Sci.* **52** (1997) 2653–2659.

[22] B. Girisuta, L.P.B.M. Janssen, H.J. Heeres, *Ing. Eng. Chem. Res.* **46** (2007) 1696–1708.

[23] The catalytic activity of the reused carbon material was evaluated by measuring the yields of glucose and β-1,4 glucan after 3 h at 373 K. The sealed Pyrex test tube reactor containing the catalyst and reactant (carbon material, 0.300 g; distilled water, 0.700 g; cellulose, 0.025 g) was placed in an oil bath at 373 K for 3 h and then cooled to room temperature. After 100 μL of the supernatant solution were withdrawn and analyzed for the estimation of the glucose and β-1,4 glucan yields (see Experimental Section), the reactor was placed in the oil bath again. After 3 h, the solid sample was rinsed 5 times in 2 cm^3 of distilled water added directly to the reactor.

During each rinse, the suspension was stirred vigorously for 30 min and then centrifuged to collect the solid and the supernatant solution. The solid collected in the reactor was dried overnight at 353 K and reused for the subsequent reaction. It was confirmed in each reuse reaction that all cellulose is hydrolyzed into glucose and water-soluble β-1,4 glucan by the reaction for 6 h. The collected supernatant solution was also analyzed by inductively coupled plasma atomic emission spectroscopy and ion chromatography to observe leaching of SO_3H groups.

[24] Hydrolysis of Eucalyptus flakes: Chemical analyses of monosaccharides revealed that the complete hydrolysis of 25.0 mg of Eucalyptus flakes yielded 26.6 mg of the product, comprising glucose (66 μmol, 12.0 mg, 45.1 wt%), xylose (11 μmol, 1.6 mg, 6.0 wt%), mannose (2 μmol, 0.3 mg, 1.1 wt%), galactose (1 μmol, 0.2 mg, 0.8 wt%), lignin (8.4 mg, 31.6 wt%), and unknown water-soluble products (4.1 mg, 15.4 wt%). Cellulose, hemicellulose, and lignocellulose in Eucalyptus thus consist of glucose, xylose, mannose, and galactose (total saccharides; 80 μmol, 14.1 mg, 53.0 wt%). The unknown water-soluble products could be readily dissolved in ethanol and acetone, suggestive of organic compounds other than saccharides. Cellulose conversion in the hydrolysis of Eucalyptus flakes was obtained in a similar manner as that of the hydrolysis of pure crystalline cellulose (see above). After reaction for 3 h at 373 K, 4 μmol of glucose, 11 μmol of xylose, and water-soluble polysaccharides (total saccharide monomer: 72 μmol) were obtained from the Eucalyptus flakes using the carbon material, indicating that most cellulosic materials (cellulose, hemicellulose, and lignocellulose) in the flakes had been successfully hydrolyzed into monosaccharides and water-soluble polysaccharides. Under the same reaction conditions (3 h, 373 K), sulfuric acid hydrolyzed the eucalyptus flakes into 16 μmol of glucose, 8 μmol of xylose, and water-soluble polysaccharides (total saccharide monomer: 39 μmol). In both cases, the insoluble product was produced at a yield of ca. 30 wt% (8 mg) attributable to lignin [25].

[25] Y. Nagamatsu, M. Funaoka, *Trans. Mater. Res. Soc. Jpn.* **26** (2001) 821–824.

[26] P.L. Dhepe, M. Ohashi, S. Inagaki, M. Ichikawa, A. Fukuoka, *Catal. Lett.* **102** (2005) 163–169.

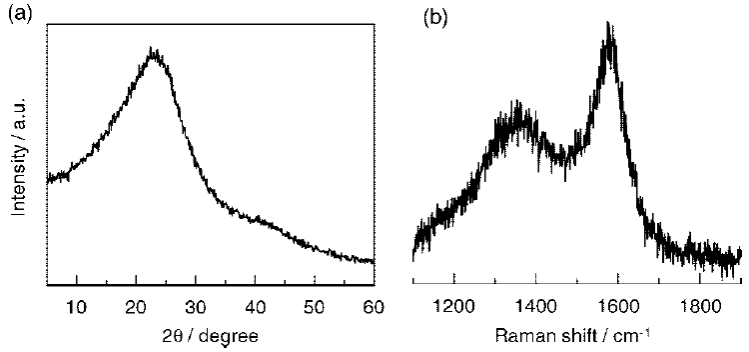

Figure 3-1. XRD pattern (a) and Raman spectrum (b) for the sample prepared by sulfonation of partial carbonized cellulose.

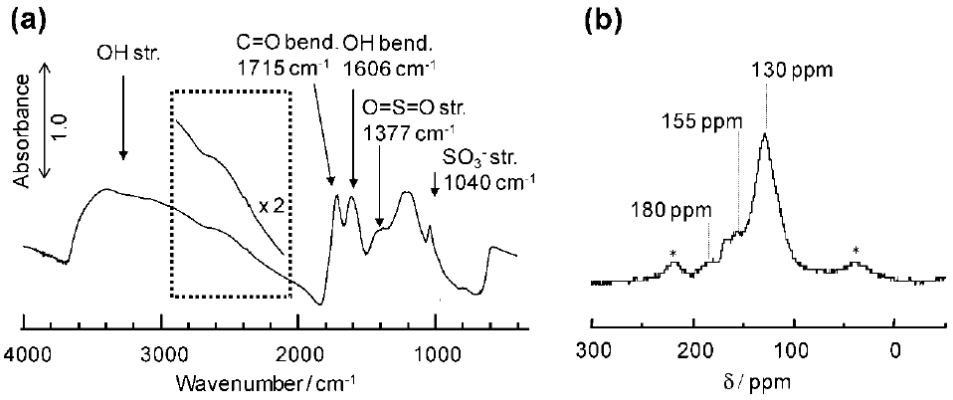

Figure 3-2. FTIR spectrum (a) and ^{13}C MAS NMR spectrum (b) for the carbon material prepared from cellulose.

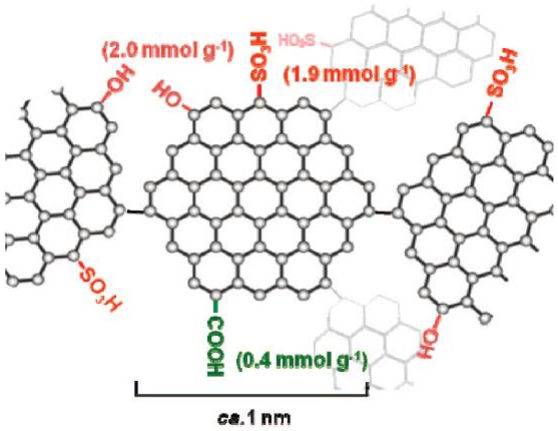

Figure 3-3. Proposed schematic structure of the prepared carbon material.

Table 3-1. Hydrolysis of Crystalline Cellulose by Various Acid Catalysts[a]

catalyst	functional groups	density / mmol g^{-1}	Maximaum Acidity H_0	surface area / m^2 g^{-1}	yields of hydrolysis products
H_2SO_4		20.4	-11	-	glucose: 10% β-1,4 glucan:38%
niobic acid	acidic OH	0.4	-5.6	90	-
H-mordenite	acidic OH	1.4	-5.6	480	-
Nafion	SO_3H	0.9	-11 to -13	<1	-
Amberlyst-15	SO_3H	4.8	-2.2	50	-
carbon material	SO_3H	1.9	-8 to -11	2	glucose: 4%
($CH_{0.62}O_{0.54}S_{0.05}$)	COOH	0.4	-		β-1,4 glucan:64%
	Phenolic OH	2.0	-		

[a] Catalyst, 0.3 g; cellulose, 25 mg; water, 0.7 g; reaction time, 3 h.

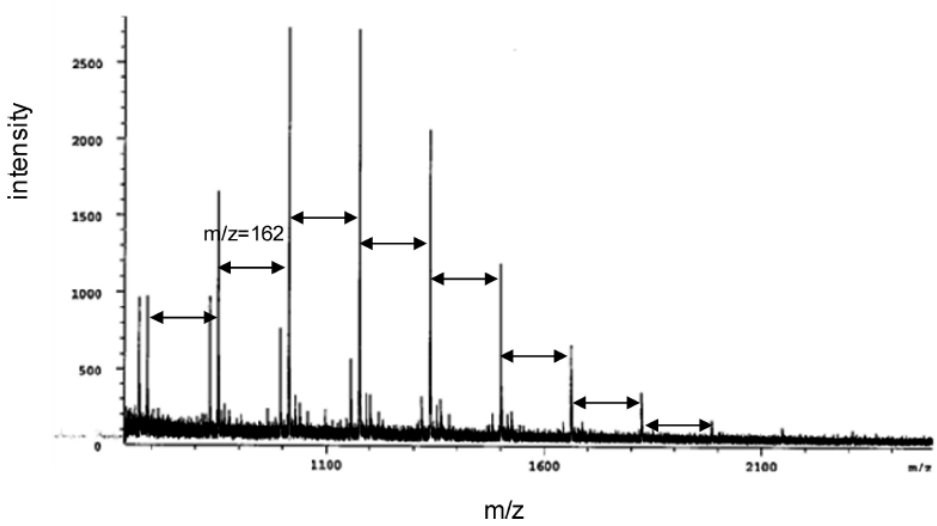

Figure 3-4. MALDI-TOF-MASS for the reaction solution. Carbon material, 0.300 g; cellulose, 0.025 g; water, 0.700 g; reaction temperature, 373 K; reaction time, 3 h; ion detection, positive; matrix, 2,5-dihydroxybenzoic acid-acetonitrile solution. *m/z* = 162 represents the mass number of glucose monomer (-(-O-$C_6H_{10}O_4$-)$_n$-) in β-1,4 glucan.

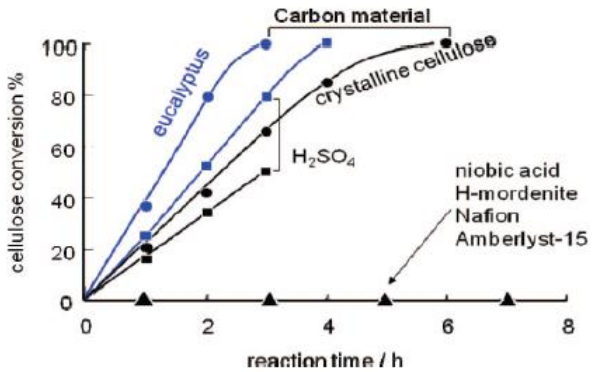

Figure 3-5. Time courses of cellulose conversion in hydrolysis (catalyst, 0.300 g; cellulosic reactant, 0.025 g; water, 0.700 g; reaction temperature, 373 K) of pure crystalline cellulose (black) and eucalyptus (blue) using carbon material (circles) and sulfuric acid (squares). Triangles represent the results for the hydrolysis of pure crystalline cellulose using niobic acid ($Nb_2O_5 \cdot nH_2O$), H-mordenite, Nafion, and Amberlyst-15.

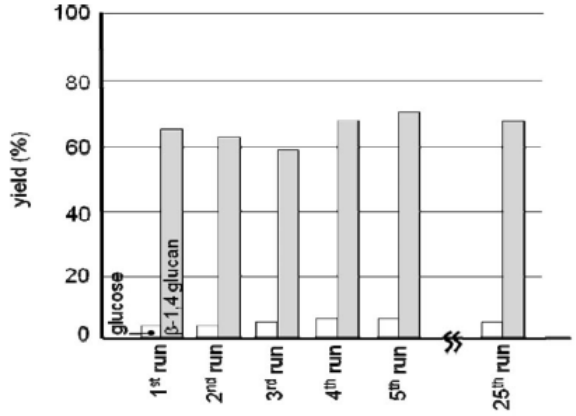

Figure 3-6. Catalytic activity of reused carbon material for hydrolysis of crystalline cellulose at 373 K. Catalyst, 0.300 g; water, 0.700 g; cellulose, 0.025 g . The yields were measured at 3 h after reaction. After reaction for 4-6 h, the conversion of cellulose into water-soluble saccharides reached ca. 100%; the catalyst was repeatedly rinsed with distilled water and was reused for the subsequent reaction.

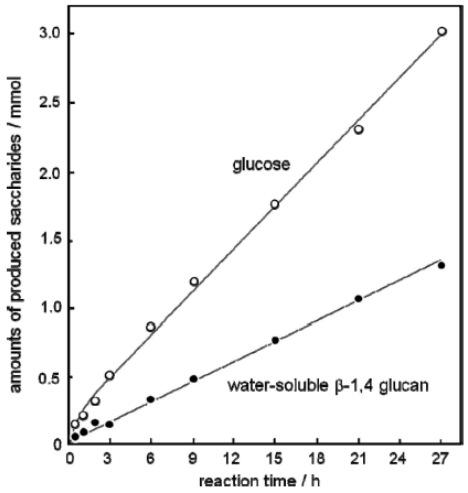

Figure 3-7. Time courses of the amounts of glucose (○) and water-soluble β-1,4 glucan (●) produced by the hydrolysis of pure crystalline cellulose in the presence of the carbon material at 373 K. Carbon material, 1.0 g; cellulose, 3.0 g; water, 0.7 g.

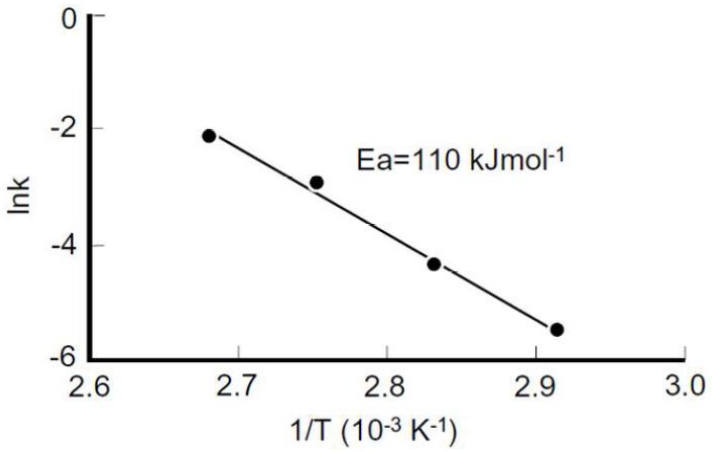

Figure 3-8. Arrhenius plots for the hydrolysis of cellulose into glucose in the presence of SO_3H-bearing carbon. Catalyst; 0.300 g, water; 0.700 g, cellulose; 0.250 g, reaction temperature; 343-373 K.

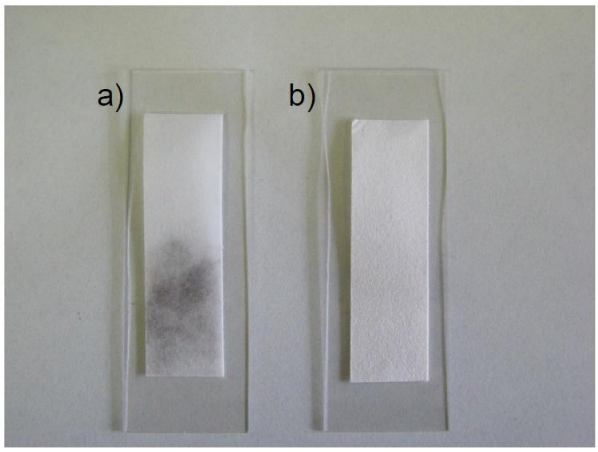

Figure 3-9. Filter papers (ADVANTEC 5A, cellulose > 99%) after soaking in solid acid-water suspensions (solid acid; 0.3 g, water; 0.7 g) at room temperature. (a) carbon material (particle size, 10–40 μm), (b) ground Amberlyst-15 (particle size, 5–70 μm). After half the filter paper was soaked in a solid acid-water suspension for 5 min, the filter paper with solid acid particles was rinsed five times in 100 cm^3 of distilled water in an ultrasonic bath for 10 min. Neither ground Amberlyst-15 particles (gray color) were observed by an optical microscope nor scanning electron microscope. H-mordenite and ground Nafion were not also adsorbed on the filter paper as well as Amberlyst-15.

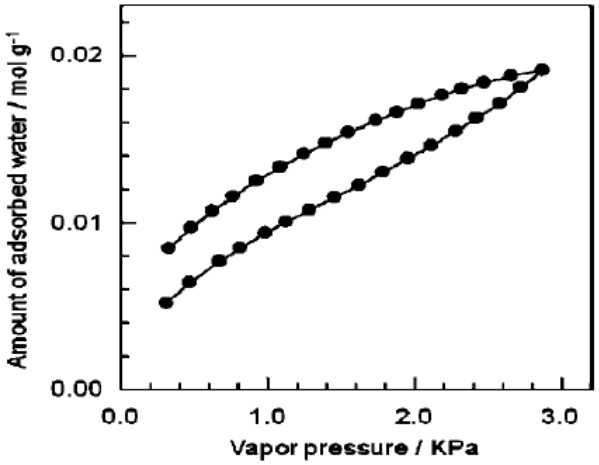

Figure 3-10. H_2O vapor adsorption-desorption isotherm of carbon material at 298 K.

Chapter 4

SO_3H-Bearing Amorphous Carbon derived from Polyvinyl Chloride as a Heterogeneous Acid Catalyst

4-1 Abstract

SO_3H-bearing amorphous carbon prepared from polyvinyl chloride (PVC) has been studied as a heterogeneous Brønsted acid catalyst. Sulfonation of partially carbonized PVC results in amorphous carbon consisting of small SO_3H-bearing carbon sheets linked by sp^3-based aliphatic hydrocarbons. This carbon material exhibits much higher catalytic performance for the hydrolysis of cellobiose than conventional heterogeneous Brønsted acid catalysts with SO_3H groups, including SO_3H-bearing amorphous carbon derived from cellulose. This can be attributed to a high density of SO_3H groups and the fast diffusion of reactants and products enabled by a flexible carbon network.

4-2 Introduction

Acid catalytic processes play a key role in the petroleum industry and in the manufacture of a wide variety of important chemicals, including pharmaceuticals, agrochemicals, and fragrances [1]. Most of these processes involve the use of homogeneous Brønsted acids (H_2SO_4, HF, HCl, and *p*-toluenesulfonic acid) in liquid-phase reactions, and subsequent neutralization leads to the generation of inorganic salts that ultimately end up in aqueous waste streams. An obvious solution to this problem is to replace traditional Brønsted acids with recyclable and highly active solid acids [1-3]. The use of solid acids facilitates the separation of catalyst from the reaction mixture and recycling, which results in a simpler process that reduces environmental impact. For this purpose, solid acid catalysts such as silica-alumina [4], zeolites [5], Cs-exchanged heteropolyacids [6], niobic acid [7], and strong ion-exchangeable resins [8] have been developed as replacements of homogeneous acids.

We have recently reported that SO_3H-bearing amorphous carbon materials can function as stable and highly active solid acid catalysts for various acid-catalyzed reactions with hydrophilic reactants, such as esterification [9-11], transesterification [11], and hydrolysis reactions [10,12,13]. These catalysts can be readily prepared by partial carbonization of organic compounds (D-glucose, starch, and cellulose), followed by sulfonation in fuming H_2SO_4 [9-13]. The materials consist of

small carbon sheets (*ca.* 1 nm) with high densities of SO_3H, COOH, and phenolic OH groups. The small carbon sheets are linked by sp^2 bonds, which provides a flexible carbon network, and high densities of hydrophilic functional groups bonded to the carbon sheets allow the smooth incorporation of large amounts of hydrophilic reactants and solvent into the carbon bulk, which results in high catalytic performance of the carbon material, despite the small surface area (up to 2 m^2 g^{-1}) [9-13]. Increased capability of the carbon material for the incorporation of hydrophilic molecules would therefore provide a higher activity alternative to homogeneous acid catalysts. The carbonization of polyvinyl chloride (PVC) produces an amorphous carbon containing polycyclic aromatic carbon sheets linked by aliphatic and olefinic hydrocarbon moieties [14]. A carbon network based on aliphatic hydrocarbons is expected to be more flexible than the typical carbon network based on sp^2 bonds. Thus, SO_3H-bearing amorphous carbon prepared by sulfonation of partially carbonized PVC may function as a more highly active heterogeneous Brønsted acid catalyst to enhance incorporation and the diffusion of reactants. In this study, SO_3H-bearing amorphous carbon prepared from PVC was studied as a heterogeneous Brønsted acid catalyst.

4-3 Experimental

Preparation of polyvinyl chloride (PVC)-derived amorphous carbon (PVC-AC)

Polyvinyl chloride (15.0 g) was pyrolyzed at 623, 673, and 723 K for 5 h under N_2 atmosphere to prepare the carbon precursors. 4.0 g of the obtained carbon precursor (powder) was heated at 353 K in 200 mL of 15 vol% fuming H_2SO_4 for 10 h under N_2 atmosphere to introduce SO_3H groups into the carbon sheets. The resulting black material was washed repeatedly with hot distilled water until the pH of the filtrate became neutral. Samples prepared at different carbonization temperatures (623, 673, and 723 K) are denoted as PVC-AC-623, PVC-AC-673 and PVC-AC-723, respectively.

Characterization of the materials

Structural information of the prepared carbon materials was obtained using Raman spectroscopy (NRS-3100, Jasco), X-ray diffraction (XRD; Ultima IV, Rigaku), ^{13}C cross-polarization (CP) magic angle spinning (MAS) nuclear magnetic resonance (NMR) spectroscopy (ASX-200, Bruker), and Fourier transform-infrared (FT-IR; FTIR-6100, Jasco) spectroscopy. ^{13}C CP/MAS NMR spectra were measured at room temperature with a Larmor frequency of 50.3 MHz using a Bruker MAS probehead with a 7 mm zirconia rotor. The spin rate used to obtain the spectra for PVC-ACs and cellulose-derived amorphous carbon bearing SO_3H groups (CAC) was 3.5 and 4.0 kHz, respectively. The frequency of the spectra is expressed with respect to pure tetramethylsilane. Experimentally, glycine was used as a second reference material with the carbonyl signal set at 176.48 ppm.

The amounts of SO_3H groups bonded to the carbon materials were estimated by elemental microanalysis (vario MICRO cube, Elemental) [12], and the acid strength of SO_3H groups bonded to the samples was examined using ^{31}P MAS NMR spectroscopy. Trimethylphosphine oxide

(TMPO) was adopted as a basic probe molecule in this study. Samples dehydrated by evacuation at 423 K for 4 h were added to a solution of TMPO in dichloromethane (CH_2Cl_2) at room temperature under an Ar atmosphere. After 2 days, the CH_2Cl_2 solvent was removed by vacuum evaporation and the TMPO-adsorbed samples were then packed into a rotor under a N_2 atmosphere. ^{31}P MAS NMR spectra of the TMPO-adsorbed samples were measured at room temperature using a spectrometer (ASX-400, Bruker) with a static magnetic field strength of 9.4 T. The Larmor frequency of ^{31}P was 162.0 MHz. The pulse sequence was a single-pulse sequence with high-power proton decoupling. A Bruker MAS probehead was used with a 4 mm zirconia rotor and a spin rate of 8 kHz. The ^{31}P chemical shift was referenced to 85% H_3PO_4 at 0.0 ppm. $(NH_4)_2HPO_4$ was used as a second reference material with the signal set at 1.33 ppm.

Nitrogen adsorption-desorption isotherms were measured at 77 K using a surface area analyzer (Nova 4200e, Quantachrome). Samples were pretreated at 423 K for 1 h under vacuum prior to measurement. The Brunauer-Emmet-Teller (BET) surface area was estimated over a relative pressure (P/P_0) range of 0.05 to 0.30. Water vapor adsorption-desorption isotherms were measured at 293 K using a volumetric adsorption equipment (Autosorb MP/VP, Quantachrome). Samples were pretreated at 423 K for 4 h under vacuum prior to measurement.

Acid-catalyzed reaction

Acid catalysis of the prepared materials was tested by the hydrolysis of cellobiose. Cellobiose (0.1 g) in water (10 mL) was reacted over the catalyst (0.2 g) at 373 K for 4 h. Samples of the reaction mixtures were taken at intervals and analyzed using high performance liquid chromatography (HPLC; LC-2000 plus, Jasco). For comparison, ion-exchange resins (Nafion resin NR50 and Amberlyst-15) and CAC, a heterogeneous strong Brønsted acid that can hydrolyze cellulose into glucose better than H_2SO_4 [12], were also tested under the same reaction conditions.

4-4 Results and discussion

Structure of prepared samples

Figure 4-1 shows the Raman spectrum for each sample after sulfonation. The spectra for all samples have two distinct signals at 1580 and 1350 cm^{-1} that are assignable to G (E_{2g} G mode) and D (A_{1g} D breathing mode) bands, respectively. These signals indicate the presence of polycyclic aromatic carbon sheets (graphene sheets) in the resulting materials [15]. The average size of graphene sheets for all samples was estimated from the intensity ratio of the G and D bands to be 1.3 nm [15]. XRD patterns for the samples are shown in Figure 4-2. Two broad and diffuse peaks at 22 and 44° observed in all XRD patterns are attributed to the graphitic (002) and (101) planes, respectively. These diffraction patterns reflect the amorphous carbon composed of graphene sheets arranged in a considerably random fashion [16]. ^{13}C CP/MAS NMR spectra for the PVC-ACs and CAC are presented in Fig. 4-3. An intense signal at 128 ppm, assignable to polycyclic aromatic carbon, was observed in all spectra. A definite peak was observed at 139 ppm in the spectra for both

PVC-AC-623 and 673. The resonance peak due to methylene groups appears in these samples at ca. 30 ppm; therefore, the peak at 139 ppm is due to polycyclic aromatic carbons bonded to methylene groups; carbon sheets linked by sp^3-derived hydrocarbons. However, these peaks due to methylene groups are not evident in PVC-AC-723 (Figure 4-3(c)), which indicates that sp^3-based linkages are thermally decomposed at carbonization temperatures above 673 K. The ^{13}C CP/MAS NMR spectrum for PVC-AC-723 suggests that most carbon sheets are linked by sp^2-bonds. While the resonance peaks of polycyclic aromatic carbon (128 ppm) and phenolic OH groups appear in the spectrum for CAC (Figure 4-3(d)), there is no signal of methylene groups, and thus CAC is composed of carbon sheets linked only by sp^2-bonds, which is distinct from PVC-AC-623 and 673. The signal for SO_3H-bonded aromatic carbon atoms (ca. 140 ppm) [17] is not distinguished in Figure 4-3, because peaks derived from aromatic carbon (130 ppm) or methylene groups (139 ppm) obscure the peak [9]. The presence of SO_3H groups in these samples was therefore directly confirmed by FT-IR. Figure 4-4 shows FT-IR spectra of the PVC-AC and CAC samples. Vibration bands at 1167 cm^{-1} (O=S=O symmetric stretching mode) and 1042 cm^{-1} (SO_3^- stretching mode) are evident in the FT-IR spectra and the amounts of SO_3H groups for each sample are summarized in Table 4-1. The PVC-AC samples have a larger amount of SO_3H groups than CAC. This can be attributed to the lack of phenolic OH groups in addition to aliphatic hydrocarbon moieties in the carbon precursor derived from PVC. CAC is synthesized by the sulfonation of partially carbonized cellulose, of which the carbon sheets possess a large amount of phenolic OH groups, because cellulose is a polymer of glucose with many OH groups. For this reason, CAC has a large amount of phenolic OH groups, as evident from the NMR spectrum of Figure 4-3(d); the density of phenolic OH groups in CAC reaches 2.0 mmol g^{-1}, which is larger than that of SO_3H groups [12]. The OH groups bonded to carbon sheets limit the introduction of SO_3H groups in CAC; however, the carbon precursor prepared from PVC has no phenolic OH groups, and therefore there are no phenolic OH groups in PVC-AC, as shown in Figure 4-3. Aliphatic hydrocarbon moieties linking carbon sheets in the carbon precursor prepared from PVC would also enhance the introduction of SO_3H groups to the carbon sheets as electron-donating groups.

The schematic structures of PVC-AC (PVC-AC-623 and 673) and CAC are illustrated in Figure 4-5. Sulfonation of partially carbonized PVC results in amorphous carbon containing small carbon sheets (*ca.* 1 nm) with a high density of SO_3H groups, and the carbon sheets are linked by aliphatic hydrocarbons. Some of the carbon sheets are likely to be linked by sp^2 bonds as well as general carbon network. Although the structure of PVC-AC is similar to that of CAC prepared from cellulose, the carbon sheets in the latter are linked only by sp^2 bonds. CAC has a lower density of SO_3H groups than PVC-AC, because CAC possesses a high density of phenolic OH groups.

Catalytic activity of PVC-AC

Table 4-1 summarizes the results for the hydrolysis of cellobiose into glucose in the presence of the tested catalysts. Cellobiose is a water-soluble β-1,4 glucan where two glucose molecules are linked by β-1,4 glycosidic bonds, as with cellulose, a water-insoluble long β-1,4 glucan. While many cellulases effectively hydrolyze cellulose into shorter cellooligosaccharides, they are not so

effective for the hydrolysis of cellobiose into glucose for biological reasons. The symmetry of cellobiose due to the β-1,4 glycosidic bonds makes the hydrolysis of cellobiose more difficult than that of maltose, an asymmetrical glucose dimer with α-1,4 glycosidic bonds. The catalysts tested were Amberlyst-15 (polystyrene-based cation-exchangeable resin with SO_3H), Nafion NR50 (perfluorosulfonated ionomer), CAC, and PVC-AC-623-723. Amberlyst-15 and Nafion NR-50 are strong polymer-based solid acids with high densities of SO_3H groups and very high activity for a range of reactions [8]. Nafion NR-50 and Amberlyst-15 can efficiently hydrolyze cellobiose into glucose, although CAC has higher catalytic activity for the same reaction due to a higher density of SO_3H groups with strong acid strength [12]. The turnover frequency (TOF) of SO_3H groups bonded to CAC is larger than that of Nafion NR-50 and Amberlyst-15. However, the PVC-AC catalysts surpass CAC in both glucose yield and TOF, which increase with the carbonization temperature, reaching a maximum at 673 K. Carbonization temperatures beyond 673 K slightly decrease the catalytic performance, because the increase in sp^2-based cross-linking among carbon sheets decreases the SO_3H density and limits the access of reactants to the SO_3H groups [10]. The results obtained for reuse experiments of PVC-AC-673 are presented in Figure 4-6. After reaction for 4 h at 373 K, particulate PVC-AC-673 could be readily separated from the reaction solution by decantation. The recovered catalyst was repeatedly evaluated for the hydrolysis of cellobiose at 373 K over 4 h. No decrease in activity was observed, even after several reuses of the catalyst, which indicates the carbon material functions as a highly active and stable heterogeneous catalyst.

Reactivity of SO_3H groups bonded to amorphous carbon

It should be noted that the TOFs for PVC-ACs given in Table 4-1 are larger than that for CAC, and the high catalytic performance of the PVC-ACs is due to the high densities of SO_3H groups with larger TOF. The high reactivity of the acid sites can be generally explained by acid strength; therefore, the acid strength of the SO_3H-bearing amorphous carbon was evaluated by measuring the adsorption of TMPO as basic probe molecules. Figure 4-7 shows ^{31}P MAS NMR spectra for TMPO-adsorbed on PVC-AC-673 and CAC. The amount of TMPO adsorbed corresponds to 10% of the amount of SO_3H groups in each sample. ^{31}P MAS NMR for solid acids with adsorbed TMPO has often been used to evaluate acid strength [18], and it is well-established that the resonance peak position of TMPO adsorbed on Brønsted acid sites is downshifted and the degree of the peak shift is directly dependent on the acid strength of the catalyst [19-21]. There is no significant difference in the NMR spectra of PVC-AC-673 and CAC, and thus the acid strength of the SO_3H groups in PVC-AC-673 is similar to that of CAC, which indicates that the high reactivity of PVC-AC cannot be explained by acid strength.

Another possible explanation for the high catalytic performance of PVC-AC is accessibility to the SO_3H groups by the reactants, which affects the diffusion of reactants and products into carbon bulk. To evaluate the accessibility of reactants to the SO_3H groups, the adsorption capability for hydrophilic molecules was examined by H_2O adsorption-desorption. SO_3H-bearing amorphous carbon can incorporate hydrophilic molecules into the bulk structure as with cation-exchangeable resins, and large incorporation or adsorption capability of hydrophilic molecules causes high

catalytic performance of SO_3H-bearing amorphous carbon materials, despite a small BET surface area [10]. Figure 4-8 shows H_2O adsorption-desorption isotherms for PVC-AC-673 and CAC at 293 K. Despite their small BET surface areas (<5 m^2 g^{-1}), both PVC-AC-673 and CAC can adsorb large amounts of H_2O vapor. Assuming that the adsorption cross sectional area of H_2O is 0.125 nm^2, the effective surface area of PVC-AC-673 and CAC at P/P_0=0.3 are estimated to be 869 and 657 m^2 g^{-1}, respectively. This suggests that PVC-AC-673 has a larger adsorption capability for hydrophilic molecules than CAC.

To further understand the reactivity of SO_3H groups bonded to amorphous carbon, time courses for the hydrolysis of cellobiose were investigated in detail. Figure 4-9 shows the time courses of cellobiose conversion and glucose yield over PVC-AC-673 and CAC. The glucose produced was not further decomposed into byproducts such as formic acid under the reaction conditions employed [12,13]. For PVC-AC-673, cellobiose conversion exceeds the glucose yield during the early stage of the reaction. However, the difference between cellobiose conversion and glucose yield decreases with reaction time and was nonexistent after 7 h. In contrast, the difference between cellobiose conversion and glucose yield over CAC did not narrow, even after 7 h. This indicates that the access of cellobiose molecules in solution to SO_3H groups in the carbon bulk, or the transfer of glucose produced from the carbon bulk to solution is more facile with PVC-AC-673 than with CAC, which results in the higher catalytic performance of PVC-AC-673. Such facile diffusion may be attributed to aliphatic hydrocarbons linking carbon sheets in PVC-AC. In CAC prepared by the sulfonation of carbonized cellulose, an increase in the carbonization temperature significantly decreases the catalytic performance, because the increase in sp^2 cross-linking among carbon sheets limits access of the reactants to SO_3H in the carbon bulk [10]. PVC-AC has a different carbon network from that of CAC; carbon sheets of PVC-AC are linked by sp^3-based aliphatic hydrocarbons. It is therefore expected that PVC-AC has a more flexible carbon network than CAC, which suggests that the higher reactivity of SO_3H groups in PVC-AC is due to fast diffusion of reactants.

4-5 Conclusion

SO_3H-bearing amorphous carbon prepared by sulfonation of partially carbonized PVC is composed of sulfonated carbon sheets linked by flexible aliphatic hydrocarbons, which is distinct from conventional SO_3H-bearing amorphous carbon where sulfonated carbon sheets are linked by rigid sp^2 bonds. The flexible carbon network derived from carbonized PVC facilitates the diffusion of reactants and enhances the reactivity of SO_3H groups bonded to the carbon sheets, which results in much higher catalytic performance than conventional SO_3H-bearing amorphous carbon.

References and notes

[1] Clark, J.M. *Acc. Chem. Res.* **2002**, *35*, 791-797.

[2] Sheldon, R.A.; Downing, R.S. *Appl. Catal., A* **1999**, *189*, 163-183.

[3] Tanabe, K.; Hölderich, W.F. *Appl. Catal., A* **1999**, *181*, 399-434.

[4] Boer, J.H.D.; Visseren, W.J. *Catal. Rev.* **1972**, *5*, 55-66.

[5] Corma, A. *J. Catal.* **2003**, *216*, 298-312.

[6] Okuhara, T. *Chem. Rev.* **2002**, *102*, 3641-3666.

[7] Nowak, I.; Ziolek, M. *Chem. Rev.* **1999**, *99*, 3603-3624.

[8] Harmer, M.A.; Sun, Q. *Appl. Catal., A* **2001**, *221*, 45-62.

[9] Okamura, M.; Takagaki, A.; Toda, M.; Kondo, J.N.; Tatsumi, T.; Domen, K.; Hara, M.; Hayashi, S. *Chem. Mater.* **2006**, *18*, 3039-3045.

[10] Fukuhara, K.; Nakajima, K.; Kitano, M.; Kato, H.; Hayashi, S.; Hara, M. *ChemSusChem* **2011**, *4*,778-784.

[11] Hara, M. *ChemSusChem* **2009**, *2*, 129-135.

[12] Suganuma, S.; Nakajima, K.; Kitano, M.; Yamaguchi, D.; Kato, H.; Hayashi, S.; Hara, M. *J. Am. Chem. Soc.* **2008**, *130*, 12787-12793.

[13] Kitano, M.; Yamaguchi, D.; Suganuma, S.; Nakajima, K.; Kato, H.; Hayashi, S.; Hara, M. *Langmuir* **2009**, 25, 5068-5075.

[14] Marongiu, A.; Faravelli, T.; Bozzano, G.; Dente, M.; Ranzi, E. *J. Anal. Appl. Pyrolysis* **2003**, 7*0*, 519-553.

[15] Ferrari, A.C.; Robertson, J. *Phys. Rev. B* **2000**, *61*, 14095-14107.

[16] Tsubouchi, N.; Xu, K.; Ohtsuka, Y. *Energy Fuels* **2003**, *17*, 1119-1125.

[17] Melero, J.A.; Grieken, R.V.; Morales, G.; Nũno, V. *Catal. Commun.* **2005**, *5*, 131-136.

[18] Baltusis, L.; Frye, J.S.; Maciel, G.E. *J. Am. Chem. Soc.* **1987**, *109*, 40-46.

[19] Rakiewicz, E.F.; Peters, A.W.; Wormsbecher, R.F.; Sutovich, K.J.; Mueller, K.T. *J. Phys. Chem. B* **1998**, *102*, 2890-2896.

[20] Karra, M.D.; Sutovich, K.J.; Mueller, K.T. *J. Am. Chem. Soc.* **2002**, *124*, 902-903.

[21] Zhao, Q.; Chen, W.H.; Huang, S.J.; Wu, Y.C.; Lee, H.K.; Liu, S.B. *J. Phys. Chem. B* **2002**, *106*, 4462-4469.

Table 4-1. Catalytic activity for the hydrolysis of cellobiose over PVC-ACs, CAC, Nafion NR50, and Amberlyst-15.

Catalyst	SO_3H groups[1] / mmol g^{-1}	Hydrolysis of cellobiose	
		Glucose Yield[2] (%)	TOF[2] / h^{-1}
Nafion NR-50	0.9	6.7	0.058
Amberlyst-15	4.8	7.0	0.011
CAC	1.8	17.7	0.078
PVC-AC-623	2.2	23.6	0.086
PVC-AC-673	2.3	30.1	0.105
PVC-AC-723	2.4	26.8	0.089

[1] Amount of SO_3H groups estimated by elemental analysis. [2] Turnover frequency at 4 h.

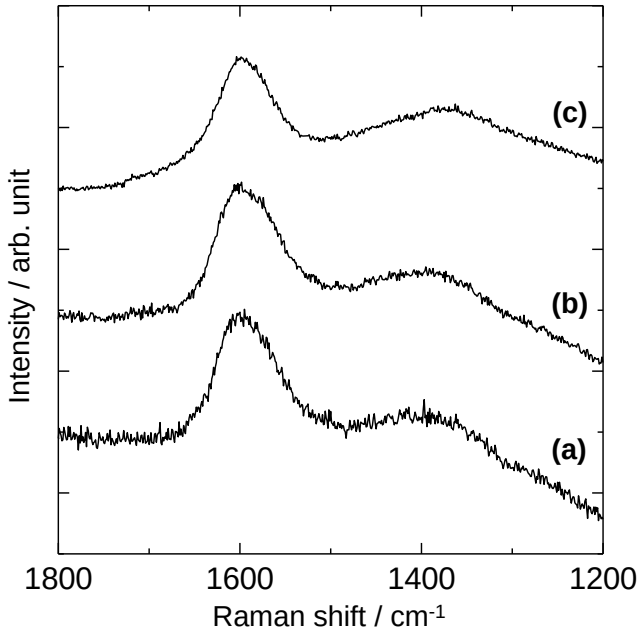

Figure 4-1. Raman spectra for (a) PVC-AC-623, (b) PVC-AC-673, and (c) PVC-AC-723.

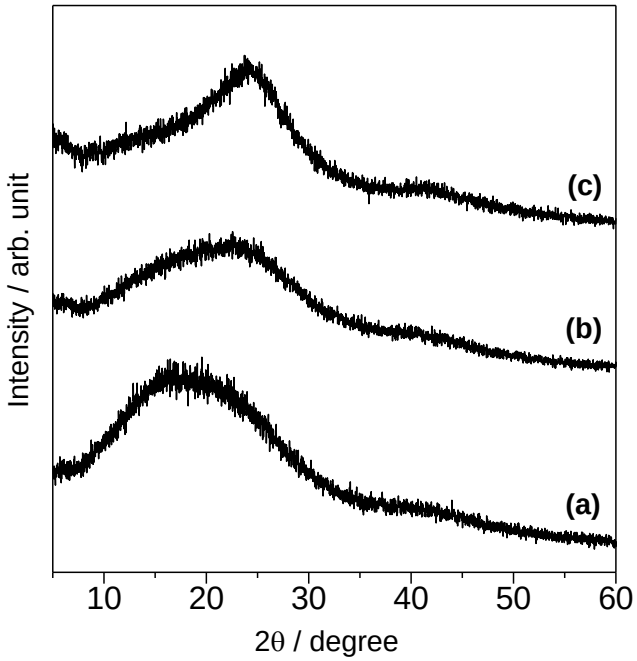

Figure 4-2. XRD patterns for (a) PVC-AC-623, (b) PVC-AC-673, and (c) PVC-AC-723.

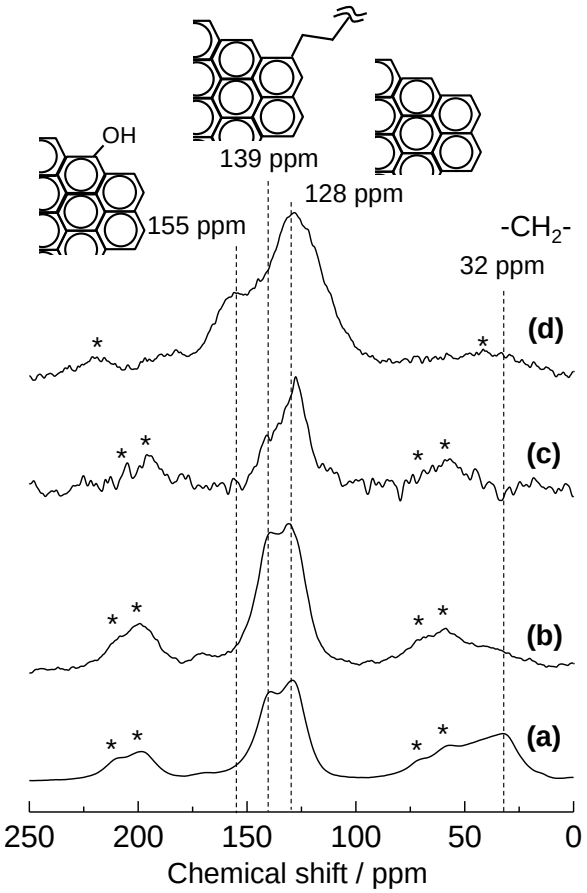

Figure 4-3. ^{13}C CP/MAS NMR spectra for (a) PVC-AC-623, (b) PVC-AC-673, (c) PVC-AC-723 and (d) CAC. * denotes spinning sideband.

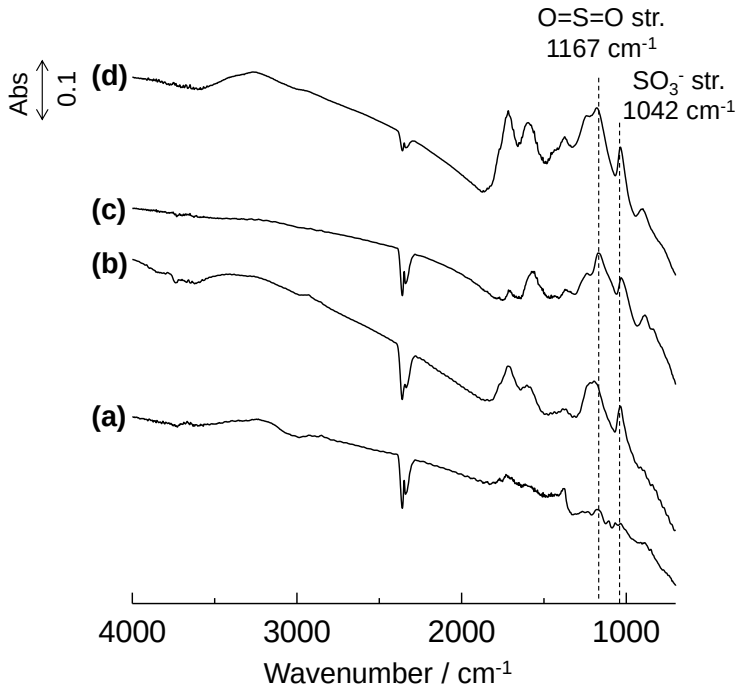

Figure 4-4. FT-IR spectra for the (a) PVC-AC-623, (b) PVC-AC-673, (c) PVC-AC-723, and (d) CAC.

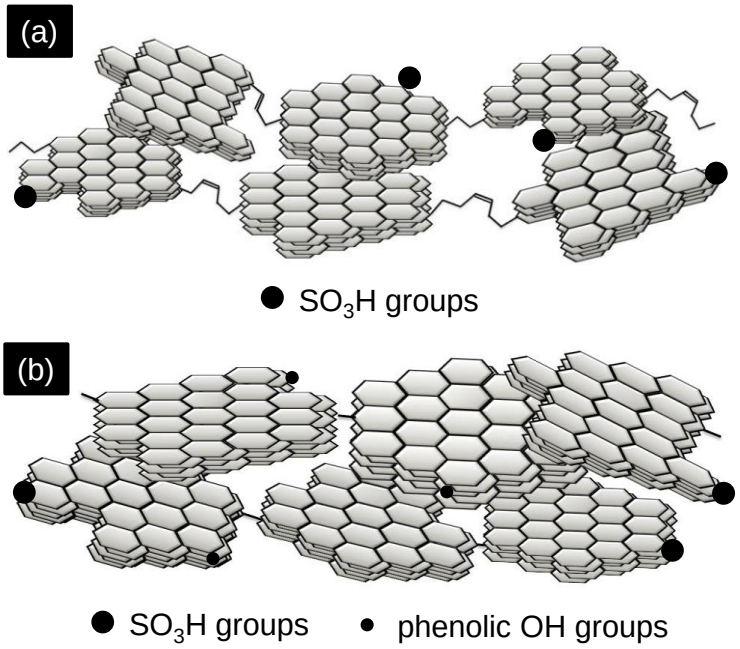

Figure 4-5. Schematic structure of (a) PVC-ACs and (b) CAC.

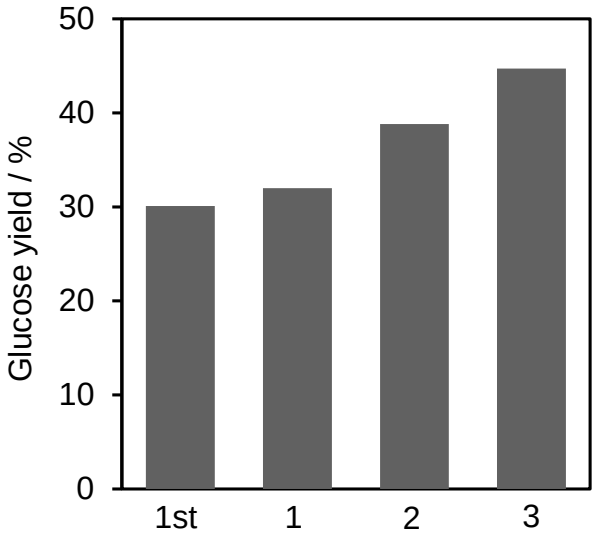

Figure 4-6. Catalyst reuse experiment for the hydrolysis of cellobiose over PVC-AC-673.

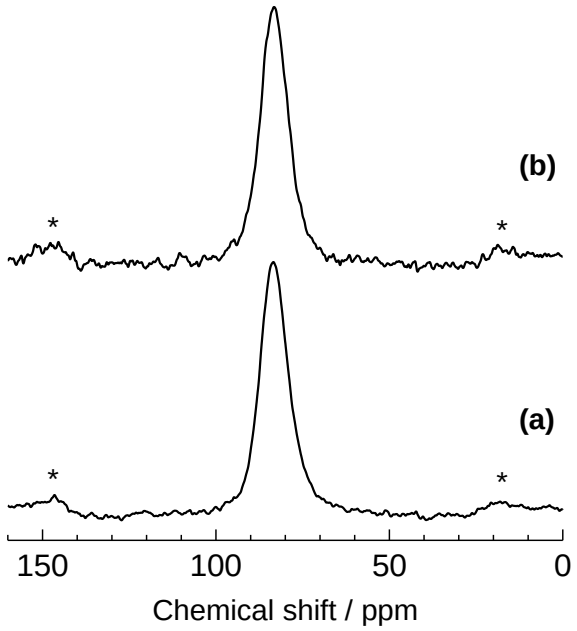

Figure 4-7. ^{31}P MAS NMR spectra for (a) PVC-AC-673 and (b) CAC after TMPO adsorption. The TMPO corresponding to 10 % of the amount of SO_3H group in each sample was adsorbed.
* denotes spinning sideband.

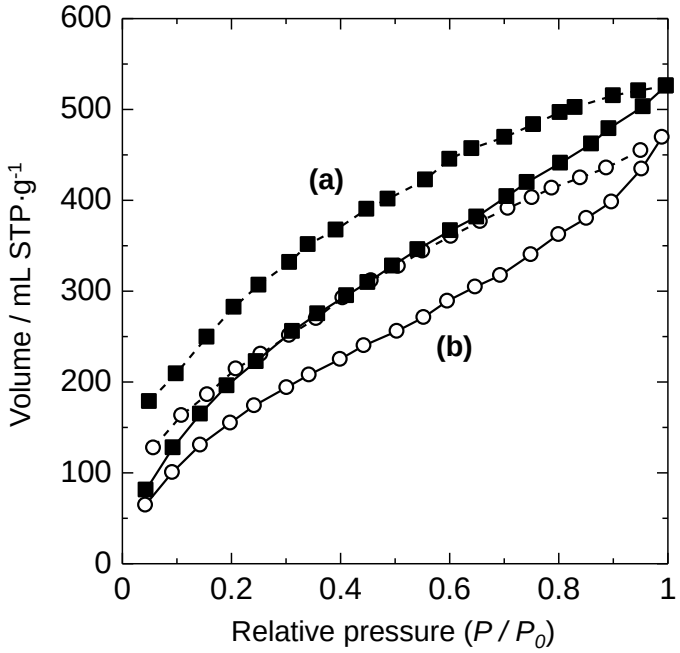

Figure 4-8. H_2O vapor adsorption-desorption isotherms for (a) PVC-AC-673 and (b) CAC.

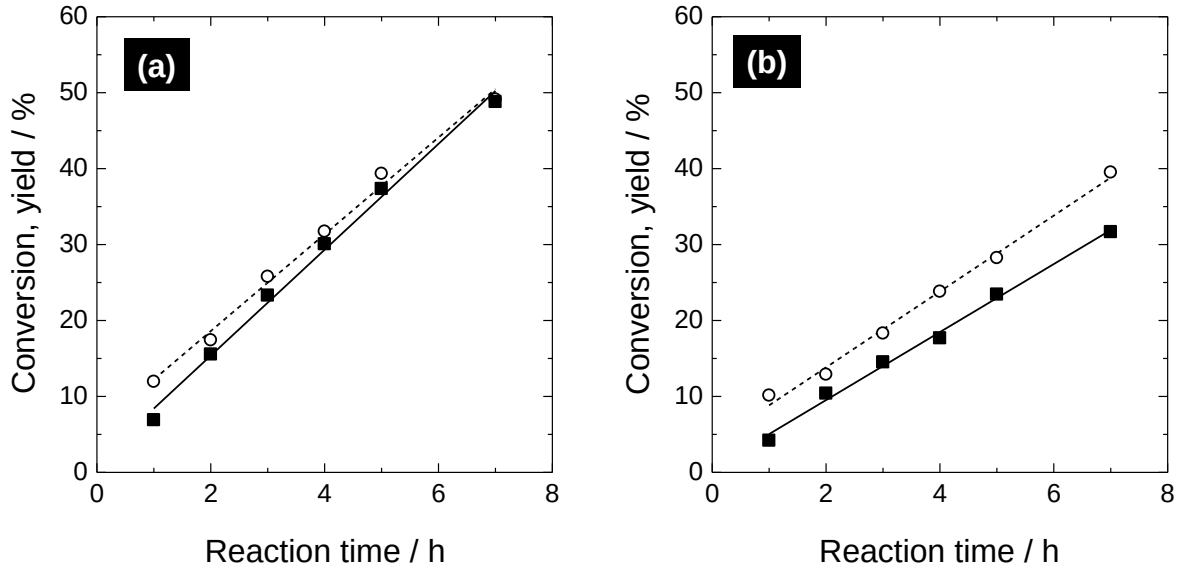

Figure 4-9. Time courses of cellobiose conversion (open circle) and glucose yield (filled square) for hydrolysis of cellobiose on (a) PVC-AC-673 and (b) CAC.

Chapter 5

SO_3H-bearing Mesoporous Carbon as a Highly Selective Catalysis

5-1 Abstract

A SO_3H-bearing mesoporous carbon material was investigated as a new type of heterogeneous catalyst. Carbonization of resorcinol-formaldehyde resin at 773 K, followed by sulfonation results in amorphous carbon consisting of graphene with high densities of SO_3H (0.9 mmol g^{-1}) and phenolic OH (2.0 mmol g^{-1}) groups. The mesoporous carbon that has a large surface area (433 m^2 g^{-1}) due to uniform mesopores (ca. 10 nm) exhibits remarkable catalytic performance for the selective dimerization of α-methylstyrene (AMS); the selectivity for unsaturated AMS dimers exceeds 99%. This catalysis is attributed to not only the large surface area based on large mesoporosity, but also to preventing intramolecular Friedel-Crafts alkylation.

5-2 Introduction

Homogeneous acids such as H_2SO_4 and HF have been widely used as acid catalysts for a large variety of industrial chemical processes. However, the use of these catalysts is hazardous and requires special energy-inefficient processes for the separation, recycling, and treatment of waste acid [1-3]. This has motivated the development of recyclable, easily separable, and highly active heterogeneous catalysts for the development of environmentally sustainable chemical processes. Over the years, a number of different types of solid acids have been developed as replacements for homogeneous liquid acids, ranging from sulfated zirconia [4], insoluble heteropolyacids [5], zeolites [6], and ion-exchangeable resins [7-11].

Recently, we have developed a new type of solid acid; an amorphous carbon consisting of nanosized carbon sheets with large amounts of SO_3H groups [12-21]. This material can be readily prepared by the partial carbonization of organic compounds (D-glucose, starch, and cellulose), followed by sulfonation in fuming H_2SO_4 solution [13-21]. SO_3H-bering amorphous carbons exhibited remarkable catalytic performance for various acid-catalyzed reactions with hydrophilic reactants, such as esterification [13-15,20,22], transesterification [21], hydration [14], and hydrolysis reactions [16-18]; the catalytic activity is much higher than that of conventional insoluble solid acid catalysts. The carbon material can incorporate large amounts of hydrophilic

reactants into the flexible carbon bulk, due to the high density of hydrophilic functional groups bonded to carbon sheets. Ready incorporation of reactants can enhance their accessibility to Brønsted acid sites in the carbon material, which results in high catalytic performance, despite the low surface area (ca. 2 $m^2 g^{-1}$) [13-18,21]. On the other hand, hydrophilic functional groups inside the carbon particles prevent the incorporation of hydrophobic reactants into the carbon bulk. Therefore, hydrophobic reactions do not proceed with SO_3H groups in the carbon bulk, which comprise most of the SO_3H groups in the carbon material, but proceed only on a small amount of surficial SO_3H groups on the low surface area. As a result, the carbon material exhibits poor or no catalytic activity for hydrophobic reactions.

Recently we reported SO_3H-bearing amorphous carbon deposited in the mosopores in SBA-15 [19]. The SO_3H-bearing amorphous carbon/mesoporous silica composite prepared by sulfonation of amorphous carbon deposited in SBA-15 has a large surface area (the surface area of deposited carbon material, > 900 $m^2 g^{-1}$) and shows high catalytic performance for hydrophobic reactions. However, such composite requires much effort to be synthesized and is unsuitable for large-scale catalyst production. In this study, the introduction of SO_3H groups into mesoporous carbon materials synthesized by carbonization of porous resins was adopted in order to develop an active carbon catalyst available for acid-catalyzed hydrophobic reactions. Hydrophobic reactants would readily access SO_3H groups on carbon mesopore walls in such materials, resulting in high catalytic performance. Resorcinol-formaldehyde (RF) resin is suitable as a starting material. The resin, which is composed of methylene (-CH_2-) and methylene ether (-CH_2-O-CH_2-), is a bridged phenolic compound can be simply synthesized from resorcinol and formaldehyde in the presence of an acid or base catalyst [23,24] and then converted into mesoporous carbon by carbonization, resulting in large surface area (400-1000 $m^2 g^{-1}$), large pore volume (<2 $cm^3 g^{-1}$), and uniform mesopore size (<10 nm) [24-27].

5-3 Experimental

Preparation of SO_3H-bearing mesoporous carbons

Resorcinol, formaldehyde (an aqueous solution of 36-37 wt% formaldehyde and 10-15 wt% methanol), and sodium carbonate (Na_2CO_3) were used for the preparation of RF aerogel [23-27]. The molar ratios of resorcinol to formaldehyde and resorcinol to sodium carbonate were 5 and 200, respectively. In a typical synthesis, 11.0 g of resorcinol, 16.5 mL of formaldehyde, and 0.053 g of Na_2CO_3 were added to 44.0 mL of distilled water. The solution was aged at room temperature for 3 days, followed by treatment at 353 K for 8 h for gradual conversion to an aerogel. The resulting aerogel was warmed in 150 mL of *tert*-butanol at 323 K for 8 h and was filtered three times to remove H_2O and methanol in the resin. The aerogel was dried at 333 K for 2 days under reduced pressure and was pyrolyzed at 523 K for 2 h under N_2 atmosphere to obtain the precursor. The resulting precursor was further heated at 573, 673, 773, or 973 K for 2 h under a N_2 atmosphere. Black powder obtained (4.0 g) was warmed in 200 mL of 15 vol% fuming H_2SO_4 at 353 K for 10 h

under N_2 atmosphere. The resulting material was washed repeatedly with hot distilled water until the pH of the filtrate became neutral. The samples prepared at different carbonization temperatures (573, 673, 773, and 973 K) are denoted as RF-573, RF-673, RF-773, and RF-973, respectively.

Characterization of the materials

Structural information of the prepared carbon materials was obtained using thermogravimetric (TG) analysis (TG8120, Rigaku), Raman spectroscopy (NRS-3100, Jasco), X-ray diffraction (XRD, Ultima IV , Rigaku), ^{13}C cross-polarization (CP) magic angle spinning (MAS) nuclear magnetic resonance (NMR), Fourier transform-infrared (FT-IR, FTIR-6100, Jasco) spectroscopy, N_2 adsorption analysis, and scanning electron microscopy (SEM). ^{13}C CP/MAS NMR spectra were measured at room temperature using a Bruker ASX-200 spectrometer at a Larmor frequency of 50.3 MHz. A Bruker MAS probehead was used with a 7-mm zirconia rotor. The spin rate used to obtain the spectra was 4.0 kHz. The frequency of the spectra is expressed with respect to pure tetramethylsilane. Experimentally, glycine was used as a second reference material, with a carbonyl signal set at 176.48 ppm. Nitrogen adsorption-desorption isotherms were measured at 77 K using a surface area analyzer (Nova 4200e, Quantachrome). Prior to the measurement, the samples were pretreated at 423 K for 1 h under vacuum. The Brunauer-Emmet-Teller (BET) surface area was estimated over a relative pressure (P/P_0) range of 0.05 to 0.30. The pore size distribution was obtained from analysis of the adsorption branch of the isotherms using the Barrett-Joyner-Halenda (BJH) method. SEM images were obtained using an ultra-high-resolution SEM system (S-5200, Hitachi) without metal deposition.

The amounts of functional groups bonded to the prepared materials were estimated by elemental microanalysis (vario MICRO cube, Elemental) and cation-exchange analysis [16]. The densities of the SO_3H groups were estimated based on the sulfur content determined from sample compositions obtained by elemental analysis. The total contents of SO_3H + COOH groups and SO_3H + COOH + phenolic OH groups were estimated from the exchange of Na^+ in aqueous NaCl and NaOH solutions, respectively. The amount of phenolic OH groups was afforded from the difference between the two results [16].

The acid strength of the prepared catalysts was examined by ^{31}P MAS NMR spectroscopy. Trimethylphosphine oxide (TMPO)-adsorbed samples were prepared in CH_2Cl_2. Samples were pretreated by evacuation at 423 K for 1 h and soaked overnight in a CH_2Cl_2 solution containing an adequate amount of TMPO at room temperature under an Ar atmosphere. After evaporation to remove the CH_2Cl_2 solvent, the TMPO-adsorbed samples were then packed into a rotor under a N_2 atmosphere. ^{31}P MAS NMR spectra of the TMPO-adsorbed materials were measured using a Bruker ASX-400 spectrometer at a Larmor frequency of 162.0 MHz. A Bruker MAS probehead was used with a 4-mm zirconia rotor. The spin rate used to obtain the spectra was 8.0 kHz. The frequency of the spectra was expressed with respect to 85% H_3PO_4. Experimentally, $(NH_4)_2HPO_4$ was used as a second reference material, with the carbonyl signal set at 1.33 ppm.

Acid-catalyzed reaction

Acid catalysis of the prepared materials was tested by the dimerization of AMS. For comparison, ion-exchange resins (Nafion resin NR50, Nafion-silica composite SAC-13, and Amberlyst-15) and cellulose-derived bulky amorphous carbon bearing SO_3H and phenolic OH groups (CAC) were also tested under the same reaction conditions. Prior to reaction, all catalysts were dehydrated by heating at 373-423 K for 1 h. AMS (25 mmol) in cumene (31.32 mL) was reacted over the catalyst (0.2 g) at 308 K for 16 h. Samples from the reaction mixtures were withdrawn at intervals and analyzed using gas chromatography (GC-16A, Shimadzu) with a capillary column.

The effect of phenolic OH groups on the selectivity toward unsaturated dimers was examined over a H_2SO_4 catalyst by the addition of p-cresol to the reaction mixture. AMS (25 mmol) in cumene (31.32 mL) was reacted with concentrated H_2SO_4 (0.1 g) at 298 K for 2 h in the presence or absence of *p*-cresol (2.4 mL).

5-4 Results and discussion

Structure of SO_3H-bearing mesoporous carbons

The pyrolysis behavior of RF resin was firstly studied with TG analysis at a heating rate of 10 K min^{-1} under N_2 flowing condition. The TG profile of RF resin in Figure 5-1 shows weight loss of approximately 11 wt% at 340–450 K, which can be attributed to desorption of physisorbed water and decomposition of small organic molecules such as aliphatic hydrocarbons [27]. Further heating decreases the sample weight down to 55%, reaching a plateau. The carbonization of the resin, therefore, starts at around 600 K under N_2 flowing condition.

Figures 5-2 and 5-3 show Raman spectrum and XRD pattern for each sample after sulfonation. The Raman spectra for all prepared samples have two distinct signals at 1580 and 1350 cm^{-1} that are assignable to G band (E_{2g} G mode) and D band (A_{1g} D breathing mode), respectively. These signals indicate the presence of polycyclic aromatic carbon sheets (graphene sheets) in the resulting materials [28,29]. The average size of graphene sheets for the materials can be estimated with the intensity ratio of G and D bands to be 1.3 nm [28]: there is no significant difference in average graphene size among samples. Because graphitization of carbon framework would need severe carbonization temperature at > 1473 K [30,31], the formation of cross-linking network among graphene sheets is expected to proceed during carbonization in preference to increase in carbon sheet size under the carbonization condition. Two broad and weak peaks at 22 and 44° observed in all XRD patterns are attributed to graphitic (002) and (101) planes, respectively. These diffraction patterns reflect amorphous carbon composed of graphene sheets in a considerably random fashion [32].

Figure 5-4 displays ^{13}C CP/MAS NMR spectra for the samples. The spectra for RF-573 and RF-673 in Figs. 5-4(b) and (c) are similar to that of the original RF resin (Fig. 5-4(a)). An intense and broad signal at 100-140 ppm composed of three resonances, a symmetric signal at 153 ppm and broad signals at 15 and 30 ppm are assignable to fundamental aromatic carbons of the cross-linked resorcinol ring (2-4), phenolic carbon (1) and different types of methylene bridges (5 and 6), as

shown in the inset of Fig. 5-4 [33]. This means that the original skeleton of the resin reflects the sample structure in the case of mild carbonization. The resonance signals due to aromatic carbons of the cross-linked resorcinol ring, phenolic carbon and methylene bridges decrease with increasing carbonization temperature (Fig. 5-4(d)), and only the broad signal due to aromatic rings is observed at 973 K. The RF-573 and RF-673 samples are therefore regarded as a mixture of polycyclic aromatic carbon (or amorphous carbon) and RF resin, rather than pure carbon material. The RF-773 and RF-973 samples are amorphous carbon, and the former has larger amounts of phenolic OH groups than the latter. The signal due to Ar-SO_3H is not distinguished in these spectra, because it is obscured by the broad peak for polycyclic aromatic carbon (129 ppm) [14]. The presence of SO_3H groups in these samples was directly confirmed by FT-IR spectroscopy (Fig. 5-5). The vibration bands at 1167 (O=S=O symmetric stretching mode in SO_3H) and 1042 cm^{-1} (SO^{3-} stretching mode) are clearly observed in the FT-IR spectra (Figs. 5-5(a)-(d)). The band due to OH bending (ca. 1600 cm^{-1}) that appears for RF-773 (Fig. 5-5(c)) is not observed in the spectrum for RF-973, which is consistent with the ^{13}C CP/MAS NMR results. These results indicate that RF-773 consists of carbon sheets with both SO_3H and phenolic OH groups. While RF-973 is also expected to possess SO_3H and OH groups, the density of OH groups is smaller than that of RF-773.

Figure 5-6 shows N_2 adsorption-desorption isotherms (A) and BJH pore size distribution curves (B) for the samples. The isotherms for RF-773 and RF-973 (Figs. 5-6A(c) and (d)) are typical type-IV patterns with a H1 type hysteresis loop, which is characteristics for mesoporous materials [34]. The sharp and large N_2 uptake over a narrow P/P_0 range (P/P_0 = 0.4-0.8) of the adsorption isotherms for these samples reflects uniform mesopores (8.5 and 5.0 nm) with a narrow size range in the corresponding pore size distribution curves (Figs. 5-6B(c) and (d)). The BET surface areas of RF-773 and RF-973 are ca. 430 and 360 $m^2\ g^{-1}$, respectively. On the other hand, RF-573 and RF-673 show no clear hysteresis loop and are therefore regarded as nonporous amorphous carbon with BET surface areas of ca. 1 $m^2\ g^{-1}$ and 59 $m^2\ g^{-1}$, respectively. Mesoporosity of RF-573 and RF-673 was confirmed to be drastically collapsed during sulfonation. Table 5-1 shows BET surface areas and mesopore volumes for the carbon precursors before and after sulfonation. All carbon precursors have larger BET surface areas and mesopore volumes than the original RF-resin (301 $m^2\ g^{-1}$ and 0.28 mL g^{-1}). The BET surface area and pore volume of RF-573 and RF-673 are smaller than those of the corresponding carbon precursors. RF-573 and RF-673 contain certain amounts of RF resin in the framework; therefore, further shrinkage and/or carbonization would proceed during severe sulfonation treatment in fuming H_2SO_4, which would result in degradation of the original mesoporosity. In contrast, the RF-773 and RF-973 samples have large BET surface areas and mesopore volumes even after sulfonation. Because RF-773 and RF-973 consist mainly on amorphous carbon with graphene sheets, the mesoporosity of these samples remains unchanged even after severe sulfonation.

The morphology of the samples was observed by SEM. The SEM image for RF-573 in Fig. 5-7(A) shows a smooth and flat surface on a large particle (ca. 20-40 μm), which indicates the formation of bulk carbon. RF-673, RF-773, and RF-973 have rather rough surfaces. Mesopores are not observed in RF-673 (Fig. 5-7(B)) but only in the RF-773 and RF-973 samples (Figs. 5-7(C) and

7(D)), which is consistent with the results of the N_2 adsorption-desorption isotherms and pore size distribution curves.

Catalytic performance of the SO_3H-bearing mesoporous carbon

The acid catalytic activity of the prepared carbon materials has been demonstrated through the dimerization of AMS. Acid-catalyzed AMS dimerization produces a mixture of valuable unsaturated dimers (2,4-diphenyl-4-methyl-1-pentene (III) and 2,4-diphenyl-4-methyl-2-pentene (IV)) and an undesirable saturated dimer (1,1,3-trimethyl-3-phenylindan (V)), as shown in Fig. 5-8 [35-38]. The unsaturated dimers synthesized by this reaction are industrially important chemicals that are used as chain-transfer agents or molecular weight regulators in the syntheses of acrylonitrile-butadiene-styrene (ABS) resin and styrene-butadiene-rubber (SBR) [35,36]. In the catalytic reaction, protonated AMS (I) is reacted with an AMS monomer to form a dimeric carbocation intermediate (II). The intermediate is transformed into two dimeric pentene derivates (III and IV) by equilibrium E1 reactions, and irreversibly into the cyclic indan derivate (V) by intramolecular Friedel-Crafts alkylation (S_N1 reaction).

The catalytic activities for AMS dimerization together with the structural parameters of the samples are summarized in Table 5-2. In the presence of sulfuric acid, most of the AMS is converted into the undesirable saturated cyclic indan, because the intramolecular Friedel-Crafts alkylation occurs parallel to the equilibrium E1 reactions of the carbocation intermediate (Fig. 5-8 (II)). CAC (cellulose-derived carbon-based solid acid) prepared by sulfonation of partially carbonized cellulose [16] and the commercially-available Nafion NR-50 [8,11], Nafion SAC-13 (Nafion-deposited SiO2) [9-11], and Amberlyst-15[7,8,11] ion-exchangers were used for comparison. These conventional polymer-based strong solid acids with high densities of SO_3H groups can act as highly active solid acids for a variety of reactions [7-11]. While Nafion NR-50 does not function as an efficient catalyst for AMS dimerization, due to its small surface area, Nafion SAC-13 and Amberlyst-15 with relatively large surface areas result in better AMS conversion. The selectivities for the objective unsaturated dimers of these two conventional solid acids are 59% and 8%, which indicates that these resin catalysts form the saturated cyclic indan in parallel with the unsaturated dimers, as is the case for sulfuric acid. In contrast to CAC, RF-573 and RF-673, RF-773 exhibits remarkable catalytic performance; AMS conversion and unsaturated dimers selectivity exceed 86% and 99%, respectively. The results for the catalyst reuse experiment of RF-773 are shown in Figure 5-9. While the catalytic activity decreases with reuse experiment, most of SO_3H groups retains intact after 4th runs. Decrease in catalytic activity is probably due to adsorbed reactant and/or product on SO_3H groups that prevents access of reactant to SO_3H groups [39]. On the other hand, RF-973 does not catalyze the reaction at all although this sample has sufficient amount of SO_3H groups and large surface area due to mesopores. These results suggest the high AMS conversion is simply attributed to neither large surface area nor the amount of SO_3H groups. The difference in catalytic performance for these two samples would depend on the acid strength and/or the accessibility of introduced SO_3H groups.

The acid strength of the solid acid catalysts was evaluated using ^{31}P MAS NMR spectroscopy

for samples treated with trimethylphosphine oxide (TMPO) as a basic probe molecule [40]. The advantage of using phosphorus molecules over other basic probes, such as pyridine and acetonitrile, is associated with the higher sensitivity and wider chemical shift range of ^{31}P resonance in the NMR spectrum [41]. It is well-established that the peak position of TMPO adsorbed on a Brønsted acid site is downshifted and the degree of peak shift is directly dependent on the acid strength of the catalyst [42-44]. Figure 5-10 shows ^{31}P MAS NMR spectra of CAC, RF-773, and RF-973. The chemical shift for TMPO-adsorbed CAC appears at 83 ppm (Fig. 5-10(a)) that is attributed to TMPO adsorbed on SO_3H groups. The spectrum for RF-773 (Fig. 5-10(b)) exhibits three distinct signals at 78, 63, and 41 ppm that are assignable to the SO_3H-adsorbed TMPO, phenolic OH-adsorbed TMPO, and self-aggregated TMPO on the solid surface, respectively [14,16]. In the case of RF-973, only one signal appears at 41 ppm (Fig. 5-10(c)), indicating that the introduced TMPO in the CH_2Cl_2 cannot interact with SO_3H or the phenolic OH groups in RF-973, despite the large surface area (361 $m^2 g^{-1}$): there are no SO_3H groups available for the hydrophobic reaction on the carbon mesopore walls in RF-973. Therefore, RF-973 does not catalyze the reaction at all in AMS dimerization. From the ^{31}P MAS NMR spectra in Fig. 5-10, 0.2 mmol g^{-1} of SO_3H group in RF-773 is estimated to react with TMPO. However, SO_3H group of RF-973 cannot adsorb TMPO at all. This suggests that the high AMS conversion depends on the amount of accessible SO_3H groups, rather than large surface area.

To investigate the difference in catalytic performance among RF-773, Amberlyst-15, and Nafion SAC-13, the dependence of AMS conversion and yields of two unsaturated dimers and saturated cyclic indan on reaction time was examined (Figure 5-11). Most of AMS was converted over Amberlyst-15 and Nafion SAC-13 with a short reaction time under the reaction condition (Figs. 5-11(A) and (B)). The unsaturated dimers and saturated cyclic indan were formed over Amberlyst-15 in the initial stage of the reaction. However, the evolved unsaturated dimers were gradually converted into indan, and the yield of unsaturated dimers is reduced to 8% after 15 h (Fig. 5-11(A)). This indicates that the intramolecular Friedel-Crafts alkylation proceeded continuously over Amberlyst-15. Nafion SAC-13 also formed both two unsaturated dimers and saturated cyclic indan at initial 3 h (Fig. 5-11(B)). While Nafion SAC-13 produced the unsaturated dimers larger than saturated cyclic indan, final yield toward unsaturated dimer was moderate (59%). This suggests that Nafion SAC-13 promotes E1 reaction in parallel with S_N1 reaction. In contrast to these conventional solid acid catalysts, most of AMS was directly converted into the unsaturated dimers over RF-773, and the final yield of two unsaturated dimers reached 86% (Fig. 5-11(C)). Apparently, the selective production of the unsaturated dimers in AMS dimerization by RF-773 can be attributed to the blocking of intramolecular Friedel-Crafts alkylation. As a result, AMS dimerization on RF-773 depends largely not only on both a large surface area based on large mesoporosity and ready access of reactants to SO_3H groups on the carbon walls in mesopores, but also on E1 reaction in preference to S_N1.

Many elimination reactions have been conducted in protic media and the olefin yield usually increases along the series H_2O < ethanol < isopropyl alcohol < *tert*-butanol, in order of decreasing nucleophilicity [45]. The solvent stabilizes the carbocation intermediates by solvolysis and

decreases the reactivity for the S_N1 reaction. In the present catalytic system, a high density of phenolic OH groups attached to carbon sheets may contribute to the stabilization of carbocation intermediates. The effect of phenolic OH groups on the selectivity toward unsaturated dimers was examined over a H_2SO_4 catalyst by the addition of p-cresol to the reaction mixture. Figure 5-12 shows time courses for AMS conversion and yield of products over H_2SO_4 in the presence and absence of *p*-cresol at 298 K. AMS was simultaneously converted into saturated cyclic indan over H_2SO_4 in the absence of *p*-cresol, as was the case for Amberlyst-15, and the final selectivity toward the unsaturated dimers was moderate (11%), as shown in Fig. 5-12(A). On the other hand, the selectivity for unsaturated dimers was largely improved in the presence of *p*-cresol; the selectivity reached ca. 72% in the early stage of the reaction (Fig. 5-12(B)), clearly indicating that the phenolic OH groups in *p*-cresol prevents intramolecular Friedel-Crafts alkylation by solvolysis. Thus, the high selectivity of RF-773 can be attributed to phenolic OH groups that restrict intramolecular Friedel-Crafts alkylation (S_N1 reaction) and promote the E1 reaction.

SO_3H-bearing amorphous carbon/mesoporous silica composite that had been reported also shows high catalytic performance for the reaction: the AMS conversion and desirable dimers selectivity are comparable to those of RF-773 [19]. The composite catalysts has larger surface areas (600-1000 m^2 g^{-1}) and mesopore volumes (0.4-1.2 mL g^{-1}) than SO_3H-bearing mesoporous carbon prepared from RF resin, indicating that the reaction does not depend only on surface area and pore volume. SO_3H-bearing amorphous carbon/mesoporous silica composite also possesses phenolic OH and silanol (Si-OH) groups [19]. The amounts of accessible SO_3H groups on amorphous carbon is crucial factor for promoting the AMS dimerization efficiently as mentioned above. High catalytic performance on RF-773 and carbon/mesoporous silica composite is therefore attributed to OH groups that restrict the conversion of unsaturated dimers by S_N1 reaction, in addition to large surface area, pore volume and the amounts of accessible SO_3H groups.

5-5 Conclusion

SO_3H-bearing mesoporous carbon prepared by sulfonation of RF resin carbonized at 773 K selectively converts AMS into unsaturated dimers (ca. 99%). The high catalytic performance of the mesoporous carbon is attributed to the large surface area and mesoporosity, which provides high accessibility of hydrophobic reactants in solution to SO_3H, and a high density of phenolic OH groups bonded to the carbon that prevent side reactions (intramolecular Friedel-Crafts alkylation) by stabilization of the dimeric carbocation intermediate.

References and notes

[1] J.A. Cusumano, *Chemtech.*, **1992**, 482-489.

[2] K. Tanabe, *Appl. Catal. A,* **113** (1994) 147-152.

[3] J.M. Clark, *Green. Chem.*, **1** (1999) G1-G2.

[4] B.M. Reddy, M.K. Patil, *Chem. Rev.*, **109** (2009) 2185-2208.

[5] N. Mizuno, M. Misono, *Chem. Rev.*, **98** (1998) 199-218.

[6] A. Corma, *Adv. Mater.*, **7** (1995) 137-144.

[7] K. Kun, R. Kunin, *J. Polym. Sci. Part A*, **6**, (1968), 2689-2701.

[8] D.C. Kennedy, *Ind. Eng. Chem. Prod. Dev.* **12** (1973) 56-61.

[9] M.A. Harmer, W.E. Farneth, Q. Sun, *J. Am. Chem. Soc.*, **118** (1996) 7708-7715.

[10] M.A. Harmer, Q. Sun, A.J. Vega, W.E. Farneth, A. Heidekum, W.F. Hoelderich, *Green Chem.*, **2** (2000) 7-14.

[11] M.A. Harmer, Q. Sun, *Appl. Catal. A*, **221** (2001) 45-62.

[12] M. Hara, T. Yoshida, A. Takagaki, T. Takata, J.N. Kondo, S. Hayashi, K. Domen, *Angew. Chem. Int. Ed.*, **43** (2004) 2955-2958.

[13] M. Toda, A. Takagaki, M. Okamura, J.N. Kondo, S. Hayashi, K. Domen, M. Hara, *Nature*, **438** (2005) 178.

[14] M. Okamura, A. Takagaki, M. Toda, J.N. Kondo, T. Tatsumi, K. Domen, M. Hara, S. Hayashi, *Chem. Mater.*, **18** (2006) 3039-3045.

[15] A. Takagaki, M. Toda, M. Okamura, J.N. Kondo, K. Domen, S. Hayashi, M. Hara, *Catal. Today*, **116** (2006) 157-161.

[16] S. Suganuma, K. Nakajima, M. Kitano, D. Yamaguchi, H. Kato, S. Hayashi, M. Hara, *J. Am. Chem. Soc.*, **130** (2008) 12787-12793.

[17] D. Yamaguchi, M. Kitano, S. Suganuma, K. Nakajima, H. Kato, M. Hara, *J. Phys. Chem. C*, **113** (2009) 3181-3188.

[18] M. Kitano, D. Yamaguchi, S. Suganuma, K. Nakajima, H. Kato, S. Hayashi, M. Hara, *Langmuir*, **25** (2009) 5068-5075.

[19] K. Nakajima, M. Okamura, J.N. Kondo, K. Domen, T. Tatsumi, S. Hayashi, M. Hara, *Chem. Mater.*, **21** (2009) 186-193.

[20] M. Kitano, K. Arai, A. Kodama, T. Kousaka, K. Nakajima, S. Hayashi, M. Hara, *Catal. Lett.*, **131** (2009) 242-249.

[21] M. Hara, *ChemSusChem*, **2** (2009) 129-135.

[22] X. Tian, F. Su, X.S. Zhao, *Green Chem.* **10** (2008) 951-956.

[23] R.W. Pekala, *J. Mater. Sci.*, **24** (1989) 3221-3227.

[24] S.A. Al-Muhtaseb, J.A. Ritter, *Adv. Mater.*, **15** (2003) 101-114.

[25] S.Q. Zhang, J. Wang, J. Shen, Z.S. Deng, Z.Q. Lai, B. Zhou, S.M. Attia, L.Y. Chen, *Nanostruct. Mater.*, **11** (1999) 375-385.

[26] Y. Yamamoto, T. Nishimura, T. Suzuki, H. Tamon, *J. Non-Cryst. Solids*, **288** (2001) 46-55.

[27] A. Lu, B. Spliethoff, F. Schüth, *Chem. Mater.*, **20** (2008) 5314-5319.

[28] A.C. Ferrari, J. Robertson, *Phys. Rev. B*, **61** (2000) 14095-14107.

[29] C. Casiraghi, A.C. Ferrari, J. Robertson, *Phys. Rev. B*, **72** (2005), 085401.

[30] C. Liang, K. Hong, G. A. Guiochon, J. W. Mays, *Angew. Chem. Int. Ed.*, **43** (2004) 5785-5789.

[31] Y. Meng, D. Gu, F. Zhang, Y. Shi, L. Cheng, D. Feng, Z. Wu, Z. Chen, Y. Wan, A. Stein, D. Zhao, *Chem. Mater.*, **18** (2006) 4447-4464.

[32] N. Tsubouchi, K. Xu, Y. Ohtsuka, *Energy Fuels*, **17** (2003) 1119-1125.

[33] S. Mulik, C. Sotiriou-Leventis, N. Leventis, *Chem. Mater.*, **19** (2007) 6138-6144.

[34] M. Kruk, M. Jaroniec, *Chem. Mater.*, **13** (2001) 3169-3183.

[35] B. Chaudhuri, M.M. Sharma, *Ind. Eng. Chem. Res.*, **28** (1989) 1757-1763.

[36] Q. Sun, W.E. Farneth, *J. Catal.*, **164** (1996) 62-69.

[37] M. Fujiwara, K. Kurokawa, T. Yazawa, Q. Xu, M. Tanaka, Y. Souma, *Chem. Commun.*, **16** (2000) 1523-1524.

[38] M. Fujiwara, S. Terashima, Y. Endo, K. Shiokawa, H. Ohue, *Chem. Commun.*, **44** (2006) 4635-4637.

[39] D.E. López, J. G. Goodwin Jr., D. A. Bruce, E. Lotero, *Appl. Catal. A: Gen.* **295** (2005) 97-105.

[40] L. Baltusis, J.S. Frye, G.E. Maciel, *J. Am. Chem. Soc.*, **109** (1987) 40-46.

[41] G.E. Maciel, P.D. Ellis, In *NMR Technique in Catalysis* (Eds.: A.T. Bell, A. Pines), Marcel Dekker, New York, (1994) pp 231-309.

[42] E.F. Rakiewicz, A.W. Peters, R.F. Wormsbecher, K.J. Sutovich, K.T. Mueller, *J. Phys. Chem. B* **102** (1998) 2890-2896.

[43] M.D. Karra, K.J. Sutovich, K.T. Mueller, *J. Am. Chem. Soc.* **124** (2002) 902-903.

[44] Q. Zhao, W.H. Chen, S.J. Huang, Y.C. Wu, H.K. Lee, S.B. Liu, *J. Phys. Chem. B* **106** (2002) 4462-4469.

[45] A.F. Cockerill, in *Comprehensive Chemical Kinetics vol. 9* (Eds: C.H. Bamford, C.F.H. Tipper), Elsevier Science, Amsterdam (1972) pp 163-364.

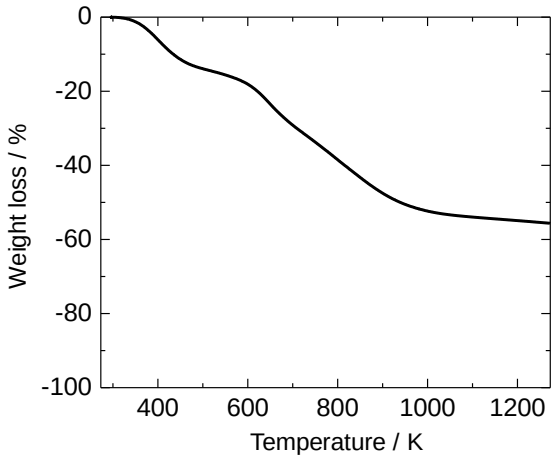

Figure 5-1. TG profile of the original RF resin. Heating rate: 10 K min^{-1}, N_2 flowing rate: 200 mL min^{-1}

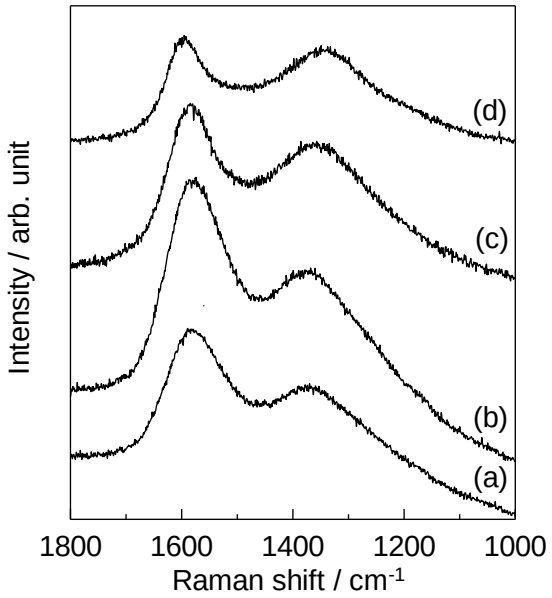

Figure 5-2. Raman spectra of the (a) RF-573, (b) RF-673, (c) RF-773, and (d) RF-973 SO_3H-bearing mesoporous carbon catalysts.

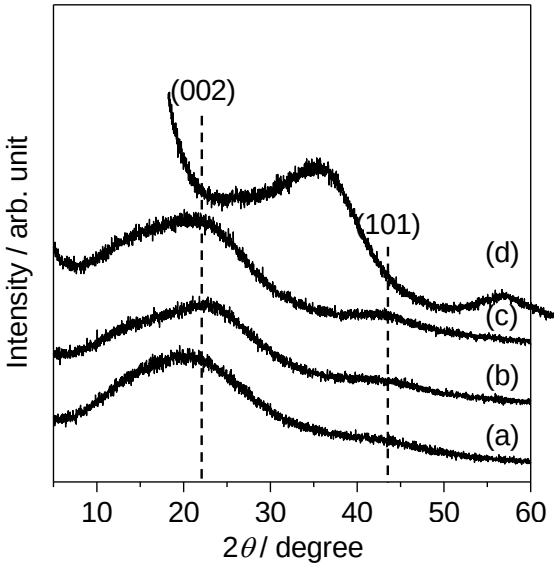

Figure 5-3. XRD patterns of the (a) RF-573, (b) RF-673, (c) RF-773, and (d) RF-973 SO_3H-bearing mesoporous carbon catalysts.

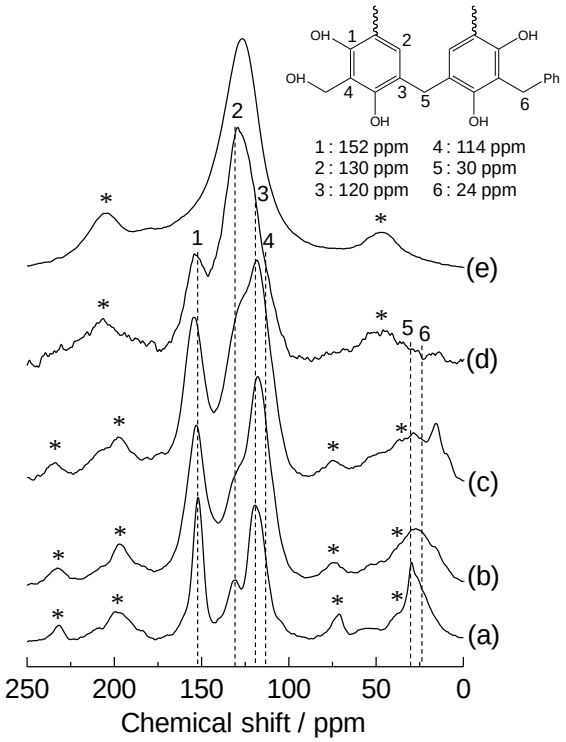

Figure 5-4. ^{13}C CP/MAS NMR spectra of (a) RF resin, and the (b)RF-573, (c) RF-673, (d) RF-773, and (e) RF-973 SO_3H-bearing mesoporous carbon catalysts. * denotes spinning sidebands.

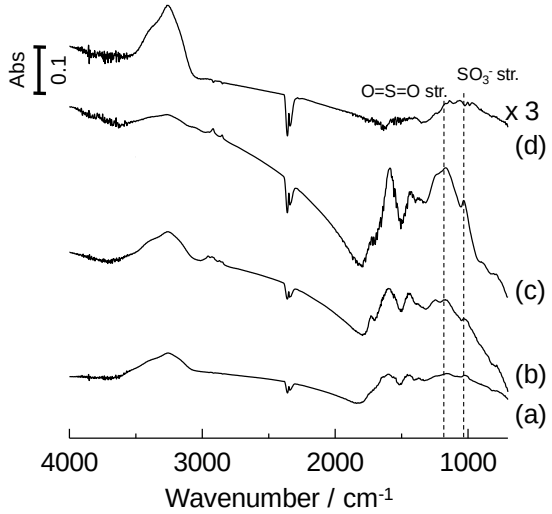

Figure 5-5. FT-IR spectra of the (a) RF-573, (b) RF-673, (c) RF-773, and (d) RF-973 SO_3H-bearing mesoporous carbon catalysts. The samples were dehydrated by heating at 423 K for 1 h under vacuum to remove physisorbed water.

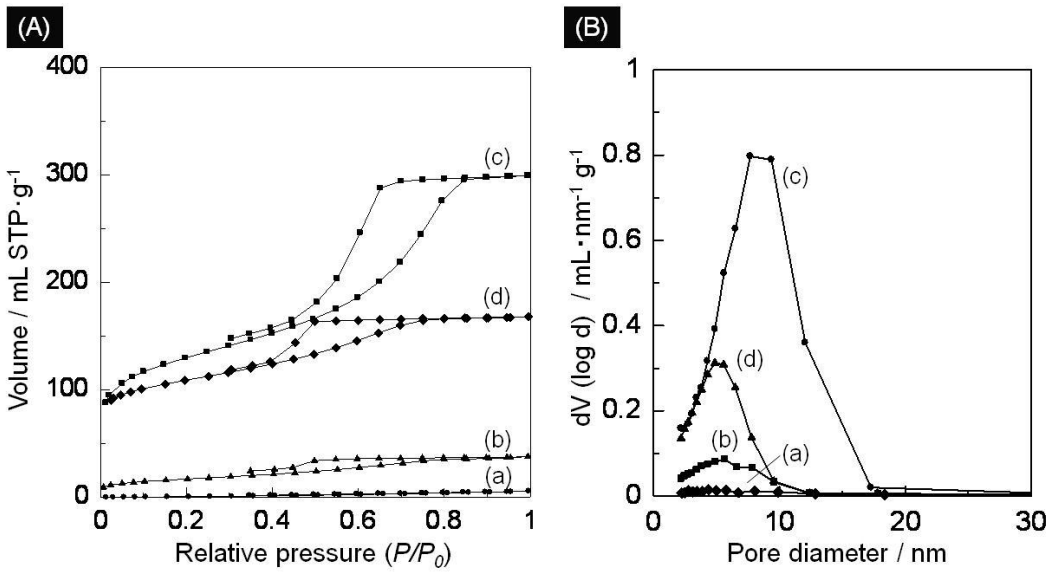

Figure 5-6. (A) N_2 adsorption-desorption isotherms and (B) BJH pore size distribution curves for the (a) RF-573, (b) RF-673, (c) RF-773, and (d) RF-973 SO_3H-bearing mesoporous carbon catalysts.

Table 5-1. BET surface areas and pore volumes for RF resin and mesoporous carbons before and after sulfonation

	BET surface area / $m^2 \cdot g^{-1}$	Mesopore volume / $mL \cdot g^{-1}$
RF resin	301	0.28
RF-573 (precursor)	307	0.38
RF-573	<1	-
RF-673 (precursor)	356	0.44
RF-673	59	0.06
RF-773 (precursor)	426	0.41
RF-773	433	0.46
RF-973 (precursor)	567	0.40
RF-973	361	0.26

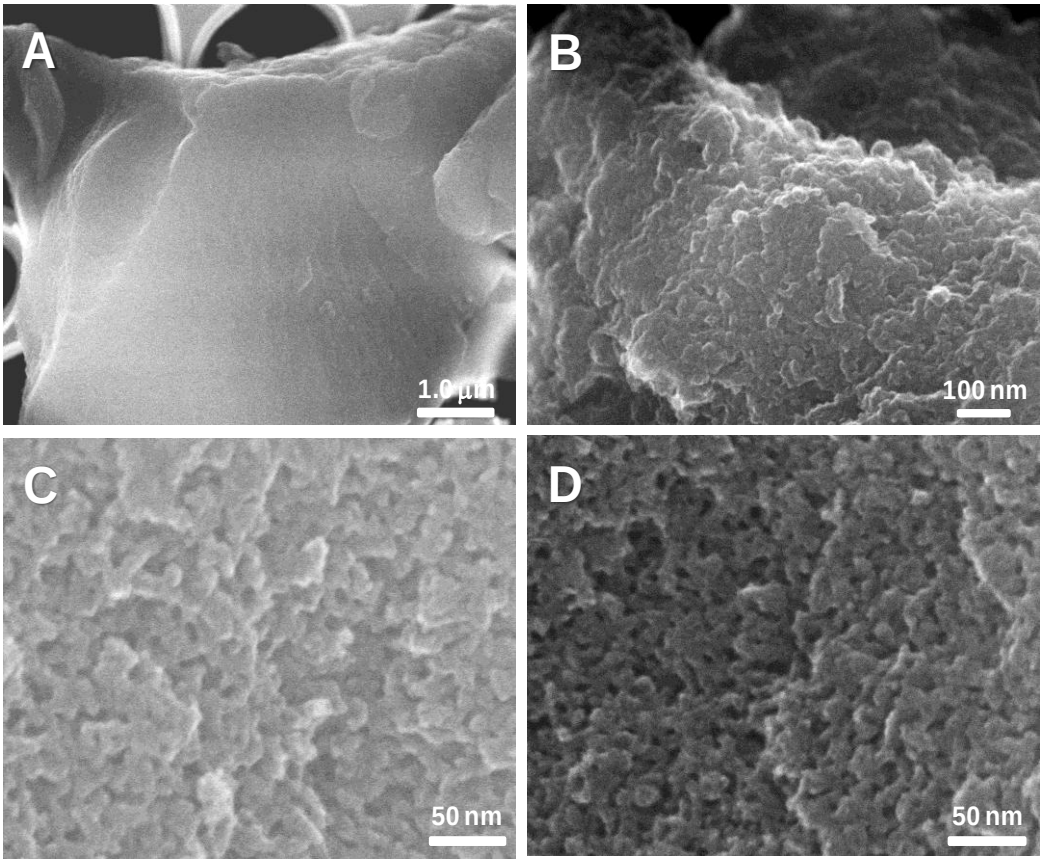

Figure 5-7. SEM images of the (A) RF-573, (B) RF-673, (C) RF-773, and (D) RF-973 SO_3H-bearing mesoporous carbon catalysts.

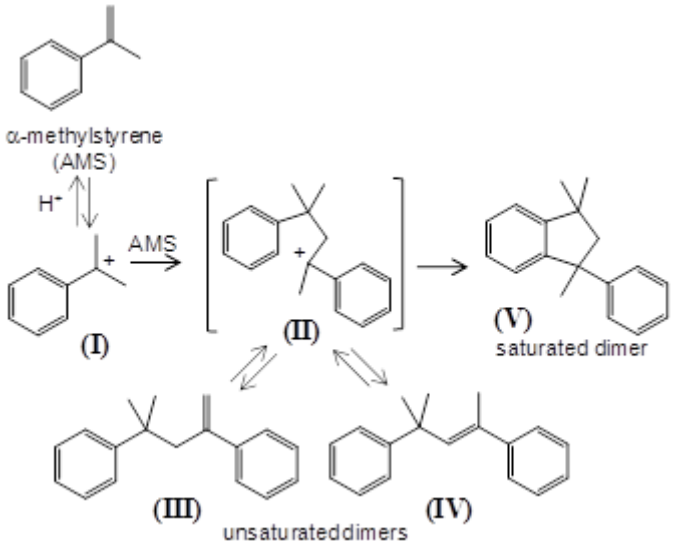

Figure 5-8. Reaction mechanism for AMS dimerization

Table 5-2. Physicochemical properties and catalytic activities for AMS dimerization by SO_3H-bearing mesoporous carbon, bulk carbon-based solid acid, Nafion NR-50, Nafion SAC-13, and Amberlyst-15 catalysts

	S_{BET} / $m^2 \cdot g^{-1}$	SO_3H [1] / $mmol \cdot g^{-1}$	Phenolic OH group [2] / $mmol \cdot g^{-1}$	AMS dimerization	
				Conv.[3] / %	Select.[4] / %
RF-573	<1	1.5	4.7	0	0
RF-673	59	1.7	3.0	4.4	>99
RF-773	433	0.9 (0.2)[6]	2.0	86	>99
RF-973	361	0.3 (0)[6]	0.8	0	0
CAC[5]	<1	1.5	5.4	0	0
Nafion NR50	<1	0.9	-	4.7	93
Nafion SAC-13	344	0.1	-	>99	59
Amberlyst-15	50	4.9	-	>99	8

[1] Amount of SO_3H groups estimated by elemental analysis; [2] amount of phenolic OH groups estimated from the combination of elemental analysis and cation-exchange analysis; [3] AMS conversion for 16 h; [4] selectivity toward unsaturated dimers for 16 h; [5] cellulose-derived carbon-based solid acid; [6] accessible SO_3H groups calculated from ^{31}P MAS NMR spectra of samples after TMPO adsorption.

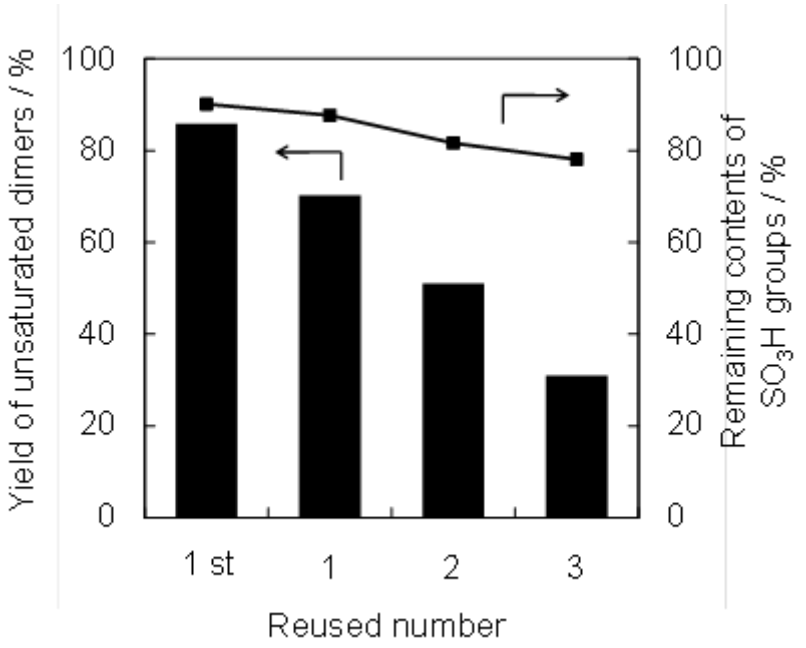

Figure 5-9. Catalytic activity of reused RF-773 for AMS dimerization and the remaining contents of SO_3H groups in the catalyst after reactions.

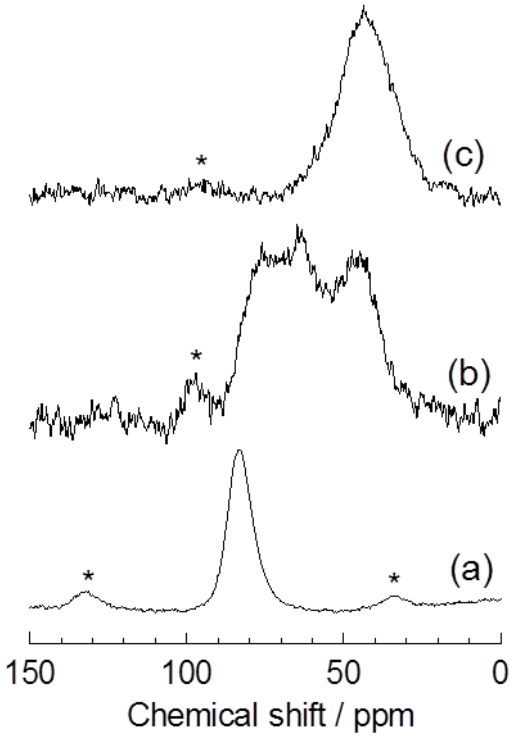

Figure 5-10. ^{31}P MAS NMR spectra of (a)CAC, (b) RF-773, and (c) RF-973 after TMPO adsorption. The SO_3H/TMPO ratio of these samples is 2. * denotes spinning sidebands.

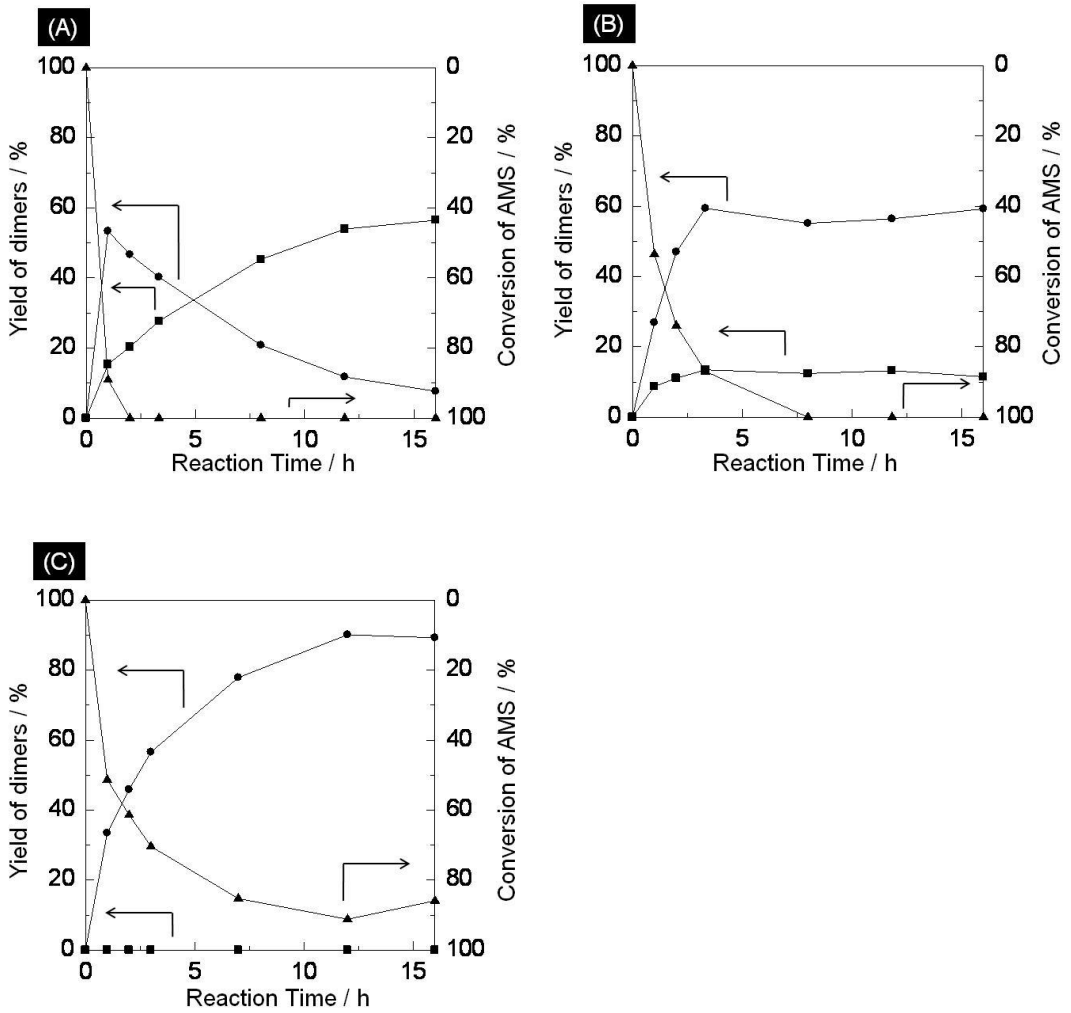

Figure 5-11. Time courses for AMS conversion (▲) and yields of unsaturated dimers (2,4-diphenyl-4-methyl-1-pentene and 2,4-diphenyl-4-methyl-2-pentene: (●)) and saturated cyclic indan (1,1,3-trimethyl-3-phenylindan: (■)) over (A) Amberlyst-15, (B) Nafion SAC-13, and (C) RF-773.

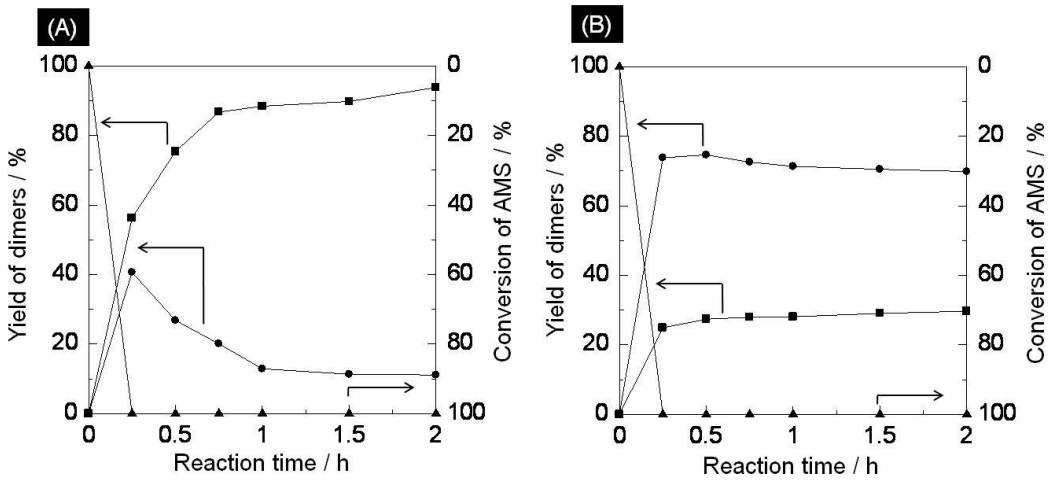

Figure 5-12. Time courses for AMS conversion (▲) and yields of unsaturated dimers (2,4-diphenyl-4-methyl-1-pentene and 2,4-diphenyl-4-methyl-2-pentene: (●) and saturated cyclic indan (1,1,3-trimethyl-3-phenylindan: (■) over H_2SO_4 in the (A) absence and (B) presence of p-cresol (2.4 mL).
AMS (25 mmol) in cumene (31.32 mL) was reacted over concentrated H_2SO_4 (0.1 g) at 298 K for 2 h in the presence or absence of p-cresol (2.4 mL).

Chapter 6

Summary

Chapter 2

SO_3H-bearing amorphous carbon, prepared by partial carbonization of cellulose followed by sulfonation in fuming H_2SO_4, was applied as a solid catalyst for the acid-catalyzed hydrolysis of β-1,4 glucan, including cellobiose and crystalline cellulose. Structural analyses revealed that the resulting carbon material consists of graphene sheets with 1.5 mmol g^{-1} of SO_3H groups, 0.4 mmol g^{-1} of COOH, and 5.6 mmol g^{-1} of phenolic OH groups. The carbon catalyst showed high catalytic activity for the hydrolysis of β-1,4 glycosidic bonds in both cellobiose and crystalline cellulose. Pure crystalline cellulose was not hydrolyzed by conventional strong solid Brønsted acid catalysts such as niobic acid, Nafion NR-50, and Amberlyst-15, whereas the carbon catalyst efficiently hydrolyzes cellulose into water-soluble saccharides. The catalytic performance of the carbon catalyst is due to the large adsorption capacity for hydrophilic reactants and the adsorption ability of β-1,4 glucan, which is not adsorbed to other solid acids.

Chapter 3

The hydrolysis of cellulose into saccharides using a range of solid catalysts is investigated for potential application in the environmentally benign saccharification of cellulose. Crystalline pure cellulose is not hydrolyzed by conventional strong solid Brønsted acid catalysts such as niobic acid, H-mordenite, Nafion and Amberlyst-15, whereas amorphous carbon bearing SO_3H, COOH, and OH function as an efficient catalyst for the reaction. The apparent activation energy for the hydrolysis of cellulose into glucose using the carbon catalyst is estimated to be 110 kJ mol^{-1}, smaller than that for sulfuric acid under optimal conditions (170 kJ mol^{-1}). The carbon catalyst can be readily separated from the saccharide solution after reaction for reuse in the reaction without loss of activity. The catalytic performance of the carbon catalyst is attributed to the ability of the material to adsorb β-1,4 glucan, which does not adsorb to other solid acids.

Chapter 4

SO_3H-bearing amorphous carbon prepared from polyvinyl chloride (PVC) has been

studied as a heterogeneous Brønsted acid catalyst. Sulfonation of partially carbonized PVC results in amorphous carbon consisting of small SO_3H-bearing carbon sheets linked by sp^3-based aliphatic hydrocarbons. This carbon material exhibits much higher catalytic performance for the hydrolysis of cellobiose than conventional heterogeneous Brønsted acid catalysts with SO_3H groups, including SO_3H-bearing amorphous carbon derived from cellulose. This can be attributed to a high density of SO_3H groups and the fast diffusion of reactants and products enabled by a flexible carbon network.

Chapter 5

A SO_3H-bearing mesoporous carbon material was investigated as a new type of heterogeneous catalyst. Carbonization of resorcinol-formaldehyde resin at 773 K, followed by sulfonation results in amorphous carbon consisting of graphene with high densities of SO_3H (0.9 $mmol \cdot g^{-1}$) and phenolic OH (2.0 $mmol \cdot g^{-1}$) groups. The mesoporous carbon that has a large surface area (433 $m^2 \cdot g^{-1}$) due to uniform mesopores (ca. 10 nm) exhibits remarkable catalytic performance for the selective dimerization of α-methylstyrene (AMS); the selectivity for unsaturated AMS dimers exceeds 99%. This catalysis is attributed to not only the large surface area based on large mesoporosity, but also to preventing the intramolecular Friedel-Crafts alkylation.

List of Publications

1. **Satoshi Suganuma**, Kiyotaka Nakajima, Masaaki Kitano, Daizo Yamaguchi, Hideki Kato, Shigenobu Hayashi, and Michikazu Hara
   "Hydrolysis of Cellulose by Amorphous Carbon Bearing SO_3H, COOH, and OH Groups" (Chapter 3)
   Journal of the American Chemical Society, **2008**, 130, 12787-12793.

2. Daizo Yamaguchi, Masaaki Kitano, **Satoshi Suganuma**, Kiyotaka Nakajima, Hideki Kato and Michikazu Hara
   "Hydrolysis of Cellulose by a Solid Acid Catalyst under Optimal Reaction Conditions"
   The Journal of Physical Chemistry C, **2009**, 113, 3181-3188.

3. Masaaki Kitano, Daizo Yamaguchi, **Satoshi Suganuma**, Kiyotaka Nakajima, Hideki Kato, Shigenobu Hayashi and Michikazu Hara
   "Adsorption-Enhanced Hydrolysis of β-1,4-Glucan on Graphene-Based Amorphous Carbon Bearing SO_3H, COOH, and OH Groups"
   Langmuir, **2009**, 25, 5068–5075

4. **Satoshi Suganuma**, Kiyotaka Nakajima, Masaaki Kitano, Daizo Yamaguchi, Hideki Kato, Shigenobu Hayashi, Michikazu Hara
   "Synthesis and acid catalysis of cellulose-derived carbon-based solid acid" (Chapter 2)
   Solid State Sciences, **2010**, 12, 1029-1034.

5. **Satoshi Suganuma**, Kiyotaka Nakajima, Masaaki Kitano, Hideki Kato, Asako Tamura, Hidesato Kondo, Shinichiro Yanagawa, Shigenobu Hayashi, Michikazu Hara
   "SO_3H-bearing mesoporous carbon with highly selective catalysis" (Chapter 5)
   Microporous and Mesoporous Materials, **2011**, 143, 443-450

6. **Satoshi Suganuma**, Kiyotaka Nakajima, Masaaki Kitano, Shigenobu Hayashi, Michikazu Hara
   "sp^3-linked Amorphous Carbon with SO_3H Groups as a Heterogeneous Acid Catalyst" (Chapter 4)
   ChemSusChem, to be accepted.

Acknowledgements

This thesis is the result of six years of the studies which have been supported by many people. I am grateful for eminent research environment and the opportunity to meet all of them.

First of all, I wish to express my deepest thanks to my supervisor, Professor Michikazu Hara for his guidance of experimental approach and logical way of thinking. His wide knowledge and understanding have been of great value of me.

Special acknowledgement is made to Professor Takashi Tatsumi for hearty encouragement and constructive guidance throughout this work. He also gave me the understanding of what is science.

I am sincere grateful to Dr. Kiyotaka Nakajima for instructive discussion, hearty encouragement, and personal guidance throughout this study. Thanks are made to Dr. Masaaki Kitano and Dr. Hideki Kato at Institute of Multidisciplinary Research for Advanced Materials, Tohoku University for their suggestion and relevant guidance in present study.

I am deeply indebted to Dr. Shigenobu Hayashi at National Institute of Advanced Industrial Science and Technology (AIST) for his help in the measurement, analysis, and discussion of solid-state NMR study.

I thank Professor Akihiko Kudo at Department of Applied Chemistry, Tokyo University of Science, for introducing me to the Hara laboratory.

During this work I have cooperated with many colleagues in the laboratory, and I deeply appreciate warm encouragement and helpful kindness of them, especially, Yasunori Inoue and Kiichi Fukuhara.

Finally, I would like to acknowledge my parents for their hearty support as well as financial assistance.

February, 2012

Satoshi Suganuma

Appendix 1

Lactic Acid Synthesis over Hydrous Ta_2O_5 as a Heterogeneous Lewis Acid Catalyst

1-1 Abstract

Amorphous Ta_2O_5 has been studied as heterogeneous Lewis acid catalyst for the transformation of 1,3-dihydroxyacetone (DHA) into lactic acid in water. Ta_2O_5 has both Brønsted and Lewis acid sites on the surface and converts DHA into lactic acid in water. Lewis acid sites on Ta_2O_5 workable in water effectively promote the dehydration of DHA into pyruvaldehyde (PVA) and subsequent hydride shift of PVA into lactic acid. The introduction of phosphate species on the Ta_2O_5 resulted in a great improvement of lactic acid yield, due to the decrease in the production of undetectable materials through complex side reactions.

1-2 Introduction

Lactic acid has been expected as an important intermediate in pharmaceutical, food, cosmetic and chemical industries, and used as a platform chemical for the production of biodegradable polymers and renewable solvents [1-3]. An anaerobic microbial fermentation of glucose and cornstarch using bacteria has been utilized for large-scale production of lactic acid in the industrial process. However, this process requires the use of calcium hydroxide to neutralize the product, resulting in waste generated during the separation of lactic acid from the fermentation broth [4]. Recently, chemical synthesis routes have attracted much attention as a replacement of the biological synthesis route. Zn(II), Cr(III), Co(II), and Ni(II) salts have been used as Lewis acid catalysts for the chemical transformation of glucose into lactic acid in water at subcritical conditions [5-7]. But, lactic acid yields were usually lower than that of biological route. The conversion of trioses into lactic acid and lactate derivatives has been a subject of intense investigation in recent years. Trioses, such as DHA and glycelaldehyde (GLA), can be obtained by aerobic oxidation of glycerol using various oxidation catalysts [8-12]. Scheme 1-1 illustrates the proposed reaction pathway of LA synthesis from DHA over an acid catalyst [13-15]. DHA is isomerized into GLA in equilibrium reaction. PVA is a reaction intermediate through the dehydration of DHA or GLA. It should be noted that PVA exists in three forms in water; hydrate form; aldehyde, mono-hydrate, and dehydrate form with a typical distribution of trace, 56%, and 44%, respectively [16]. Mono-hydrated PVA is

converted though a hydride shift reaction into lactic acid. Homogeneous Lewis acids, such as Cr or Rh complexes, have been investigated for the transformation of trioses into lactic acid in water [17,18]. However, the use of homogeneous Lewis acids has generally some problems in separation of the catalyst from reaction mixture and reusability. This has stimulated the use of stable and highly active solid acids with water-tolerant Lewis acid sites for the development of environmentally benign chemical production of lactic acid in water. Representative example of such solid Lewis acid is Sn–containing Beta zeolite that can convert DHA into methyl lactate with high yield in methanol [7,19]. This process can realize easy separation of the product from reaction mixture, due to insoluble Lewis acid catalysts, and would be suitable for large scale production of lactic acid derivatives with minimizing environmental load.

Recently, we reported that niobic acid, $Nb_2O_5{\cdot}nH_2O$, can function as a heterogeneous catalyst with water-tolerant Lewis acid sites for the conversion of glucose into 5-(hydroxymethyl)furfural (HMF) [20]. The Lewis acid sites workable in water are due to NbO_4 tetrahedra that still have effective positive charges as Lewis acid sites even after the formation of NbO_4-H_2O adducts. In addition, H_3PO_4 treatment of $Nb_2O_5{\bullet}nH_2O$ resulted in drastic improvement of HMF selectivity, due to a large decrease in the production of undetectable by-products. Transition metal oxide including groups 5 metals would be expected to function as a similar water-tolerant Lewis acid catalyst to $Nb_2O_5{\bullet}nH_2O$. We have focused on Ta_2O_5 as a potential heterogeneous Lewis acid catalyst and have applied the oxide to lactic acid production in water. Hydrated Ta_2O_5 have been reported as a strong solid acid catalyst similar to $Nb_2O_5{\bullet}nH_2O$. Acid property of Ta_2O_5 relies mainly on strong Brønsted acid sites and Lewis acid sites are considered as TaO_4 tetrahedra [21]. Du et al. reported that Ta_2O_5 efficiently promotes saccharide dehydration into HMF in a water/2-butanol biphasic system [22], indicating that Ta_2O_5 is also useful catalyst for the acid-catalyzed conversion of biomass-derived sugars into chemicals in water. In this study, Lewis acidity of Ta_2O_5 was studied with FT-IR measurement using basic probe molecules in the presence of water. Catalytic performance was examined for lactic acid production from aqueous DHA solution. In addition, H_3PO_4 treatment was attempted for of Ta_2O_5 to improve the catalytic performance of the samples.

1-3 Experimental

Catalyst preparation

Ta_2O_5 was prepared from tantalum ethoxide through a simple sol-gel reaction. In a typical synthesis, a mixture of 5 g tantalum (V) pentaethoxide and 100 mL water was stirred for 15 h at room temperature. The evolved white precipitate was collected by filtration and washed with excess amounts of distilled water. The white powder was stirred in 250 mL of 0.1 M aqueous HCl solution to promote the hydrolysis of residual unreacted ethoxide. After stirring the solution for 3 h at room temperature, the resulting sample was further washed repeatedly with distilled water until the pH of the filtrate reached neutral. After drying the material at 353 K overnight, Ta_2O_5 was obtained. Phosphoric acid-modified Ta_2O_5 was prepared by immobilizing H_3PO_4 on the resulting Ta_2O_5. 1.5 g

of Ta_2O_5 was added to aqueous H_3PO_4 solution (0.1 M, 100 mL) for 48 h at room temperature. The collected sample was washed repeatedly with distilled water until phosphate ions were no longer detected. The resulting material was dried overnight at 353 K and then used as the catalyst. The resulting material is denoted as PA-Ta_2O_5.

Characterization

Structural information of the prepared samples was obtained by powder X-ray diffraction (XRD; ULTIMA IV, Rigaku), Fourier transform-infrared spectroscopy (FT-IR; FT/IR-6100, Jasco), and N_2 adsorption analysis (NOVA-4200e, Quantachrome). Nitrogen adsorption-desorption isotherms were measured at 77 K. Prior to measurement, the samples were pretreated at 423 K for 1 h under vacuum. The Brunauer-Emmett-Teller (BET) surface areas were estimated over a relative pressure (P/P_0) range of 0.05-0.30.

The acid properties of the prepared samples were examined using FT-IR, equipped with a mercury cadmium telluride detector. The samples were pressed into self-supporting disks (20 mm diameter, 20-30 mg) and placed in an IR cell attached to a closed circulation system. The sample was dehydrated at 423 K for 1 h under vacuum and was exposed to pyridine vapor at 423 K. The intensities of the bands at 1540 and 1445 cm^{-1} (pyridinium ion formed on Brønsted acid sites, molecular absorption coefficient: 7.24 $\mu mol \cdot cm^{-1}$ and pyridine coordinatively bonded to Lewis acid sites, molecular absorption coefficient: 3.49 $\mu mol \cdot cm^{-1}$, respectively) were plotted against the amounts of pyridine adsorbed on the Brønsted and Lewis acid sites of the samples. The band intensity increased with increasing amount of chemisorbed pyridine, reaching a plateau with the appearance of a band due to physisorbed pyridine (1440 cm^{-1}). After evacuation of the samples at room temperature, the maximum intensity of the band at 1540 and 1445 cm^{-1} corresponds to the total amount of Brønsted and Lewis acid sites with adsorbed pyridine.

Acid-Catalyzed Reaction

The catalytic performance was demonstrated through the conversion of DHA and pyruvaldehyde (PVA) into lactic acid (383 K). Some homogeneous and heterogeneous acid catalysts ($Sc(OTf)_3$, $Yb(OTf)_3$, Nafion NR50, H_2SO_4, H_3PO_4, Nb_2O_5, H_3PO_4-treated Nb_2O_5 (represented as PA-Nb_2O_5)) were used as reference materials for comparison. The reactions were carried out in a 2 mL of 0.1 M aqueous solution. 0.1 g of each catalyst was used in the reactions without any pretreatments. The solutions were analyzed using a high-performance liquid chromatography (LC-2000 plus, Jasco) equipped with an Aminex HPX-87H column (BioRad Laboratories).

1-4 Results and discussion

Structural characteristics and acid property for Ta_2O_5 and PA-Ta_2O_5

Structural characteristics and acid property were examined with XRD, N_2 adsorption analysis,

and FT-IR measurement using basic probe molecules. XRD patterns for Ta_2O_5 and PA-Ta_2O_5 are shown in Figure 1-1. There is no clear diffraction in Figures 1-1(a) and 1(b), which reflects amorphous structure. BET surface area of the Ta_2O_5 and PA-Ta_2O_5 was estimated from N_2 adsorption isotherm to be 186 and 139 $m^2 \cdot g^{-1}$, respectively. The samples therefore consist of amorphous Ta_2O_5 oxide with large surface area. H_3PO_4 treatment slightly decreases surface area, due to the polycondensation of OH groups, but PA-Ta_2O_5 still have large surface area suitable for catalytic reaction. Figure 1-2 shows FT-IR spectra for the Ta_2O_5 and PA-Ta_2O_5. The signals for OH stretching (3735 cm^{-1}) mode of isolated surficial Ta-OH groups, hydrogen-bonded OH stretching (3600-2800 cm^{-1}) mode of Ta-OH groups and physisorbed H_2O, and OH bending (1600 cm^{-1}) mode of physisobed H_2O is observed for both spectra. A broad and intense signal at 1100 cm^{-1} in Figure 1-2(b) is attributed to P-O stretching mode in phosphoric acid groups. In addition, sharp signal also appears at 3669 cm^{-1} after H_3PO_4 treatment. This would be assignable to OH stretching mode of phosphate species. These results indicate that a certain amount of phosphate groups is immobilized on Ta_2O_5 surface during H_3PO_4 treatment.

FT-IR spectroscopy of basic probe molecules adsorbed on solid acid catalysts is useful method for understanding the active sites of the catalysts [23-28]. Pyridine has been widely used as a probe molecule for the characterization of both Brønsted and Lewis acid sites. Pyridine adsorption measurement can identify Lewis and Brønsted acid sites on the surface. Figure 1-3 displays FT-IR spectra of pyridine-adsorbed samples after evacuation at 298 K. The spectra for Ta_2O_5 and PA-Ta_2O_5 have two distinct signals at 1447 and 1542 cm^{-1}, which is assignable to coordinated pyridine species on Lewis acid sites and pyridinium ions formed on Brønsted acid sites, respectively. The intensities of the two bands increase with the amount of introduced pyridine and finally reach plateaus. The amounts of Brønsted and Lewis acid sites on Ta_2O_5 and PA-Ta_2O_5 were estimated from these band intensities and molecular adsorption coefficient to be ca. 0.01 and 0.10 mmol g^{-1}, and 0.01 and 0.05 mmol g^{-1}, respectively. Figure 1-4 shows the results for introduction of pyridine to Ta_2O_5 in the presence of saturated H_2O vapor. Two large and diffuse bands due to physisorbed water are observed at 2500–3700 and 1500–1700 cm^{-1} in these spectra. Even in the case of such water-saturated Ta_2O_5, the band due to pyridine adsorbed on Lewis acid sites (1444 cm^{-1}) appears. The total amounts of Lewis acid sites on Ta_2O_5 in the presence of saturated water vapor (water-tolerant Lewis acid density) were 0.09 mmol g^{-1}. This implies that most of unsaturated TaO_4 tetrahedra still act as Lewis acid sites, even in the presence of water, because water does not deactivate these Lewis acid sites. The amount of water-tolerant Lewis acid sites was also estimated to be 0.05 mmol g^{-1} with the FT-IR measurement.

Catalytic performance in lactic acid synthesis

The catalytic performance of Ta_2O_5 and PA-Ta_2O_5, together with reference materials, in the transformation of DHA into lactic acid in water was summarized in Table 1-1. $Sc(OTf)_3$ and $Yb(OTf)_3$ as homogeneous Lewis acid catalysts, efficiently converts DHA into lactic acid and undetectable by-product. Lewis acid catalysts workable in water are effective in producing lactic acid from DHA in aqueous solution: However, relatively high yield for unknown species indicates

that Lewis acid sites promote complex side reactions to form undetectable by-product, in addition to the dehydration of DHA and hydride shift of PVA. Homogeneous (H_3PO_4 and H_2SO_4) and heterogeneous (Nafion NR50) Brønsted acid catalysts exhibit higher PVA yield than lactic acid yield in the reaction. Brønsted acids effectively proceed on the dehydration of DHA into PVA, but are not so active for subsequent hydride shift reaction. Nb_2O_5 and Ta_2O_5 can produce lactic acid in high yield: Lactic acid yields are comparable to that of $Sc(OTf)_3$, a homogeneous Lewis acid. In addition, H_3PO_4 treatment of Nb_2O_5 and Ta_2O_5 leads to a great improvement in catalytic performance for the reaction. PA-Ta_2O_5 shows higher catalytic performance among the tested catalysts: DHA conversion and lactic acid yield reaches >99% and 88%, respectively. High lactic acid yield for these materials is mainly derived from water-tolerant Lewis acid sites that promote hydride shift of PVA, because Brønsted acid are not effective in the hydride shift reaction. Phosphoric acid modification causes a significant improvement in lactic acid yield by decreasing side reactions. Phosphoric acid itself cannot work as an effective catalyst for the reaction: H_3PO_4 shows much smaller lactic acid yield than other tested catalyst. To clarify the difference of these two catalysts, time courses of DHA conversion and product yields for Ta_2O_5 and PA-Ta_2O_5 (Figure 1-5) was examined. Ta_2O_5 converts DHA into lactic acid and undetectable materials within a short reaction time (Figure 1-5 (A)). In the case of PA-Ta_2O_5, DHA is converted into PVA at the initial stage of the reaction and the evolved PVA decreases with the increase in lactic acid (Figure 1-5 (B)). We also examined catalytic performance in hydride shift of PVA over Ta_2O_5 and PA-Ta_2O_5, as shown in Figure 1-6. Ta_2O_5 effectively converts PVA into lactic acid (ca. 86% in yield) within 30 minute but simultaneously produces a small amount of undetectable material (ca. 10% in yield). PA-Ta_2O_5 converts most of PVA into lactic acid without the production of by-product. These results suggest that Ta_2O_5 promotes the dehydration of DHA and hydride shift of evolved PVA in parallel with side reactions at each step. The introduction of phosphate species effectively suppresses these side reactions which form undetectable materials. It should be noted that phosphate species are immobilized on Ta-OH groups on the surface. This means that H_3PO_4 treatment effectively decrease in weakly acidic Ta-OH groups that are regarded as active sites for side reactions.

1-5 Conclusion

Ta_2O_5 functioned as water-tolerant Lewis acid catalysts and converted DHA into lactic acid in water. Acid catalysis of Ta_2O_5 is derived from Lewis acid sites that promote the dehydration of DHA and the hydride shift of PVA. The selectivity of lactic acid for Ta_2O_5 was improved by H_3PO_4 modification on surface, resulting from suppresion of side reactions. This is attributed to the decrease in weakly acidic Ta-OH groups that would act as active sites for side reactions.

References and notes

[1] T. Ooi, T. Miura, K. Maruoka *Angew. Chem., Int. Ed.* **37** (1998) 2347-2349.

[2] Datta, R.; Henry, M. *J. Chem. Technol. Biotechnol.* **81**(2006) 1119-1129.

[3] A. Takasu, Y. Narukawa, T. Hirabayashi, *J. Polym. Sci., Part A:Polym. Chem.* **44** (2006) 5247-5253.

[4] K.L. Wasewar, A.A. Yawalkar, J.A. Moulijn, V.G. Pangarkar, *Ind. Eng. Chem. Res.* **43** (2004) 5969-5982.

[5] L. Kong, G.Li, H. Wang, W. He, F. Ling *J. Chem. Technol. Biotechnol.* **83** (2008) 383-388.

[6] M. Bicker, S. Endres, L. Ott, H. Vogel *J. Mol. Catal. A: Chem.***239** (2005) 151-157.

[7] E. Taarning, S. Saravanamurugan, M. Spangsberg Holm, J. Xiong, R.M.West, C.H. Christensen, *ChemSusChem* **2** (2009) 625-627.

[8] H. Kimura, K. Tsuto, T. Wakisaka, Y. Kazumi, Y. Inaya, *Appl. Catal., A* **96** (1993) 217-228.

[9] R. Ciriminna, G. Palmisano, C.D. Pina, M. Rossi, M. Pagliaro, *Tetrahedron Lett.* 47 (2006) 6993-6995.

[10] S. Demirel, K. Lehnert, M. Lucas, P. Claus, *Appl. Catal., B* **70** (2007) 637-643.

[11] R.M. Painter, D.M. Pearson, R.M. Waymouth, *Angew. Chem., Int. Ed.* **49** (2010) 9456-9459.

[12] C. Gätgens, U. Degner, S. Bringer-Meyer, U. Herrmann, *Appl. Microbiol. Biotechnol.* **76** (2007) 553-559.

[13] Y. Hayashi, Y. Sasaki, *Chem. Commun.* (2005) 2716-2718.

[14] K.P.F. Janssen, J.S. Paul, B.F. Sels, P.A. Jacobs, *Stud. Surf. Sci. Catal.* **170B** (2007) 1222-1227.

[15] E. Taarning, S. Saravanamurugan, M. Spangsberg Holm, J. Xiong, R.W. West, C.H. Christensen, *Chem. Sus. Chem.* **2** (7) (2009) 625-627.

[16] A.C. McLellan, P.J. Thornalley, *Anal. Chim. Acta.*, **263** (1992) 137.

[17] J. Eriksen, O. Mønsted, L. Mønsted, *Transition Met. Chem.* **23** (1998) 783-787.

[18] J.E. Bang, L. Monsted, O. Monsted, *Acta Chem. Scand.* **48** (1994) 12-19.

[19] Y. Román-Leshkov, M.E. Davis, *ACS Catal.* **1** (2011) 1566-1580.

[20] K. Nakajima, Y. Baba, R. Noma, N. Kitano, J.N. Kondo, S. Hayashi, M. Hara, *J. Am. Chem. Soc.* **133** (2011) 4224-4227.

[21] M. Baltes, A. Kytökivi, B.M. Weckhuysen, R.A. Schoonheydt, P.V.D. Voort, E.F. Vansant, J. Phys. Chem. B **105** (2001) 6211-6220.

[22] F. Yang, Q. Liu, M.Yue, X. Baia, Y. Du, *Chem. Commun.* **47** (2011) 4469-4471.

[23] G. Busca, *Phys. Chem. Chem. Phys.* **1** (1999) 723-736.

[24] E.P. Parry, *J. Catal.* **2** (1963) 371-379.

[25] J.W. Ward, *J. Catal.* **9** (1967) 225-236.

[26] M.B. Sayed, K.A. Kydd, R.P. Cooney, *J. Catal.* **88** (1984) 137-149.

[27] N. Echoufi, P.J. Gelin, *Chem. Soc., Faraday Trans.* **88** (1992) 1067-1073.

[28] A. Zecchina, S. Bordiga, G. Spoto, D. Scarano, G. Petrini, G. Leofanti, M. Padovan, C.O. Arean, *J. Chem. Soc., Faraday Trans.* **88** (1992) 2959-2969.

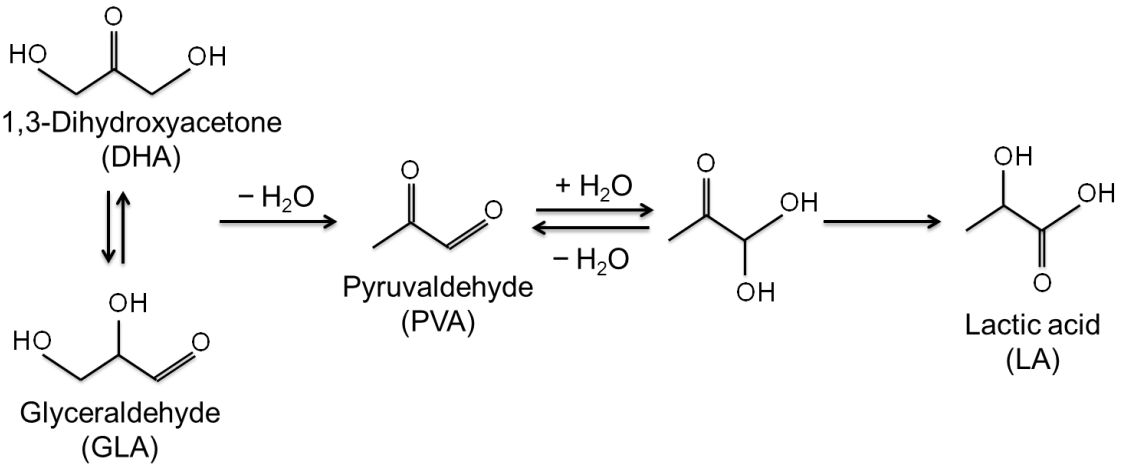

Scheme 1-1. Schematic illustration of reaction pathway in acid-catalyzed transformation of 1,3-dihydroxyacetone into lactic acid.

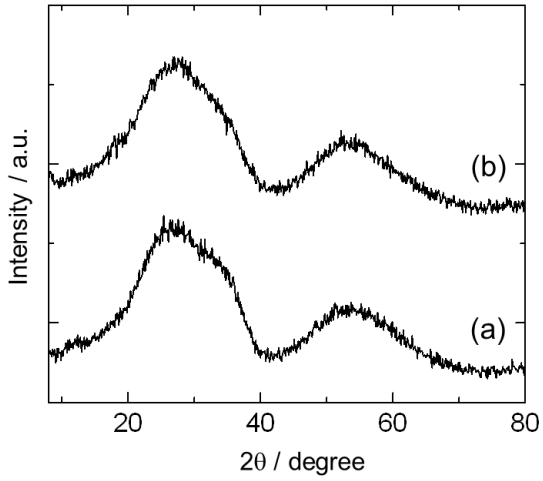

Figure 1-1. XRD patterns for (a) Ta_2O_5 and (b) PA-Ta_2O_5

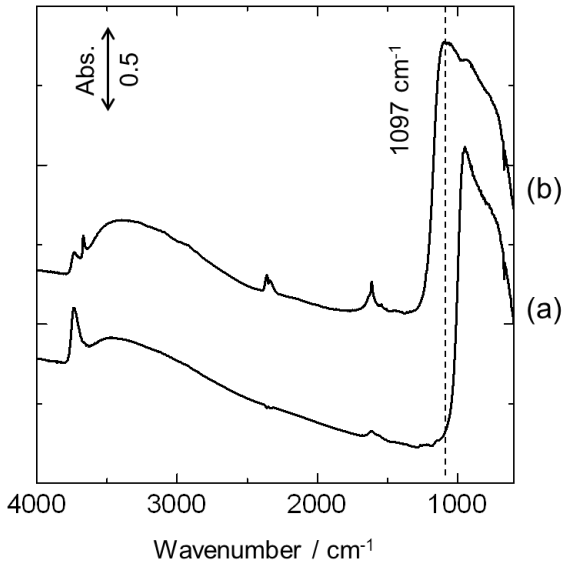

Figure 1-2. FT-IR spectra for (a) Ta_2O_5, and (b) PA-Ta_2O_5. The samples were dehydrated at 298 K for 0.5 h under vacuum to remove weakly physisorbed water.

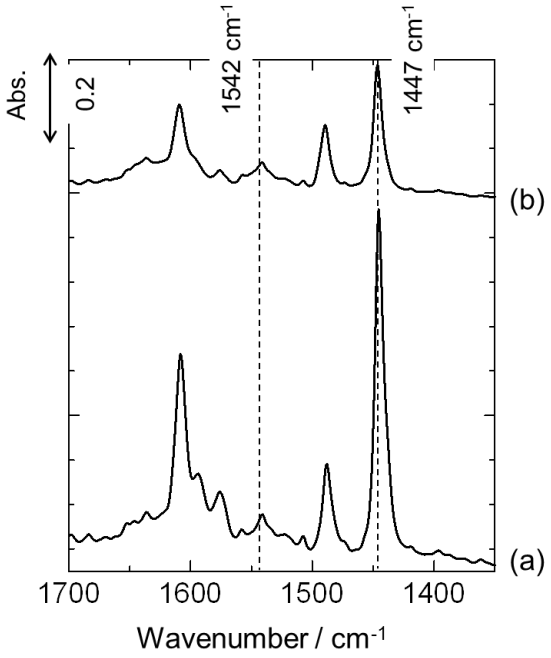

Figure 1-3. Differential FT-IR spectra for pyridine-adsorbed (a) Ta_2O_5 and (b) PA-Ta_2O_5. at room temperature. Prior to measurement, the samples were dehydrated at 473 K for 1 h under vacuum to remove physisorbed water. After pyridine adsorption, the samples were again evacuated at room temperature to remove weakly physisorbed pyridine.

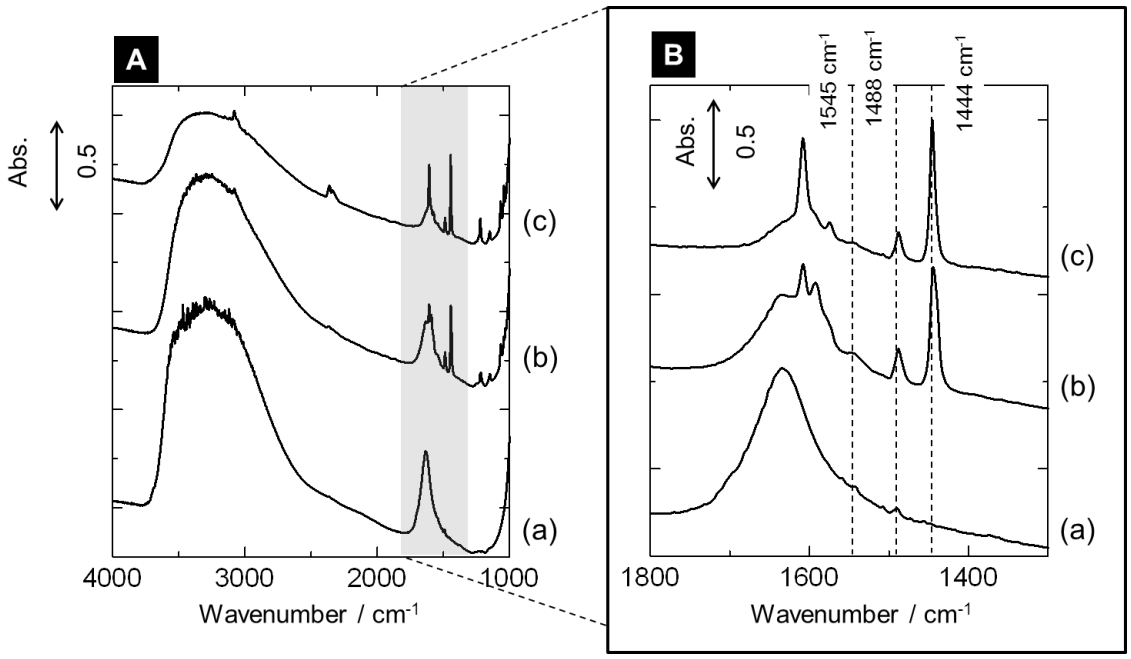

Figure 1-4. FT-IR spectra of hydrated Ta_2O_5. (a) hydrated Ta_2O_5 in saturated H_2O vapor, (b) the hydrated Ta_2O_5 after introduction of saturated pyridine vapor under saturated H_2O vapor, and (c) Ta_2O_5 sample obtained by evacuation at room temperature for 140 min after (b). The marked grey area in A is enlarged in B.

Table 1-1. Catalytic performance of Ta_2O_5, PA- Ta_2O_5 and reference materials in the transformation of DHA into lactic acid.

	LAS [a] (mmol g^{-1})	BAS [b] (mmol g^{-1})	Conversion [c] (%)	Yield (%) [c]		
				Lactic acid	PVA	Unknown [d]
Nb_2O_5	0.15 (0.03) [e]	0.17	>99	51.3	0	48.7
Ta_2O_5	0.10 (0.09) [e]	0.01	>99	55.2	0	44.8
PA-Nb_2O_5	0.11 (0.02) [e]	0.04	>99	77.7	10.0	12.3
PA-Ta_2O_5	0.05 (0.05) [e]	0.01	>99	87.9	3.3	8.8
$Sc(OTf)_3$	2.0	–	>99	65.5	0	34.5
$Yb(OTf)_3$	1.6	–	>99	30.3	0	52.0
Nafion NR50	–	0.9	82.0	2.6	51.9	27.6
H_2SO_4	–	20.4	>99	32.6	58.8	8.6
H_3PO_4	–	30.6	>99	2.5	81.9	15.6

[a] Lewis acid amounts, [b] Brønsted acid amounts, [c] Reagents and conditions: 0.1 M DHA aq., 2 mL; catalyst, 0.1 g; temperature, 383 K; reaction time, 3h, [d] undetectable by-product, [e] water-adsorbed sample.

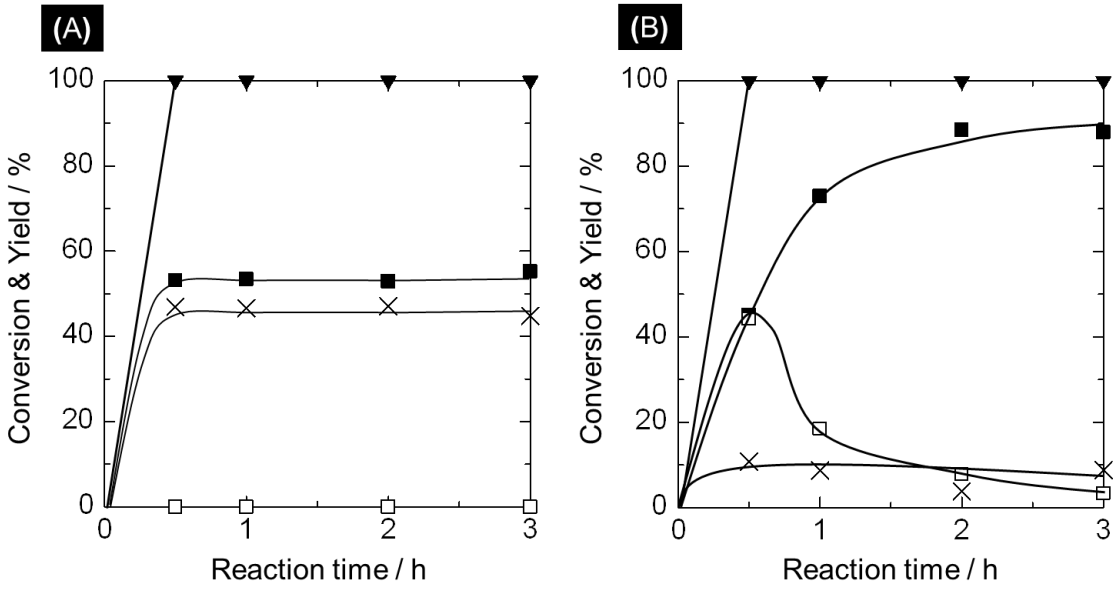

Figure 1-5. Time courses of DHA conversion and product yields for (A) Ta_2O_5 and (B) PA-Ta_2O_5. ▼: DHA conversion, ■: lactic acid yield, □: PVA yield, ×: undetectable by-product yield.

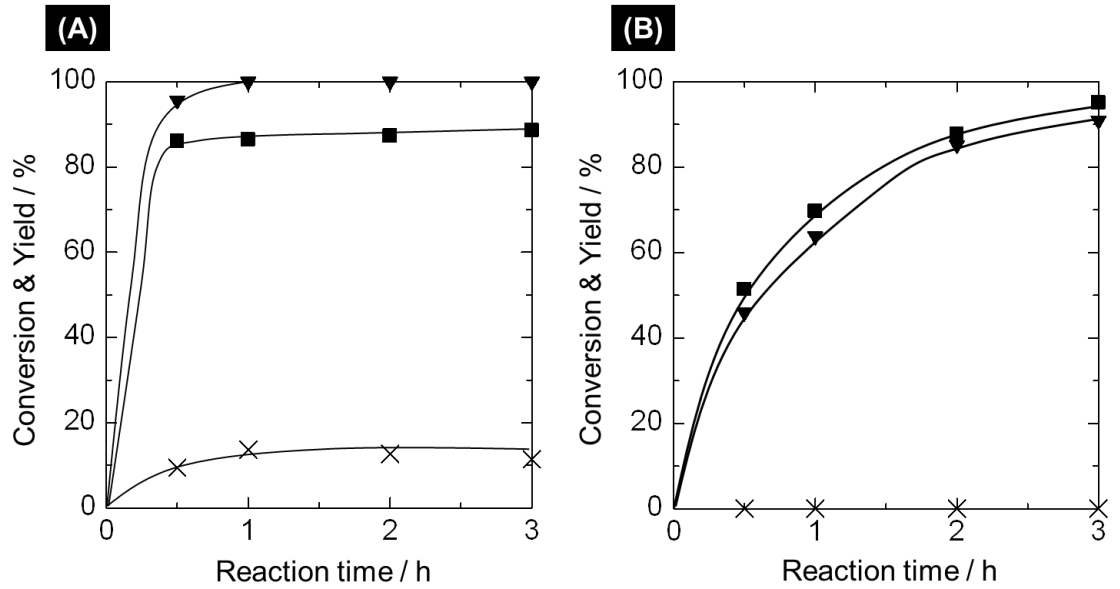

Figure 1-6. Time courses of PVA conversion and product yields for (A) Ta_2O_5 and (B) PA-Ta_2O_5. ▼: PVA conversion, ■: lactic acid yield, ×: undetectable by-product yield.